Characterisation and Modelling of Flow Mechanisms for Direct Contact Condensation of Steam Injected into Water

Anka Petrovič - de With

A thesis submitted in partial fulfilment of
the requirements of the University of Hertfordshire
for the degree of Doctor of Philosophy

The programme of research was carried out in the
School of Aerospace, Automotive and Design Engineering,
Faculty of Engineering and Information Sciences,
University of Hertfordshire

Hatfield, June 2006

Abstract

Direct contact condensation of steam injected into water is a special mode of condensation where condensation occurs on the interface between steam and water. This type of condensation forms an essential part of various industrial applications and correct prediction and modelling of the condensation behaviour is crucial to obtain an optimised design of such devices.

While present prediction models for direct contact condensation are valid for a limited range of flow conditions only, the work presented in this thesis provides improved models for direct contact condensation. The models are developed in the form of diagrams and include: a condensation regime diagram, for predicting the condensation behaviour, a steam plume length diagram, for predicting the penetration distance of steam into water, and a heat transfer coefficient diagram.

These models are derived using a wide range of data and therefore provide more accurate predictions compared with alternative models available in literature. In contrast to present models, the derived models presented in this work are constructed using an additional physical parameter to describe the process.

The diagrams are validated against independent experiments and demonstrate close agreement. Furthermore, the predictions from the condensation regime diagram and steam plume length diagram are self-consistent.

The models developed in this study are capable of predicting condensation behaviour for a wide range of initial conditions and can be used in conjunction with computational fluid dynamics techniques for direct contact condensation.

Key words: direct contact condensation, condensation regime, steam plume length, steam plume shape, heat transfer coefficient

Acknowledgements

This thesis presents the results of my work performed at the University of Hertfordshire for a period of three years. I would like to express my gratitude to Dr. Raj K. Calay for the trust she had in me before and during my research project. Her supervision and guidance were an important factor in completing this thesis. I would also like to thank my second supervisors, Professor Arne E. Holdø and Professor Peter R. Bullen, for their contribution and feedback.

Part of this thesis deals with the direct contact condensation of steam into a water flow and includes results and photographic material, obtained during experiments performed for the development of a ballast water treatment system. Therefore I would like to thank Ocean Saver AS, Norway and Det Norske Veritas, Norway, for allowing me to use their experimental material.

My gratitude also goes to Jason, John and Ian for their support during my research and to some of my colleagues from the Science and Technology Research Institute for their friendship.

Finally, my special thanks go to my parents and to Govert, who was giving me indispensable support during all three years of my PhD.

Contents

Notation

Symbol	Description
A	area
A	plume surface area
a	x-coordinate of a centre of a sphere, ellipsoid
B	condensation potential
C	coefficient of virtual mass
c_p	specific heat at constant pressure
D	diameter of steam injector
e	internal energy
FI	coefficient of drag
f	shape function
G	steam flow rate
h	heat transfer coefficient
h_{fg}	latent heat
I	Integral
j	molecular flux
k	thermal conductivity
L	plume length
L	length
l	plume extension coefficient
M	molecular weight
M	momentum transfer
m	surface tension force
$\dot{m}$	rate of change of mass
p	pressure
Q	heat exchange
R	gas constant
R	injector radius
R	plume radius
Re	steam Reynolds number
r	radius
r	plume expansion coefficient

S	transport modulus
T	temperature
$\underline{T}$	stress tensor
ΔT	temperature of water subcooling
t	time
v	velocity
W	work exchange
x, y, z	space coordinates
y	section of function f

α	volume fraction
Γ	volumetric mass transfer rate
Δ	absolute value of fluctuation
ϵ	energy source
η	viscosity
η	plume shape factor
ν	frequency
ν	kinematic viscosity
ρ	density
Φ	condensation energy flux

Subscripts

Symbol	Description
a	average conditions
b	bubble
i	interface
i	surface of a volume
in	interface
j	surface area
k	phase k
k'	opposite phase to phase k
ki	contact between phase k and interface
m	maximum size
m	mixture
m	mean value
p	plume
s	steam
s	sine function
sp	sphere
w	water
∞	free stream conditions
0	initial conditions/at the injector
$1, 2$	referring to parts of a function

Abbreviations

Abbreviation	Description
BWT	Ballast Water Treatment
CFD	Computational Fluid Dynamics
CR	Condensation Regime
DCC	Direct Contact Condensation
HTC	Heat Transfer Coefficient
SDJP	Steam Driven Jet Pump
SPL	Steam Plume Length

1 Introduction

A condensation of steam injected into water is an example of multiphase flows in which fluids have different physical or thermodynamic properties and are separated by interfaces. Multiphase flows are the most common flows of fluids in nature and they appear in many industrial devices. Some examples of multiphase flows are boiling and condensing liquids, the drifting of clouds in the atmosphere and liquid sprays.

The frequent appearance and industrial significance of multiphase flows has resulted in intensive investigation of the subject, both experimentally and theoretically. Studies by Guha [1], Whalley [2], Hetsroni [3] and Drew and Passman [4] have contributed significantly to our present understanding of multi-phase flows and their work has formed the basis for most of the multi-phase computer models. Despite these substantial developments in the field of multi-phase flows, accurate modelling remains out-of-reach when the phenomenon of phase transition is the dominant flow feature, as seen in condensation and cavitation. At present, experimental study of such flows is essential to develop an understanding of the flow behaviour and the interaction from one phase to another. Nevertheless, it is well recognized that an understanding of this flow behaviour is essential to optimize the performance of a range of engineering devices. Some examples of engineering applications which rely on a well-controlled phase transition are steam ejectors, steam turbines, and various other devices used in the pharmaceutical and food industry and in nuclear reactors. Unfortunately, the physical behaviour of phase-transition is complicated. It includes two different phases in the system and, subject to environmental conditions, rapid, erratic and uncontrolled transition from one phase to another can take place. Consequently, both analytic and numerical modelling of such process remains a challenging task.

The theme of this thesis is to study the phase transition that takes place when steam is injected into water. The condensation of steam injected into water is a form of a Direct Contact Condensation (DCC) and is one of the least studied forms of condensation. While surface condensation and homogeneous condensation are studied extensively, DCC is given limited attention. Nevertheless, there is a range of devices which rely heavily on

effective use of DCC. One of them is the Steam Driven Jet Pump (SDJP) [5]-[7]. When DCC takes place there is a transfer of water vapour from gas into liquid form, causing heat, momentum and energy transfer. During DCC the transfer of mass, energy and momentum is subject to the local characteristics of the condensation process; hence, the performance of such engineering devices depends strongly on the local condensation characteristics and therefore detailed knowledge of the process is required to optimize the performance. The information that is required includes an understanding of the break-up of the condensation surface, the dynamic behaviour at the condensation interface and the formation of steam bubbles.

The behaviour of DCC has been investigated in various experimental studies [8]-[15] and while this has resulted in a substantial increase in experimental data, a generic understanding of condensation of steam in water is still very limited. Existing models for predicting the performance of devices which involve DCC [7], [16], [17] simplify the condensation process and use empirical correlations in their model. Consequently, these empirical correlations and model assumptions limit the capability of these models. It is this distinct lack of knowledge in DCC which requires further investigation and which is selected as the main theme of this thesis.

Crucial in modelling of the process of DCC is the behaviour of the injected steam, the penetration distance of steam into water and the heat transfer coefficient. The condensation behaviour of the steam is commonly termed as a regime. As part of this work a three-dimensional condensation regime diagram and a two-dimensional steam plume length diagram were developed and are presented in this thesis. For a wide range of flow conditions, these are capable of predicting the behaviour of condensing steam, the regime, and the length of a plume, the penetration distance of steam into water. They were constructed from experimental data available in literature. The experimental data has been obtained from a comprehensive set of independent experimental studies that has been published during the last three decades. The thesis will discuss in detail the construction of the condensation regime diagram and the steam plume length diagram. Further experimental data and correlations from the literature are used for validation. Modifications in the condensation regime diagram and steam plume

length diagram to enhance their functionality and to allow for prediction of steam condensation in water flow are discussed.

Furthermore, a mass conservation model for a steam plume is proposed in the thesis. A number of shapes, including shapes with interfacial structures, describing developed steam plumes at different flow conditions is proposed in combination with the model. Following the condensation regime diagram and the steam plume length diagram, different shapes are incorporated into the model in order to calculate the heat transfer coefficient for DCC of steam injected into water at various conditions. This leads to the development of the three-dimensional heat transfer coefficient diagram. This developed diagram is presented in the thesis and validated using correlations from the literature.

The three-dimensional condensation regime diagram, the two-dimensional steam plume length diagram and the three-dimensional heat transfer coefficient diagram characterise fully the process of DCC of steam injected into water. Furthermore, they show the dependance of the condensation process on four physical parameters of the process, which are steam inflow rate, temperature difference between steam and water, dimensions of the steam injector and velocity of the water flow.

The following chart (Figure 1.1) represents diagrammatically the developed diagrams and models presented in this thesis. A more detailed chart is presented at the end of the thesis in Chapter 8.

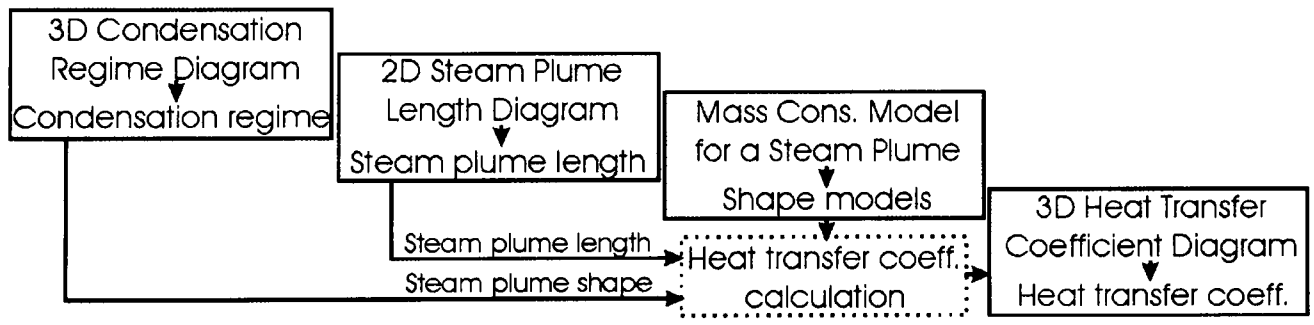

Figure 1.1: Flow chart of the developed DCC models and diagrams presented in the thesis.

1.1 Aims

In this work characterisation and modelling of flow mechanisms for a special mode of condensation DCC of steam injected into water are carried out. The purpose of the work is to use these means to predict the behaviour of the steam injected into water. The specific aims of this work are as follows:

- To increase the understanding of the DCC of steam injected into water by identifying the physical characteristics of the process.
- To propose improved correlations and models of the process of DCC of steam injected into water in order to provide the basis for more generic modelling of the process.

To achieve these aims, detailed objectives of the research were set and the research methodology to achieve the latter was proposed and followed during the research. Objectives are listed in Chapter 2, and methodology of the research is described in Chapter 3.

1.2 Outline of the Thesis

The second chapter of this thesis aims to provide a background knowledge of the subject of DCC and a clear understanding of the difficulties involved in modelling of DCC. Furthermore, regions and regimes of DCC of steam injected into water are presented in detail and key limitations of existing models are described. The chapter ends with the already-mentioned objectives listing the tasks that need to be performed in order to achieve the aims.

The thesis continues with Chapter 3 which describes the research methodology. The methodology flow chart is presented at the end of the chapter.

In the fourth chapter, the three-dimensional condensation regime diagram is developed. The section of the chapter starts with the literature review in order to gather sufficient data about regimes, used for construction of the diagram. Furthermore, the three-dimensional condensation regime diagram its validation and applicability to DCC of steam injected into a water flow are described. The Chapter finishes with a short discussion about the developed diagram. Findings from this Chapter were also suggested for the publication in the *International Journal of Heat and Mass Transfer* [18].

In Chapter 5, a two-dimensional steam plume length diagram is developed. Literature on the subject of a steam plume length is reviewed at the beginning of the Chapter. The Chapter than continues with a section about the development and validation of the steam plume length diagram. The developed diagram is than applied to DCC in a water flow. Discussion about the developed diagram finishes the Chapter.

Chapter 6 deals with the modelling of the steam-water interface. The mass conservation model for a steam plume is proposed in the Chapter. In addition, different models describing the interface with a smooth surface and with irregular structures are proposed and built into the mass conservation model.

In Chapter 7 the three-dimensional heat transfer coefficient diagram is developed. The literature review and data gathering on the subject of the heat transfer coefficient at DCC opens the Chapter. The mass conservation model for a steam plume is used in combination with the developed three-dimensional condensation regime diagram and the two-dimensional steam plume length diagram to generate the three dimensional heat transfer coefficient diagram for DCC of steam injected into water. The development of the diagram is described in the second section of Chapter 7. Further in the Chapter, the developed diagram is validated and applied to DCC in a water flow. The Chapter finishes with a discussion about the heat transfer coefficient diagram.

Chapter 8 provides a general discussion of the work. Strengths and weaknesses of the research methodology are assessed in the light of the reliability of developed diagrams and models for the DCC of steam injected into water. Furthermore, possible use of developed diagrams as means of providing the data for numerical modelling of DCC process is described. To visualize the inter-dependencies of the developed diagrams and models a flow chart is added to the Chapter.

The review in Chapter 9 leads to the conclusions that can be drawn from the work. Finally, suggestions for obtaining improved predictions and recommendations for further research are offered in Chapter 10.

2 Background

This chapter aims to introduce the key features of DCC and discusses how it can be modelled. It sets the scene by presenting the process of DCC as a special mode of condensation and as one of the multiphase flows. Furthermore, the terminology of the subject is defined in the chapter and key limitations of existing models are listed. The chapter finishes with the objectives for this study.

2.1 Condensation

Condensation is the removal of heat from a system so that part or all of the vapour phase is converted into liquid [2], [19]. Different modes of condensation exist and they are presented in Figure 2.1.

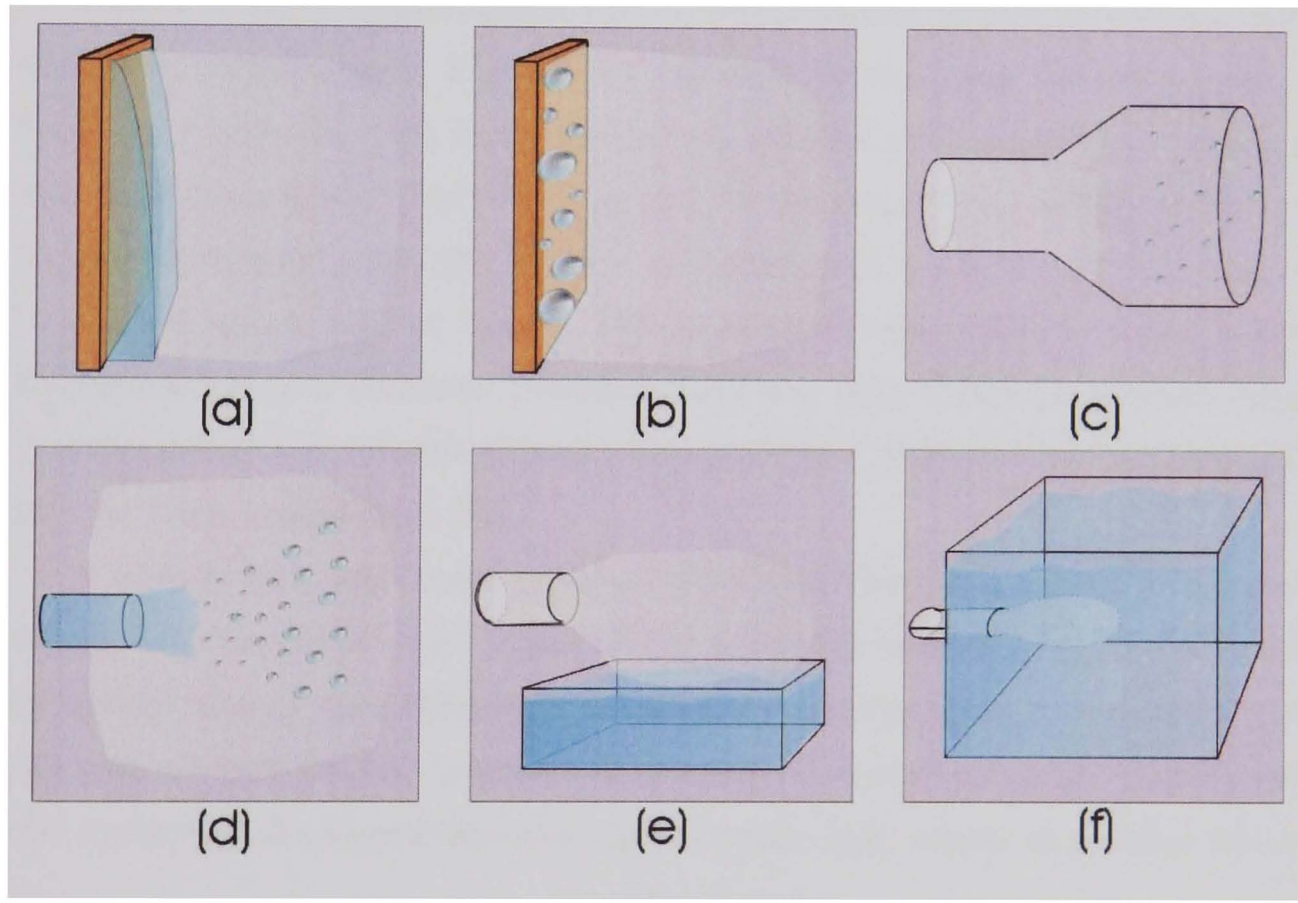

Figure 2.1: Modes of condensation: (a) Film condensation on a cold surface. (b) Dropwise condensation on a cold surface. (c) Homogeneous condensation resulting from the change in pressure. (d) DCC of vapour on the liquid jet. (e) DCC of vapour on the liquid surface. (f) DCC of vapour injected into a pool of liquid.

The most common mode is condensation of vapour on the cold surface

of a solid. Film condensation (Figure 2.1(a)) occurs when steam comes in contact with a clean, uncontaminated surface and causes the formation of a liquid film covering the entire surface. Under the action of gravity, film flows continuously from the surface. If the surface is coated with a substance that inhibits wetting, dropwise condensation occurs (Figure 2.1(b)). In this mode, drops form in cracks, pits and cavities on the surface and may grow and coalesce [20].

Another common mode of condensation is homogeneous condensation (Figure 2.1(c)), where vapour condenses to form droplets suspended in a gas phase to form a fog. Homogeneous or spontaneous condensation occurs in uncontaminated vapour as a result of isentropic expansion in steam nozzles and heterogeneous nucleation as a result of dust particles in the steam which may act as nucleation centres[1], [21].

Direct contact condensation occurs when vapour comes in a direct contact with a cold liquid. Figures 2.1 (d) to (f) show three different cases of DCC. In Figure 2.1 (d), vapour comes in contact with a liquid jet which is injected into a space filled with vapour. In the case shown in Figure 2.1 (e), vapour is injected onto the surface of liquid and in Figure 2.1 (f), vapour is injected into a pool of liquid. The later case is the subject of this study. Condensation is a common process; however, only film-wise condensation is understood and reliable theories about other types of condensation have not yet been established [22].

A special but most common case of DCC is the condensation of vapour on the interface of its own liquid. Here, the mass transfer can be described by kinetic theory as a difference between a rate of arrival of molecules from the vapour space to the interface and a rate of departure of molecules from the surface of the liquid into the vapour space [19], where molecular flux is

$$|j| = \left(\frac{M}{2\pi R}\right)^{\frac{1}{2}} \frac{\Delta p}{T^{1/2}} \,. \tag{2.1}$$

In order for condensation to occur, arrival rate must exceed the departure rate.

The driving force for condensation of vapour on the interface of its own liquid is the saturation temperature, which is dependent on the vapour pressure. Heat transfer is fixed by the heat transfer coefficient, which incorporates information about the effect of the flow on the transport of heat.

The interfacial heat transfer coefficient can be defined as

$$h_i = \frac{\Phi}{\Delta T} , \tag{2.2}$$

where the condensation energy flux Φ is a product of mass flux and latent heat ($\Phi = h_{fg} j$). This leads to an equation for a local heat transfer coefficient

$$h_i = h_{fg} \left(\frac{M}{2\pi R\, T} \right)^{\frac{1}{2}} \frac{\Delta p}{\Delta T} . \tag{2.3}$$

Equation (2.3) is only an approximation and does not contain factors describing effects of turbulence, non-condensable gases and some others. Finding a more accurate equation for the heat transfer coefficient is one of the main difficulties in developing an accurate model for DCC. The other difficulty is a definition of the shape and position of the interface. The latter are connected with properties of steam and eddies around the interface and have strong influence on the heat transfer.

Heat transfer with DCC occurs in the liquid and the heat transfer coefficient for this process is higher than for other types of condensation process. With DCC the heat transfer coefficient is of the order of $10^6 W/(m^2 K)$, with filmwise condensation $6 \times 10^2 - 6 \times 10^3 W/(m^2 K)$ and with dropwise condensation $6 \times 10^4 - 6 \times 10^5 W/(m^2 K)$ [3].

2.2 Multiphase Flows

Multiphase flows are combined flows of different phases such as bubbly flow, flow of water with solid particles, liquid droplets with dust particles in gas and many others. Special case of multiphase flows are flows with phase transition an example of which is also DCC.

Multiphase flows can be classified according to phase materials and interfacial structures in different systems and classes. The first classification gives three main systems of multiphase flows; liquid-gas, gas-solid and liquid-liquid system [3]. Classification according to interfacial structures gives three main classes of multiphase flows; separated flows, example of which is a jet flow, transitional flows, example of which is a slug flow, and dispersed flows, example of which is a bubbly flow [23], [24].

Different modelling techniques for multiphase flows can be used. The simplest is the homogeneous flow model [3], [25], [26], which assumes well

mixed phases moving at the same velocity, and can only give satisfactory results for the void fraction and overall pressure gradient. The use of the model is therefore limited only to specific cases of multiphase flows.

Another model is a drift - flux model. The model, developed by Wallis [24], looks at the relative motion of phases and is therefore applicable to flows with well-defined velocities of different phases. As a result it gives a simplified description of some separated and dispersed flows such as bubbly and slug flow, but does not give information about the motion of the individual phases and can not be extended to more complicated flow regimes and processes such as boiling and condensation [27].

More complicated multiphase processes can be better described by separate continuity, momentum and energy equations for the different phases with additional jump conditions, which describe exchanges of mass, momentum and energy between different components on their interfaces. Therefore, jump conditions act as interfacial boundary conditions. Simplified governing equations describing multiphase flows are presented by Hetsroni [3].

The most general text about modelling different multiphase flows was written by Drew and Passman [4]. In this theoretical book, the authors present the theory of multicomponent fluids and a derivation of the general equations governing three-dimensional unsteady two-fluid model from equations for one particle. Their model is constructed from three conservation equations: mass, momentum and energy conservation, which can be used for different components involved in the process separately, and from three equations for jump conditions. Jump conditions describe the mass, momentum and energy transfer between phases and connect together separate conservation equations for different components of the process. The proposed model can be used to model all different types and processes of multiphase flows.

Evidence of its huge applicability is evidenced by the works of Andrianov [23], [28], Saurel and Abgrall [29], Saurel and Lemetayer [30] and Lahey and Drew [31], who all refer to Drew and Passman's *Theory of Multicomponent Fluids* and use their general model as a basis for further work which includes compressible duct flow, vapour - liquid and particle - liquid two-phase flows,

shock wave problem in a tube and cavitation.

Many proposed multiphase models were also implemented in Computational Fluid Dynamics (CFD) codes. One of the first two-phase models, which was used for developing a CFD code, was that proposed by Spalding [32]. The model is implemented in the commercial code PHOENICS for two thermodynamic phases as a steady-state, one-dimensional flow model and it is a basis for many other models developed in recent years, such as a model for oil and air flow in a horizontal pipe proposed by Baghdadi [33].

In recent years various Nuclear System Simulation codes were built (RELAP5 [17], CATHARE [34], RETRAN [35], ATHLET [36]) and models for reactor safety proposed [37]. A major part of these codes is devoted to the prediction of steam - water two-phase flow which occurs in a nuclear reactor when steam is transported through pipes and injected into a water tank. Because of the importance of the correct prediction of processes related to nuclear power plants, these codes are being continuously evaluated and improved. They are used for the analysis of the safety of nuclear power plants and capable of predictions reasonably comparable with experimental data for the narrow range of input data specific for nuclear power plants. The most widely used program is RELAP5 [17], a one-dimensional transient two-fluid model for flow of a two-phase steam - water mixture that can contain noncondensable components in the steam phase and a soluble component in the water phase.

Two phase steam - water flow occurs also in steam ejectors and steam driven jet pumps. These devices are used in refrigerators, chemical industry, nuclear reactors and in marine and pumping applications. Modelling performance of these devices can be performed using available models for multiphase flows. Many one-dimensional two-phase models for steam ejectors and SDJP were published [5]-[7], [38]-[43] for predicting mixing and condensation of steam into water. However, these models are coupled with many empirical correlation constants in order to describe unknown processes involved in DCC and can only predict performance of these devices with limited accuracy.

In order to improve the prediction of models involving DCC, the process of condensation of steam into water should be better understood.

2.3 Direct Contact Condensation of Steam Injected into Water

The DCC of steam injected into water is a complicated process, because it appears in different regimes, depending on the environmental conditions, and it involves different regions of the process.

Independent of the condensation regime, the process of DCC of steam injected into water consists of four different regions: a steam plume, the interface between steam and water, the hot water layer and the surrounding water. Figure 2.2 shows a schematic picture of these regions.

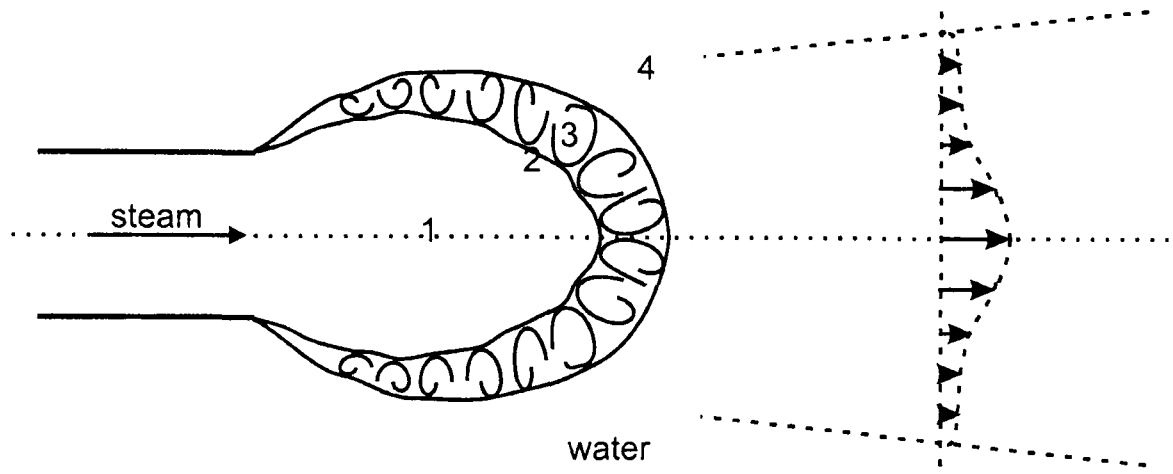

Figure 2.2: Schematic picture, showing the different regions of DCC of steam injected into water: steam plume (1), interface (2), hot water layer (3) and surrounding water (4).

The first region consists of pure steam and is called the steam plume. The plume's outer surface is the interface where condensation takes place. Surrounding the interface is a hot water layer which contains of steam bubbles and is characterized by an increase in water temperature. The hot water layer is surrounded by surrounding water. A two-phase jet is formed in the surrounding water down-stream of the plume. The exact behaviour and the precise appearance of each region will differ depending on the regime. Nevertheless, each region is always present when there is a condensation of steam into water.

Figure 2.3 shows photographs of DCC taken during two different experiments. That on the left shows DCC of steam injected into a water flow taken during the development of the ballast water treatment system. Close

Figure 2.3: Left: Photograph of DCC taken during the experiments for a ballast water treatment system. Right: Photograph of DCC from Youn *et al.* [12].

to the steam injector exit is clearly seen a white ellipsoidal steam plume. A well-developed two phase jet can be observed down-stream of the plume. The photograph on the right is by Youn *et al.* [12]. It shows a steam plume developed during the injection of steam into a pool of stagnant water. A bubbly and unstable hot water layer in the shape of ellipsoid can be seen at the pipe exit. Flow conditions in these experiments were quite different.

2.3.1 Regions of DCC

Steam Plume

The steam plume is the first region in the condensation process and occurs at the steam pipe exit. In most computational models the steam plume is approximated by a pure steam region with temperature and velocity gradients in both downstream and radial directions [8], [11]. The shape of the steam plume is predominantly dependent on the inflow conditions. These include steam inflow rate and water subcooling temperature. Steam inflow rate (G_0) is defined as a ratio between mass flux of steam and the steam injector exit area. The water subcooling is the temperature difference between steam and water ($\Delta T = T_s - T_w$). A range of steam plume shapes can be observed during experimental observations and include: hemispherical, conical, ellipsoidal and divergent shapes. Alternatively, a steam plume in the shape of a bubble can be observed and with very low rates of steam inflow the plume is reduced to a small film covering the injector exit [44]-[46].

Interface

The surface of the steam plume or interface, divides the steam from the hot water layer. It is the region where DCC occurs with convective heat and mass transfer through the interface. The size of the interface is related to the amount of condensed steam. The exact shape and position of the interface are difficult to define. As suggested by Liang & Griffith [10], this shape depends on the interfacial eddies and the local temperature in the hot water layer that surrounds the interface.

The size of the interface depends on the rate of condensation and it also affects this rate. If the interface is small, heat and mass transfer can only take place across a small area and condensation will take place comparatively slowly. If the steam plume is large, the interface is larger and the condensation will be accelerated. Fast condensation across the interface of a plume increases the instability leading to collapse of the bubble when the steam supply is insufficient to keep up with the rate of condensation.

Hot water layer

The hot water layer, or bulk water, is a two-phase layer in the vicinity of the interface with a temperature close to the value of saturation. The water layer at the interface is mixed with steam bubbles and there is a large amount of turbulent motion. Turbulence is formed by the momentum subtracted from the condensing steam and has a large effect on the shape of the interface and the condensation rate across the interface [10], [47], [48].

Surrounding Water

Stagnant or moving water surrounds the steam plume and hot water layer. As shown by Celata [47] the water velocity directly affects turbulence in the hot water layer and consequently the steam plume shape and the heat transfer coefficient. Steam, condensing in water, also generates a temperature distribution in the surrounding water. However, the temperature of the water is significantly increased only in close proximity of the interface. Further downstream of the plume the increase of the water temperature is marginal [49].

Dependent on the inflow conditions, the surrounding water can be simply water or a two-phase mixture of water and uncondensed steam bubbles.

Downstream of the condensation region a self-similar jet is developed in the water [50]. Experimental observations have shown that the surrounding water is directly affected by the formation and collapse of the steam plume, resulting in pressure oscillations in water [9], [12], [46], [51], [52].

2.3.2 Regimes of DCC

The dynamic behaviour and the geometrical appearance of the steam plume can be subdivided in three main regimes:

- Chugging regime
- Jetting regime
- Bubbling regime

Chugging Regime

The chugging regime is characterised by a flat or curved shape of steam plume located in the injector or its vicinity, and the steam plume size is close to the injector's cross-sectional area. Figure 2.4 shows a possible cycle of a chugging regime.

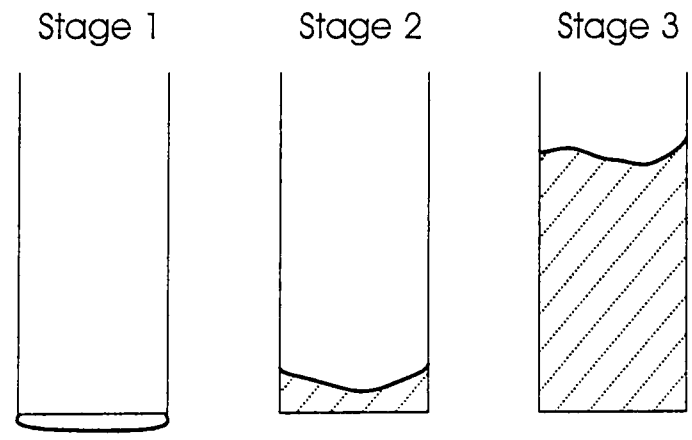

Figure 2.4: Chugging regime cycle from Chan & Lee [9]. The regime was observed with water subcooling of 66^0C. The shaded area represents water. Steam is injected vertically downwards.

The chugging regime occurs at steam inflow rates up to $80kg/\left(m^2s\right)$, depending on the surrounding water temperature and steam injector diameter. The location of the steam plume in the injector may vary continuously,

moving from the outer edge of the injector into the injector and backwards [9]. Chugging occurs because the steam inflow rate is smaller than the condensation rate which causes suction of surrounding water into the steam injector. If chugging occurs inside the injector in a pulsating manner, the process is called interfacial condensation oscillation. For this type of condensation the steam inflow rate is normally smaller than $5kg/\left(m^2s\right)$.

Jetting Regime

For steam inflow rates higher than about $100kg/\left(m^2s\right)$, steam forms a plume which holds approximately constant size and shape. This type of condensation is called the jetting regime. Jetting consists of three main plume shapes which include: conical, ellipsoidal and divergent shape (Figure 2.5).

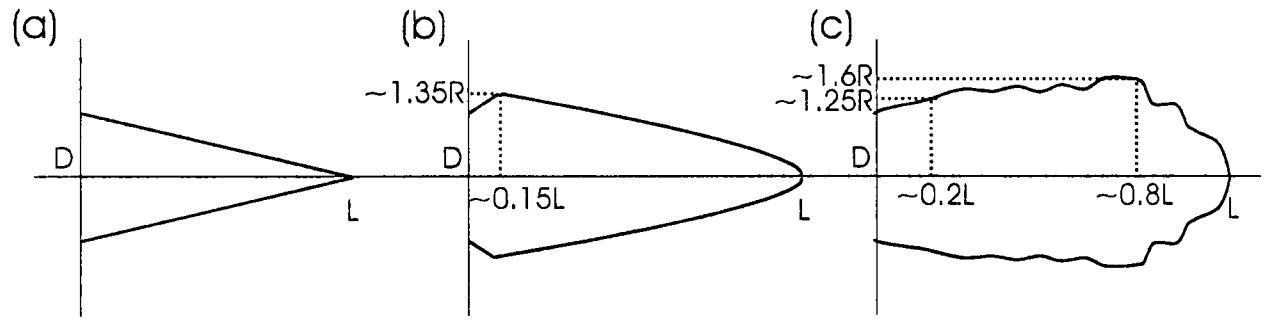

Figure 2.5: Jetting regime plume shapes observed by Chun *et al.* [45]. (a) Conical plume, $\Delta T = 76.7^0C$, $G_0 = 286kg/\left(m^2s\right)$, $D = 10.85mm$, $L = 20mm$, (b) Ellipsoidal plume, $\Delta T = 58.5^0C$, $G_0 = 312kg/\left(m^2s\right)$, $D = 7.65mm$, $L = 26mm$, (c) Divergent plume, $\Delta T = 27.1^0C$, $G_0 = 530kg/\left(m^2s\right)$, $D = 7.65mm$, $L = 34mm$. Steam injection is to the right.

For some inflow conditions close to the bubbling regime, the plume can also take a hemispherical shape. The length of the steam plume (L) in the jetting regime can vary from one millimetre to more than fifteen centimetres. If the condensation occurs in a conical or ellipsoidal jetting regime, the plume will take a regular shape with a smooth surface (Figure 2.5 (a), (b)). For water temperatures higher than 70^0C to 80^0C, the plume will take an irregular divergent shape (Figure 2.5 (c)). This regime is named divergent jetting. The length of a divergent plume is usually bigger than two centimetres.

Bubbling Regime

For steam inflow rates between chugging and jetting, bubbling occurs. Here, injected steam generates a regular or an irregular bubble at the edge of the injector. The generated bubble grows and when a maximum size of the bubble is reached, the whole or a part of the bubble is detached from the injector. The remaining part of the original bubble starts to grow until a maximum bubble size is reached [46]. In certain cases there is a collapse of the original bubble after detachment. Detached parts of the bubble are dragged away from the steam injector and continue to condense, generating a trace of smaller steam bubbles in the downstream flow [51]. Figure 2.6 shows a possible cycle of a bubbling regime of DCC.

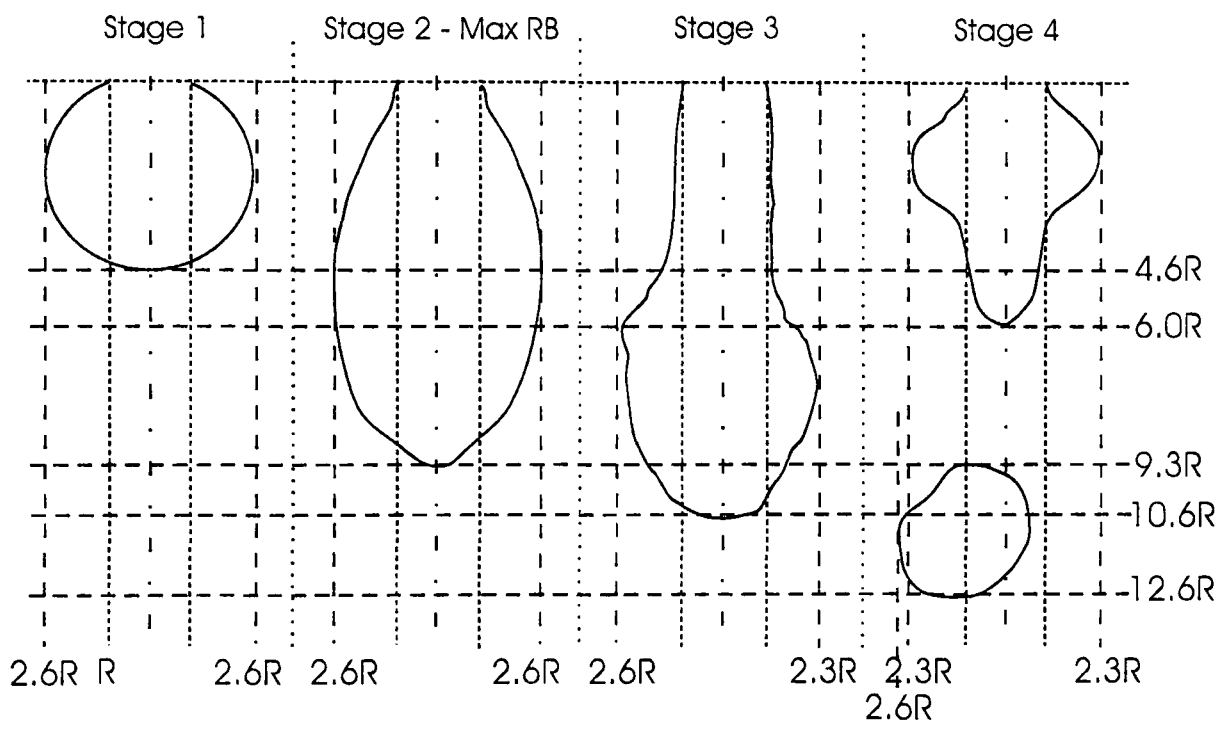

Figure 2.6: Bubbling regime cycle observed by Simpson & Chan [46]. $\Delta T = 37^0C$, $G_0 = 305.5kg/(m^2s)$, $D = 0.635cm$. Steam is injected vertically downwards.

2.3.3 Analytical Model for DCC

An appropriate analytical model describing DCC of steam injected into water must incorporate fundamental aspects of two-phase flow, flow dynamics and condensation. The one-dimensional governing equations used in this work are based on the general equations governing three-dimensional unsteady two-phase model derived by Drew and Passman [4], [53]. The new

model for DCC consists of balance equations and jump conditions for both phases and has incorporated important aspects of condensation.

The first equation of the model is the mass conservation or continuity equation

$$\frac{\partial}{\partial t}\left(\alpha_k \rho_k\right) + \frac{\partial}{\partial x}\left(\alpha_k \rho_k v_k\right) = \Gamma_k \,, \tag{2.4}$$

where the index k is replaced by the index s for the steam phase or w for the water phase for each separate equation. In Equation (2.4), α_k is the volume fraction of phase k, ρ_k is a phase density, v_k phase velocity and Γ_k is the volumetric mass transfer rate due to phase change of phase k. Additional to Equation (2.4) a mass jump condition exists

$$\Gamma_s + \Gamma_w = 0 \,, \tag{2.5}$$

where interfacial mass exchange is preserved and the system does not have any additional sources or sinks on the interface.

The second equation of the system is a momentum equation for condensation (Equation (2.6)).

$$\frac{\partial}{\partial t}\left(\alpha_k \rho_k v_k\right) + \frac{\partial}{\partial x}\left(\alpha_k \rho_k v_k^2\right) = -\frac{\partial}{\partial x}\left(\alpha_k p_k\right) - \alpha_k \rho_k F I_k \left(v_k - v_{k'}\right) -$$

$$-C \alpha_k \alpha_{k'} \rho_m \left(\frac{\partial}{\partial t}\left(v_k - v_{k'}\right) + v_{k'}\frac{\partial v_k}{\partial x} - v_k \frac{\partial v_{k'}}{\partial x}\right) + \Gamma_k \left(v_{in} - v_{k'}\right) \,. \tag{2.6}$$

The second element of the right part of the above equation adds the effect of interfacial drag, where the coefficient FI indicates the drag coefficient, and the last two elements describe the interfacial momentum transfer. Index k' indicates the opposite index that is indicated by index k, where subscript in indicates interface and m mixture. The coefficient C, indicating the virtual mass, is dependent on the flow regime. Momentum jump condition is

$$\Gamma_s \left(v_{in} - v_s\right) + \Gamma_w \left(v_{in} - v_w\right) - \alpha_s \rho_s F I_s \left(v_s - v_w\right) - \alpha_w \rho_w F I_w \left(v_w - v_s\right) = m \,, \tag{2.7}$$

where m indicates surface tension force.

The energy equation for DCC is

$$\frac{\partial}{\partial t}\left(\alpha_k \rho_k \left(e_k + \frac{v_k^2}{2}\right)\right) + \frac{\partial}{\partial x}\left(\alpha_k \rho_k v_k \left(e_k + \frac{v_k^2}{2}\right)\right) = -\frac{\partial}{\partial x}\left(\alpha_k p_k v_k\right) +$$

$$+ Q_k + W_k + \Gamma_k \left(e_{ki} + \frac{v_{ki}^2}{2}\right) \,, \tag{2.8}$$

where e_k indicates internal energy of phase k, and Q_k and W_k indicate interfacial heat and interfacial work exchange, respectively. Index ki indicates the relative phase-interface index. The energy jump condition is

$$Q_s + Q_w + W_s + W_w + \Gamma_s \left(e_{si} + \frac{v_{si}^2}{2} \right) + \Gamma_w \left(e_{wi} + \frac{v_{wi}^2}{2} \right) = \epsilon \,, \qquad (2.9)$$

where ϵ indicates interfacial energy source.

From the balance Equations (2.4), (2.6) and (2.8) with a use of jump conditions (2.5), (2.7) and (2.9), a system of six equations describing transient, one-dimensional condensation can be derived. The model was also published in Petrovic [54].

DCC of steam in water is a three-dimensional process. Although a one-dimensional mathematical model can be used to perform simulations, a three-dimensional model would provide a more realistic representation. The system of equations for a one-dimensional DCC (Equations (2.4)-(2.9)) can be extended to three dimensions. The continuity equation for DCC of steam in water in three-dimensions is

$$\frac{\partial}{\partial t} (\alpha_k \rho_k) + \nabla \cdot (\alpha_k \rho_k \vec{v}_k) = \Gamma_k \,, \qquad (2.10)$$

where the continuity jump condition is

$$\Gamma_s = \Gamma_w \,. \qquad (2.11)$$

The momentum equation and jump condition are

$$\frac{\partial}{\partial t} (\alpha_k \rho_k \vec{v}_k) + \nabla \cdot (\alpha_k \rho_k \vec{v}_k \vec{v}_k) = -\nabla (\alpha_k p_k) - \nabla \cdot (\alpha_k \underline{T}_k) +$$

$$+\Gamma_k (\vec{v}_{in} - \vec{v}_k) + M_k \qquad (2.12)$$

and

$$M_s + M_w + \vec{v}_{is}\Gamma_s + \vec{v}_{iw}\Gamma_w = m \,, \qquad (2.13)$$

where M indicates interfacial momentum transfer, $\underline{T}$ stress tensor. The energy equation for three-dimensional model describing DCC is

$$\frac{\partial}{\partial t} \left(\alpha_k \rho_k \left(e_k + \frac{\vec{v}_k \vec{v}_k}{2} \right) \right) + \nabla \cdot \left(\alpha_k \rho_k \vec{v}_k \left(e_k + \frac{\vec{v}_k \vec{v}_k}{2} \right) \right) = -\nabla (\alpha_k p_k \vec{v}_k) -$$

$$-\nabla \cdot (\alpha_k \underline{T} \cdot \vec{v}_k) + Q_k + W_k + \Gamma_k \left(e_{ki} + \frac{\vec{v}_{ki} \vec{v}_{ki}}{2} \right) \qquad (2.14)$$

and the energy jump condition is

$$Q_s + W_s + Q_w + W_w + \left(e_{si} + \frac{\vec{v}_{si}\vec{v}_{si}}{2}\right)\Gamma_s + \left(e_{wi} + \frac{\vec{v}_{wi}\vec{v}_{wi}}{2}\right)\Gamma_w = \epsilon\ . \quad (2.15)$$

To compute the unknowns of each of the systems: –pressure, steam and water density, steam and water velocity, and steam and water internal energy,– the system of equations have to be solved by approximation methods. Analytical or numerical approximation can be used, where the later is easier to apply. Crucial to the modeling of DCC of steam condensing in water is the approximation of the variables such as Q, W and Γ as well the geometry of the steam plume and the heat transfer coefficient. These quantities are computed simultaneously with the general equations describing processes involved. Geometry of the plume, the shape and the length of the plume, is important in order to specify the position, where equations of each of the phases have to be applied during the calculation. Hence, the condensation regime and the length of the plume have to be known prior to calculation. Furthermore, the computation of the quantity Γ is critical as it depends on the heat transfer process that takes place in the flow. To obtain an accurate approximation of Γ, the heat transfer coefficient must be calculated and this depends on the steam plume geometry and processes in the hot water layer.

2.3.4 Key Limitations of Existing Models

Researchers have recognised the lack of knowledge about DCC of steam in water and the process has been studied extensively in the last three decades. This involved study of the condensation behaviour, the geometry of the steam plume and calculation of the heat transfer coefficient.

The condensation behaviour has been studied through observations of the process. The most descriptive information about the steam plume behaviour is found in summary form in a regime map. This map is a graph describing the appearance of different regimes at specific conditions in terms of their geometric appearances and dynamic features. Various regime maps have been published in literature [9], [10], [12], [51], [52], [55] which show the occurrence of different regimes, depending on the steam inflow rate and the water subcooling. These two-dimensional maps obtained during ex-

periments performed at various environmental conditions, which are inflow conditions, injector geometry and the water flow conditions, show similar features of the process observed by different researchers. However, inflow conditions at which these features were observed differ from one map to another. This leads to the conclusion, that the condensation behaviour is case specific and the environmental conditions during the experiment affect the occurrence of the regime. Therefore, a single two-dimensional regime map should not serve as a basis of identifying the regimes.

Block [51] tried to solve the problem by proposing the three-dimensional regime map with the water subcooling, the steam inflow rate and the water inflow rate as axes of the map. However, this regime map is based on basic calorimetric analysis and does not identify different regimes in details. Even more, from the water subcooling and amounts of both phases involved in the process it only predicts the amounts of steam and water present after the process. Therefore, there is a distinct need for more generalised predictions of the condensation regime that is accurate across a wide range of flow conditions and injector sizes.

In the literature a number of empirical correlations for a dimensionless steam plume length is proposed [8], [14], [45], [56]. These correlations present a ratio between the steam plume length and the diameter of the injector (L/D) as a function of the water subcooling and the steam inflow rate. The error between predictions and experimental data is reported to be in the range of 10% to 35%. However, the error only relates to the sets of data obtained at limited inflow conditions.

Similarly, also correlations were obtained from limited sets of data. If environmental conditions are changed, the correlations predict the plume length poorly and are no more valid. Therefore, specific correlations should not be used as a general tool of predicting the steam plume length.

Due to the importance of the steam plume length in modelling of the process, separate correlations were used to predict the length during calculations. This resulted in a poor prediction of the flow behaviour. Therefore, there is a need for more generalised prediction of the steam plume length valid across a range of inflow conditions.

Similarly to correlations for the dimensionless steam plume length, cor-

relations for the heat transfer coefficient are proposed in literature [13], [14], [45]. Here, the heat transfer coefficient is presented as a function of the water subcooling and the steam inflow rate. Also these correlations are data specific and predict the heat transfer coefficient reasonably well only in a limited range of inflow conditions.

In addition, limited sets of data for the heat transfer coefficient are published [46], [57]. These were calculated using a mass conservation, inflow conditions and the geometry of a steam plume. However, the geometry of the plume used for calculation did not correspond entirely with the experimental observations, but the assumed averaged geometry was used. Therefore, also this data gives very limited accurate predictions of the heat transfer coefficient.

Similarly to regime predictions and the steam plume length predictions, there is also a need for more generalised heat transfer coefficient predictions. Furthermore, a different approach for obtaining new predictions should be identified.

2.4 Objectives

In order to achieve the aims set out in the Chapter 1.1, a series of detailed objectives need to be followed. These are:

- To review and analyse the literature associated with this research and collect available information about the process in order to identify existing data, models, correlations and their limitations.
- To collect and analyse all experimental data from the literature and experiments performed at the development of the ballast water treatment system.
- To identify physical parameters with which the process of DCC of steam injected into water can be described.
- To produce mass conservation model for a steam plume and propose models for various shapes of interface.
- To identify new ways of predicting the condensation regime and to

develop a new condensation regime diagram by investigating the behaviour of a steam plume at different flow conditions.

- To identify new ways of predicting the length of the plume and to develop a new steam plume length diagram and compare it with existing correlations from literature.

- To identify new ways of predicting the heat transfer coefficient and to develop a new heat transfer coefficient diagram and compare it with existing correlations from literature.

3 Research Methodology

This chapter will discuss the research methodology used to achieve the objectives and thus aims of the work. The approach during the various stages of the project will be highlighted to establish a logical procedure of this research.

3.1 Proposed Research Methodology

As discussed in Chapters 1 and 2, the principal target of this research is to investigate the behaviour of condensing steam during the injection of steam into water and to propose improved correlations and models of the process.

When steam is injected into water, condensation takes place. Depending on conditions, the process shows different types of behaviour, classified as regimes of condensation. Classification is based primarily on the appearance of the plume of the injected steam. The condensation behaviour is sensitive to steam inflow and water conditions.

Most of the research on DCC has been experimental; hence the range of flow conditions has been limited by the physical constraints on the test facilities. Consequently, the correlations for flow predictions derived from these experiments are only valid for a limited range of flow conditions. While researchers were reporting similar findings on different types of steam behaviour for different operating conditions, they failed to show the connection between their findings and the findings of other researchers. Therefore, the wider picture of direct contact condensation remained uncovered. One of the aims of this research is to develop new DCC models, capable of predicting flow characteristics across a wide range of flow conditions.

As a first step, the literature should be analysed to identify difficulties and processes involved in DCC of steam injected into water. Such a review will lead to identification of existing data and models built around this data. To avoid repetition in developing yet another model of limited applicability this research will focus on a detailed analysis of all existing data, which involves detailed study of published regime maps, steam plume length data, reported pressure pulses and photographic and illustrated material of steam behaviour when injected into water for different conditions.

Further experimental data, which has not been published in literature before, will be used during this study. The organisation OceanSaver As from Norway in cooperation with MetaFil and Det Norske Veritas, both from Norway, performed various experiments while developing a system for Ballast Water Treatment (BWT). Part of the experiments involved injecting steam into a water flow. During these experiments, various different steam injectors were used and the steam was injected at various flow rates. The steam plumes were recorded with a camera and steam plume lengths were measured. The data and photographic material was kindly provided for use in this thesis. Further in the thesis this data will be referred to as data obtained during the development of the "BWT system".

There are four main issues involved in the description of DCC of steam injected into water. These are: identification of the regime of condensation, length of the steam plume, heat transfer coefficient and modelling and a description of the shape of the plume. Although all connected, they can be studied separately and researchers investigating the DCC until now have focused on different issues of the process. Therefore, a literature review should be performed in a way that recognises this fact.

Information about regimes and two-dimensional regime maps available in the literature fail to show the connection between regimes for a wide range of conditions. This study should aim to find a new regime classification by identifying a possible third axis, proposing a further physical parameter involved in the process, and connecting available information about regimes into a three-dimensional condensation regime diagram. The new developed diagram will be validated. Using data, obtained during the development of the BWT system, regimes at DCC of steam injected into a water flow will be identified. The applicability of the new three-dimensional condensation regime diagram to DCC in a water flow will be discussed.

Correlations available in the literature for length of a steam plume, or penetration distance of steam in water, were derived using limited sets of data. The data was obtained during experiments performed using limited ranges of operating conditions. These correlations give different predictions for lengths, which are often more than 30% different from measured lengths. This study should collect all available data for a steam plume length in order

to identify improved correlation. Important physical parameters involved in the process should be identified, leading to a proposal of a new correlation for a steam plume length. This will form the basis for a new two-dimensional steam plume length diagram. The diagram will be capable of predicting length of the plume for a wide range of conditions and will be validated using correlations and data from literature. The length of a steam plume during injection into a water flow will be discussed using the data obtained during the BWT system.

In order to model the plume at different conditions, ways of presenting the interface will be investigated. For different operating conditions, steam plume appears in different shapes. Therefore, different shapes defining the interface will be proposed, including shapes with a smooth and wavy interface. These shapes will be used in the proposed mass conservation model for a steam plume.

The steam plume model can be used for the calculation of a heat transfer coefficient. Until now, researchers have used only two different shapes of plume in order to calculate the coefficient. By using different shapes at conditions specified by the new three-dimensional condensation regime diagram and predictions of a plume length from the new two-dimensional steam plume length diagram, more accurate values of heat transfer coefficient should be obtained and the new three-dimensional heat transfer coefficient diagram should be proposed.

The nature of the DCC process is such that it is strongly dependent on the operating conditions, where already a small change in one of the conditions may result in a completely different condensation behaviour. Furthermore, the process on the steam-water interface is not understood in full detail yet. Therefore, the representation of new findings in a form of diagrams, which are graphical representations of underlying matrices with constructed data, is likely to be more detailed as compared with possible analytical expressions from identified parameters.

Finally, conclusions and recommendations may then be drawn with respect to the initial aims and objectives.

3.2 Research Methodology Flow Chart

The following chart (Figure 3.1) represents diagrammatically the proposed methodology. It shows three main parts of the research, with the central part, representing the bulk of the study split into four main sections. These relate to the developed condensation regime diagram, steam plume length diagram and heat transfer coefficient diagram, and the proposed mass conservation model for a steam plume.

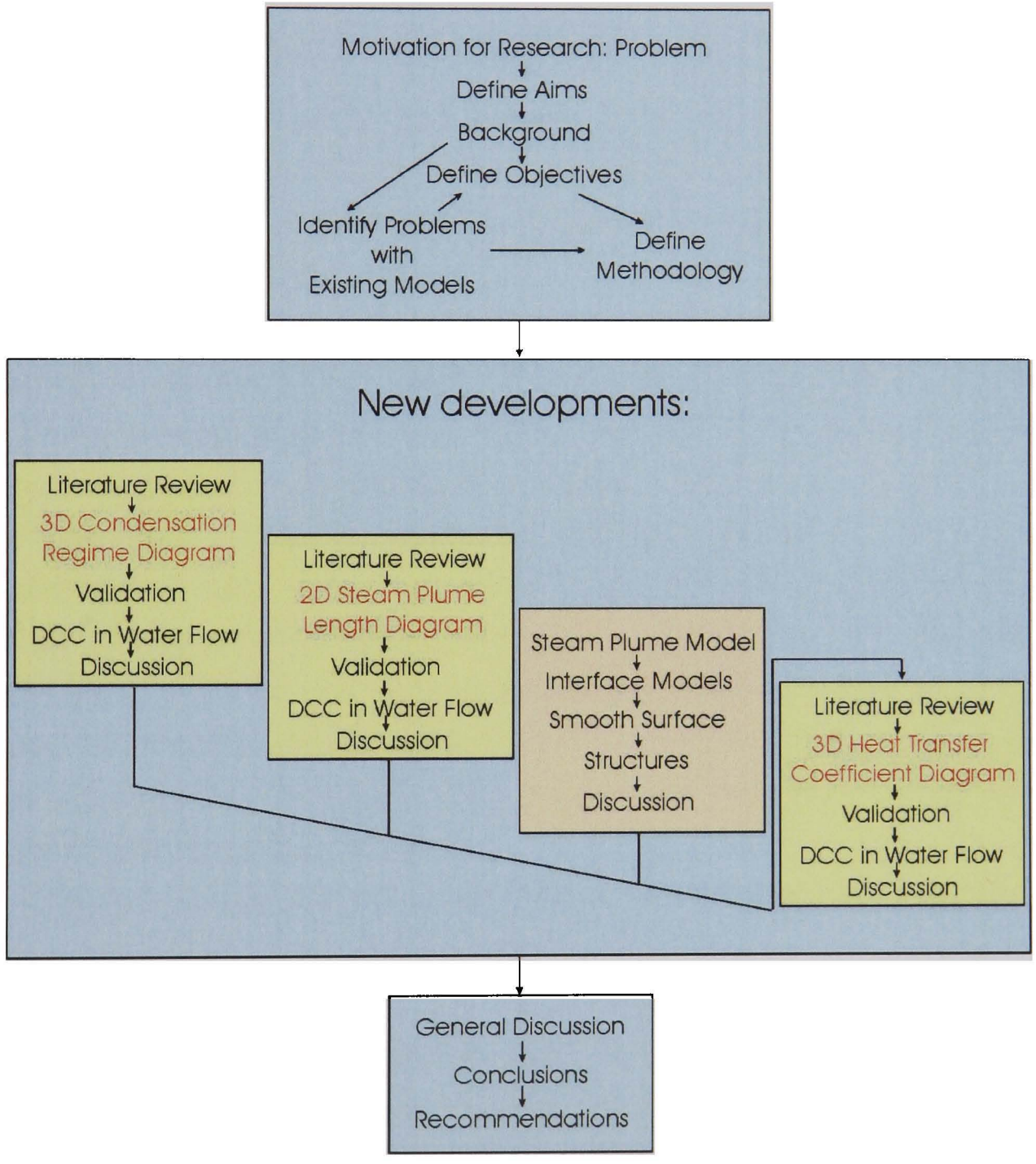

Figure 3.1: Flow chart of research methodology.

4 Identification of the Condensation Regime in DCC

Reliable and accurate prediction of the regime is essential for applications where DCC is the dominant flow feature. The regime maps from literature show only limited accuracy. Therefore, this chapter aims to provide a more general approach to prediction of the condensation regime.

4.1 Literature Review and Data Gathering

The data for the regime map was obtained from a large number of independent studies published during the last three decades [8]-[11], [13], [14], [45], [46], [51], [52], [55]. This also involves information about regimes obtained from regime maps from literature.

Regime maps were proposed by Liang & Griffith [10], for steam injected through an injector with a diameter $D = 0.02m$. Aya & Nariai [52] and [55] proposed a regime map for steam injected through injectors with diameters in the range of $D = 0.009m$ to $D = 0.038m$. Furthermore, Chan & Lee [9] constructed a map for a steam injector with diameter $D = 0.051m$. In addition, two other regime maps were presented by Block [51] and Chan & Lee [9]. Block [51] presented a regime map, which was originally taken from Chan & Lee [9], but used a different notation for the regimes. Block based his notation on the pressure variation in the water into which steam was injected. Also the regime map, presented by Youn *et al.* [12] is based on pressure variation in the water.

Figure 4.1 shows the regime map proposed by Liang and Griffith [10]. These researchers focussed their work on the problem of chugging and performed experiments at steam inflow rates up to $60kg/(m^2s)$. They identified five different regimes: chugging, low frequency bubbling with detached bubbles, high frequency bubbling with attached bubbles, oscillatory steam jet with detached bubbles and stable steam jet.

Figure 4.2 shows a regime map proposed by Aya and Nariai [52], [55]. They performed experiments for a range of different steam injectors and proposed one regime map. As Liang and Griffith, Aya and Nariai focussed their research on the chugging regime; however, they performed experiments

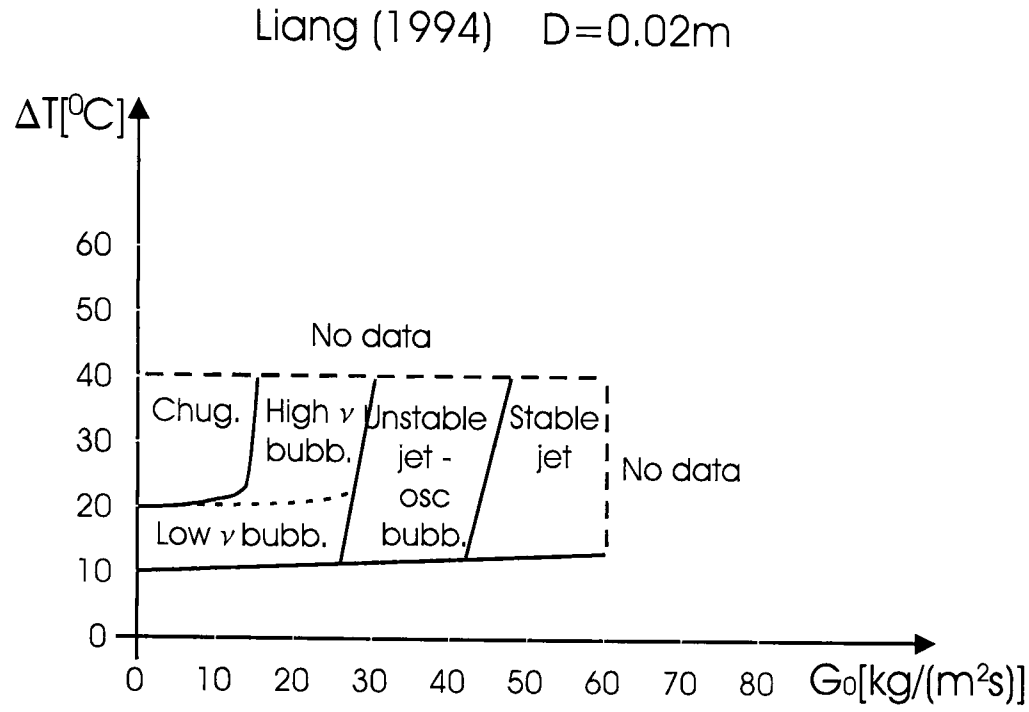

Figure 4.1: Regime map presented by Liang and Griffith [10].

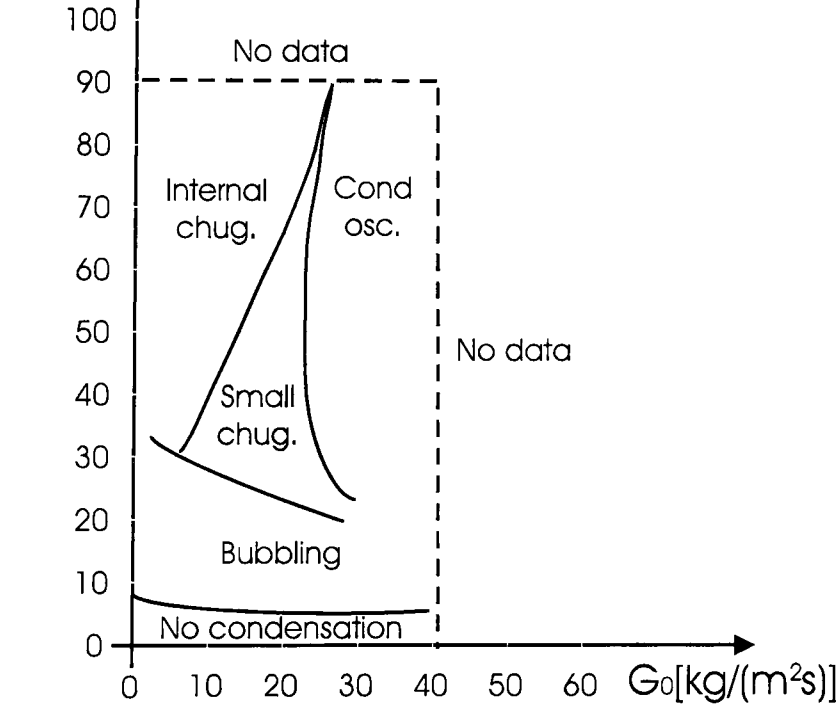

Figure 4.2: Regime map presented by Aya and Nariai [52], [55].

for a larger range of temperature of water subcooling.

Figure 4.3 shows the regime map proposed by Chan and Lee [9]. They identified seven different regimes: conical and ellipsoidal jetting, ellipsoidal and oscillatory or spherical bubbling, external and internal chugging, and

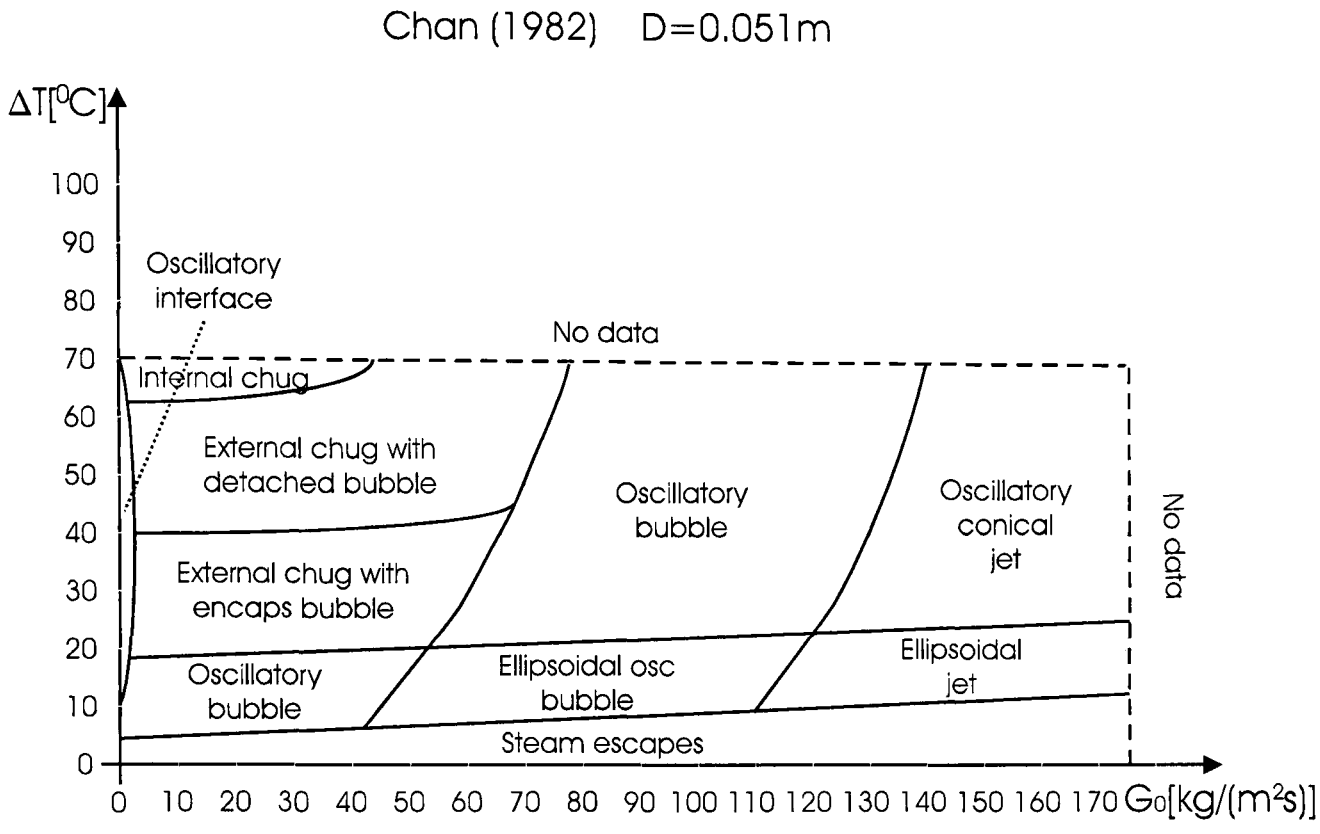

Figure 4.3: Regime map presented by Chan and Lee [9].

oscillatory interface.

The regime map proposed by Block [51] is presented in Figure 4.4.

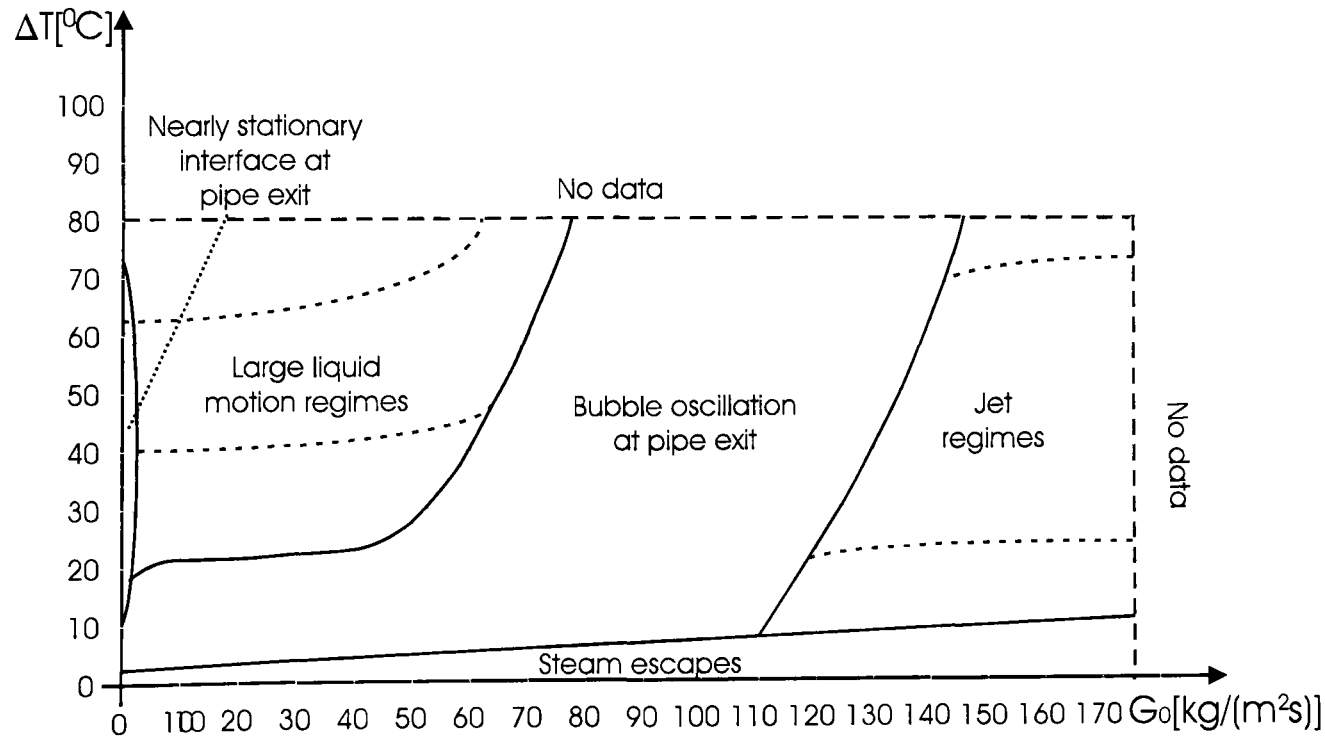

Figure 4.4: Regime map presented by Block [51].

It is based on measurements of pressure variations in water. He reproduced the map presented by Chan and Lee [9] (Figure 4.3), but grouped jetting, bubbling and chugging regimes together. He identified the chugging regime as a regime with large fluid motions.

The regime map proposed by Youn *et al.* [12] (Figure 4.5) is also based on pressure differences. Their map covers the largest range of steam inflow rates of all workers. However, no information can be found about the steam injector with which their experiments were performed.

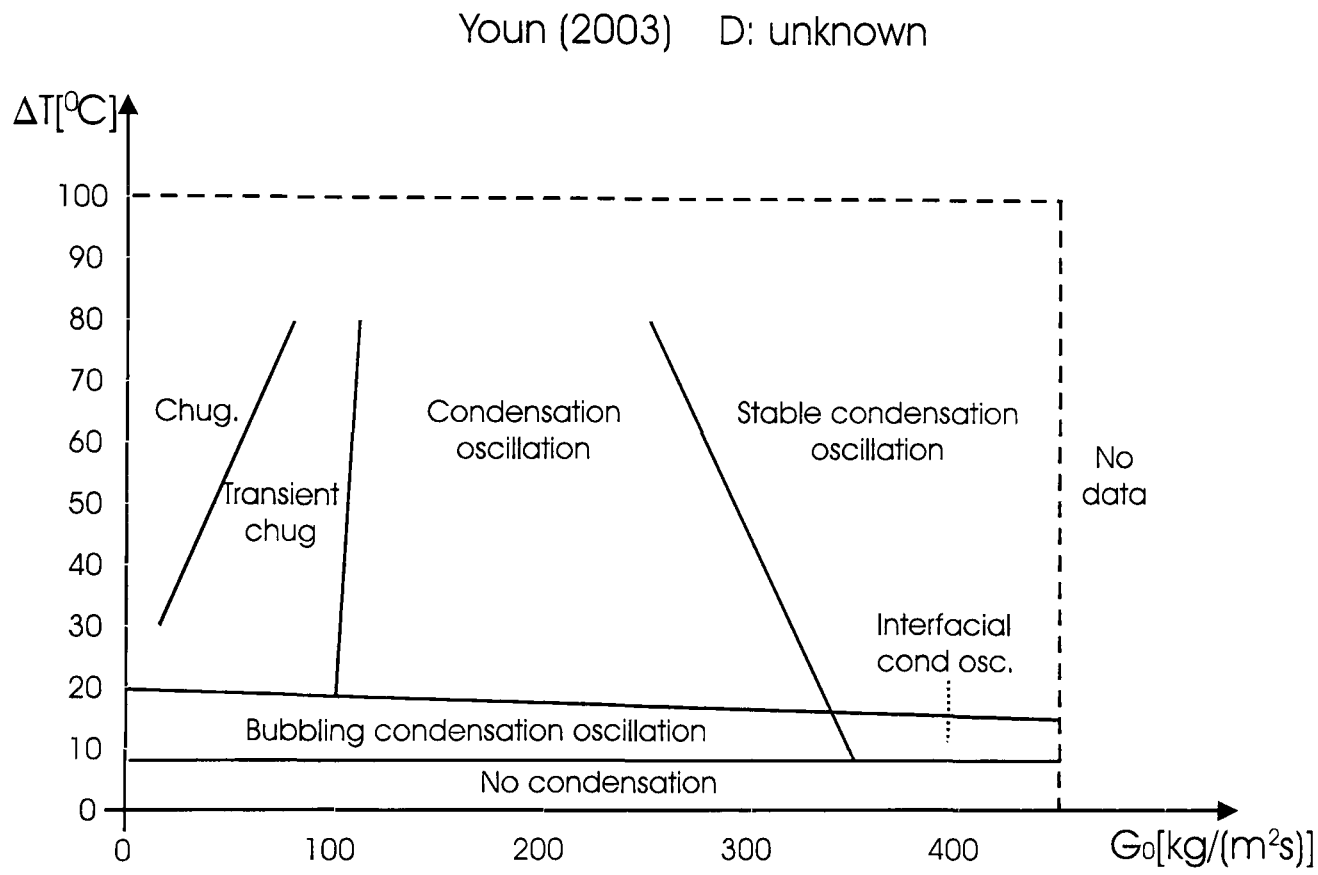

Figure 4.5: Regime map presented by Youn *et al.* [12].

All presented regime maps cover a relatively small range of steam inflow rates. At small steam inflow rates, chugging and bubbling regimes occur and all published maps show these two regimes and only the first part of a jetting regime. In addition to regime maps themselves, information about regimes detected during experiments for different flow conditions can also be found. Papers presenting observations at high steam inflow rates can contain more information about jetting regimes and the papers from Kim *et al.* [13], Kim *et al.* [14], Chen & Faeth [44] and Chun *et al.* [45] are relevant. Furthermore, some transition criteria between regimes were proposed by Liang and Griffith [10], but these were based on different models and fitting

techniques, proposed by researchers and are valid only for limited inflow conditions. Hence, the transition criteria should not be used as information about flow conditions for different regimes.

4.2 Development of a 3D Condensation Regime Diagram

A comparison of the two-dimensional regime maps (Figures 4.1-4.5) shows that all maps contain similar features. However, steam and water conditions, at which the regime pattern is observed, can vary significantly. Distinct variations are seen when comparing the regime maps based on different injector diameters. Figure 4.6 provides a detailed plot of three regime maps obtained with different injector sizes. In blue is the map from Chan & Lee [9] (Figure 4.3), in red is the map proposed by Liang & Griffith [10] (Figure 4.1) and in green is the map by Aya & Nariai [52], [55] (Figure 4.2). Each regime map lies on a separate plane of a coordinate system parallel to $x-z$ plane, placed at appropriate D. The map by Aya & Nariai is extended through the diagram with respect to D because authors reported the range in which their map should be valid.

Of the maps given in Figures 4.1 to 4.5, only three were incorporated into the three-dimensional diagram. The map from Block [51] (Figure 4.4) is the reproduction of the map by Chan & Lee [9] (Figure 4.3) and the position of the map by Youn *et al.* [12] (Figure 4.5) in the diagram is unclear. Therefore, these two maps were not added to the diagram. However, incorporated maps still provide information about relations between DCC regimes.

Figure 4.6 clearly indicates a lack of proportionality and the regime pattern is not scalable from one injector size to another if there is a substantial change in injector size. For example, while the regime map provides a distinct chugging regime with large injector diameters, chugging is marginal with a comparatively small injector diameter. This observation is very significant and implies that the regime map cannot be normalised with respect to the injector size; hence, a single two dimensional regime map is unsuitable for a wide range of injector sizes. A further aspect of consideration is the injector shape. However, studies on the injector shape

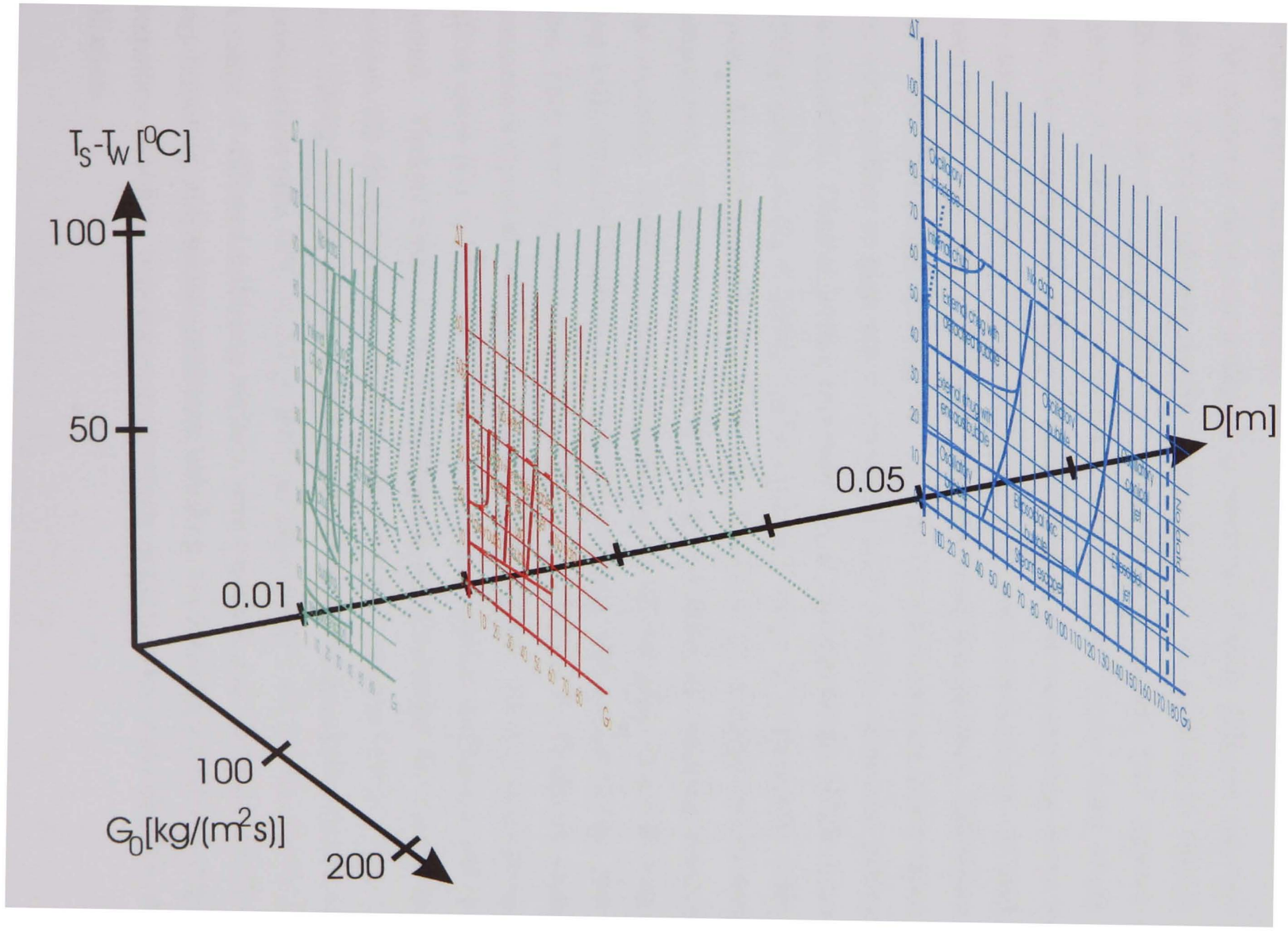

Figure 4.6: 3D diagram of regime maps. Each colour represents a regime map from different researchers. In blue is the map from Chan and Lee [9] (Figure 4.3), in red is the map proposed by Liang and Griffith [10] (Figure 4.1) and in green is the map by Aya and Nariai [52] and [55] (Figure 4.2).

reported in [8] and [49] are inconclusive. Furthermore, the majority of studies on DCC are performed using a cylindrically shaped injector.

For this reason a three-dimensional regime diagram is needed and has therefore been developed in this work. The traditional dependencies of steam mass inflow rate (G_0) and water subcooling ($\Delta T = T_s - T_w$) are used. Based on the above analysis the injector diameter (D) is selected as a third dependency. Other selections of dependency have been studied but provided very poor correlation.

All gathered data was analysed in order to identify different reported regimes. Fifteen different regimes were identified, all reported at slightly different flow conditions. For low temperature subcooling (ΔT approximately 10^0C or less) no condensation was detected. Under these conditions, the temperature difference between steam and surrounding water is too small for the steam to condense before it escapes from the water. At high steam inflow rates ($G_0 > 300kg/\left(m^2s\right)$) and small temperature differences ($\Delta T < 35^0C$) divergent jetting was reported. At similar steam inflow rates, but with medium to high water subcooling ($\Delta T > 35^0C$) ellipsoidal jetting was reported. Conical jetting was reported at medium steam inflow rates ($120kg/\left(m^2s\right) < G_0 < 300kg/\left(m^2s\right)$) across a range of temperature differences. At small steam inflow rates ($2kg/\left(m^2s\right) < G_0 < 60kg/\left(m^2s\right)$) and temperature differences above 20^0C a series of different chugging regimes was reported. These are internal chugging, small chugging, external chugging with detached bubbles and external chugging with encapsulating bubbles. They were reported at slightly different conditions. Furthermore, some researchers reported only some of the chugging regimes. At very small steam inflow rates ($G_0 < 2kg/\left(m^2s\right)$) interfacial condensation oscillation was reported. Various forms of bubbling regimes were reported for conditions between the chugging regime and the conical jetting regime ($60kg/\left(m^2s\right) < G_0 < 120kg/\left(m^2s\right)$), and for conditions between the chugging regime and no condensation area ($5^0C < \Delta T < 20^0C$ at $1kg/\left(m^2s\right) < G_0 < 60kg/\left(m^2s\right)$). A range of different bubbling regimes were reported and included: oscillatory bubbling, ellipsoidal oscillatory bubbling, low frequency bubbling, high frequency bubbling, bubbling condensation oscillation and condensation oscillation.

For a clearer description of condensation, the data was rationalised. All different chugging regimes were grouped together in one regime and similarly also all bubbling regimes were grouped into one regime. The jetting regimes cover a large range of flow conditions and give important information about the steam plume shape; hence, the jetting regime was subdivided into three jetting regimes. Rationalisation of the regime data resulted in a total of seven different regimes. These include: no condensation area, internal condensation oscillation, chugging regime, bubbling regime, conical jetting, ellipsoidal jetting and divergent jetting. They are presented in the Table 4.1.

Regime	$G_0 \left[\frac{kg}{m^2 s}\right]$	$\Delta T\,[^0C]$
no condensation		≤ 10
interfacial condensation oscillation	< 2	
chugging	$\in (2, 60)$	> 20
bubbling	$\in (60, 120)$ $\in (1, 60)$	$\in (10, 90)$ $\in (5, 20)$
conical jetting	$\in (120, 300)$	$\in (20, 90)$
ellipsoidal jetting	> 300	> 35
divergent jetting	> 30	< 35

Table 4.1: Seven main different regimes reported in the literature. Depending on the diameter of the steam injector, conditions at which regimes are reported vary and are in the ranges presented in this table.

Figure 4.7 shows data for outer boundaries of different regimes, obtained from the data used. Dots in the graph indicate the data with different colours indicating the border of different regimes.

The distribution of different coloured dots on Figure 4.7 gives an indication of conditions where different DCC regimes can be detected. For more detailed information about different regimes, three-dimensional condensation regime diagram must be generated using data indicating borders between regimes.

The three-dimensional condensation regime diagram was created from the three-dimensional surfaces representing the outer borders of the con-

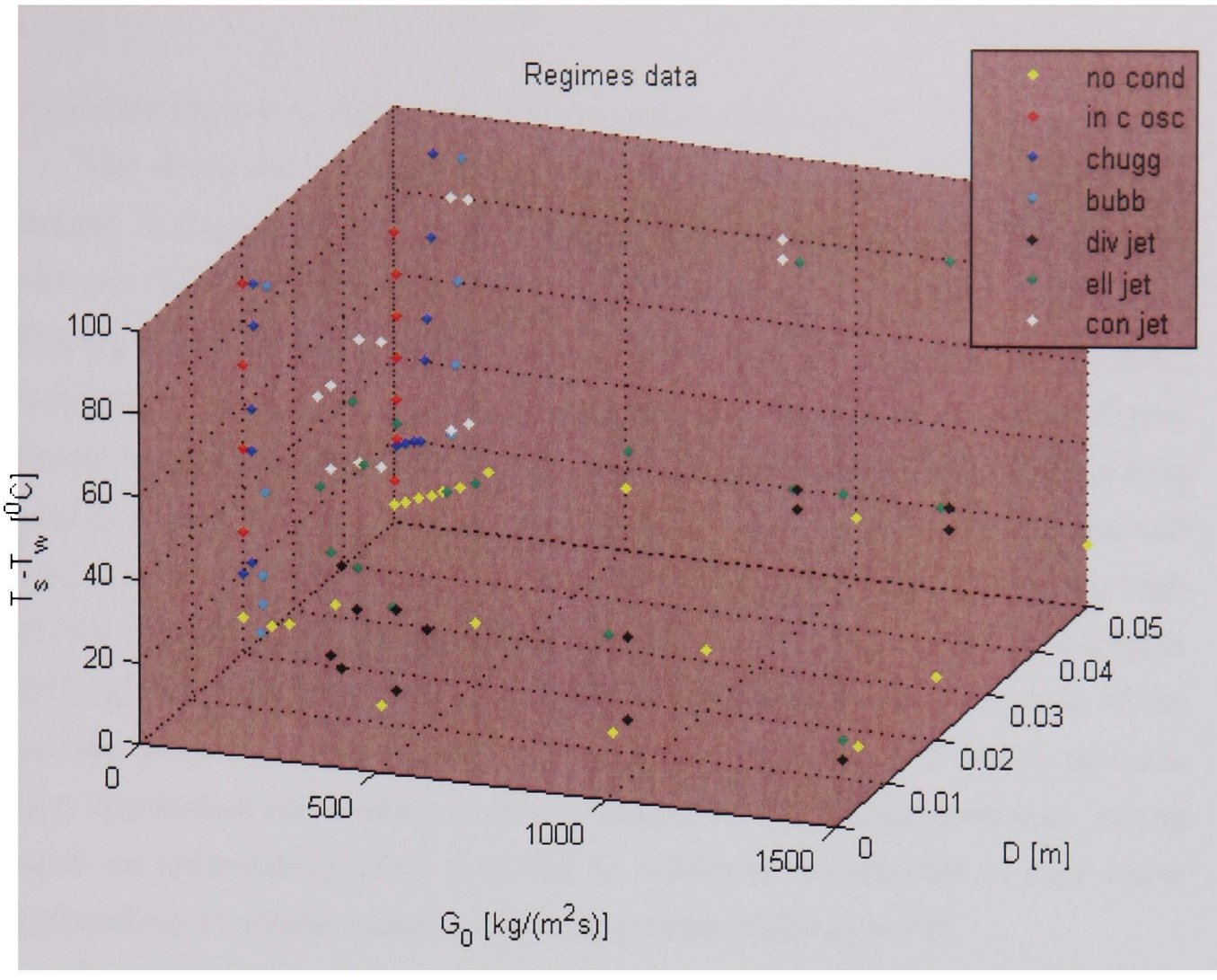

Figure 4.7: Data for outer boundaries of different regimes obtained from the literature. Each colour represents different regime: no condensation regime (no cond), interfacial condensation oscillation (in c osc), chugging regime (chugg), bubbling regime (bubb), divergent jetting (div jet), ellipsoidal jetting (ell jet) and conical jetting (con jet).

densation regime. These surfaces were generated to run through data indicating borders of different regimes. All surfaces were placed in a single graph to form a new Three-Dimensional Condensation Regime diagram for DCC of steam injected into stagnant water. Further in the thesis this diagram will be referred to as the "new 3DCR diagram". The diagram presents areas of different regimes for different steam inflow rates in the range from $0kg/\left(m^2s\right)$ to $1500kg/\left(m^2s\right)$, for steam injector diameter sizes between $0.00135m$ to $0.5m$ and for water subcooling ranging from 0^0C to 90^0C. For water subcooling between 90 and 100^0C data was not available. To ensure sufficient accuracy, the diagram is constructed such that areas with insufficient data remain white. The information from the diagram can be stored in the form of a table providing the information about the

expected regime at different environmental conditions.

The developed three-dimensional condensation regime diagram is presented in Figures 4.8 to 4.11. These Figures show four different views of the new 3DCR diagram. Figures 4.8 and 4.9 show two different side views. Figure 4.8 is from a side with small steam injector diameters and Figure 4.9 from a side with large steam injector diameters. The diagram clearly shows areas of different jetting regimes: conical jetting, ellipsoidal jetting and divergent jetting. Jetting regimes cover most of the 3DCR diagram and they appear at steam inflow rates around $200kg/\left(m^2s\right)$ and extend to high steam inflow rates. In the jetting area it can be seen that the divergent jetting appears above the no-condensation area and covers a section of the jetting area that ranges from approximately 10^0C to 25^0C water subcooling, depending on a steam injector diameter. Above the divergent jetting area, an ellipsoidal jetting area can be observed. It expands to high water subcooling at steam inflow rates higher than $1000kg/\left(m^2s\right)$.

At lower steam inflow rates, this area is diagonally cut with an area of conical jetting, which occurs at a water subcooling around 25^0C at $200kg/\left(m^2s\right)$ and expands to 90^0C at $200kg/\left(m^2s\right)$. For steam inflow rates smaller than $200kg/\left(m^2s\right)$ bubbling, chugging and interfacial condensation oscillation occur. Figures 4.10 and 4.11 show two different side views on section of the 3DCR diagram at steam inflow rates $0kg/\left(m^2s\right)$ up to $200kg/\left(m^2s\right)$. The diagram shows that for very small steam inflow rates up to $2kg/\left(m^2s\right)$ interfacial condensation oscillation ranges from 15^0C to 60^0C of water subcooling. The chugging regime starts when the water subcooling is 20^0C and extends to 90^0C and covers an area of the 3DCR diagram up to a steam inflow rate of $50kg/\left(m^2s\right)$. With lower water subcooling a bubbling regime is observed. For steam inflow rates between $50kg/\left(m^2s\right)$ and $120kg/\left(m^2s\right)$ a bubbling regime occurs with water subcooling up to 90^0C.

The new 3DCR diagram developed during this work and presented in Figures 4.8-4.11 clearly indicates where different regimes of condensation are expected for a range of steam inflow rates, temperatures of water subcooling and diameters of steam injector.

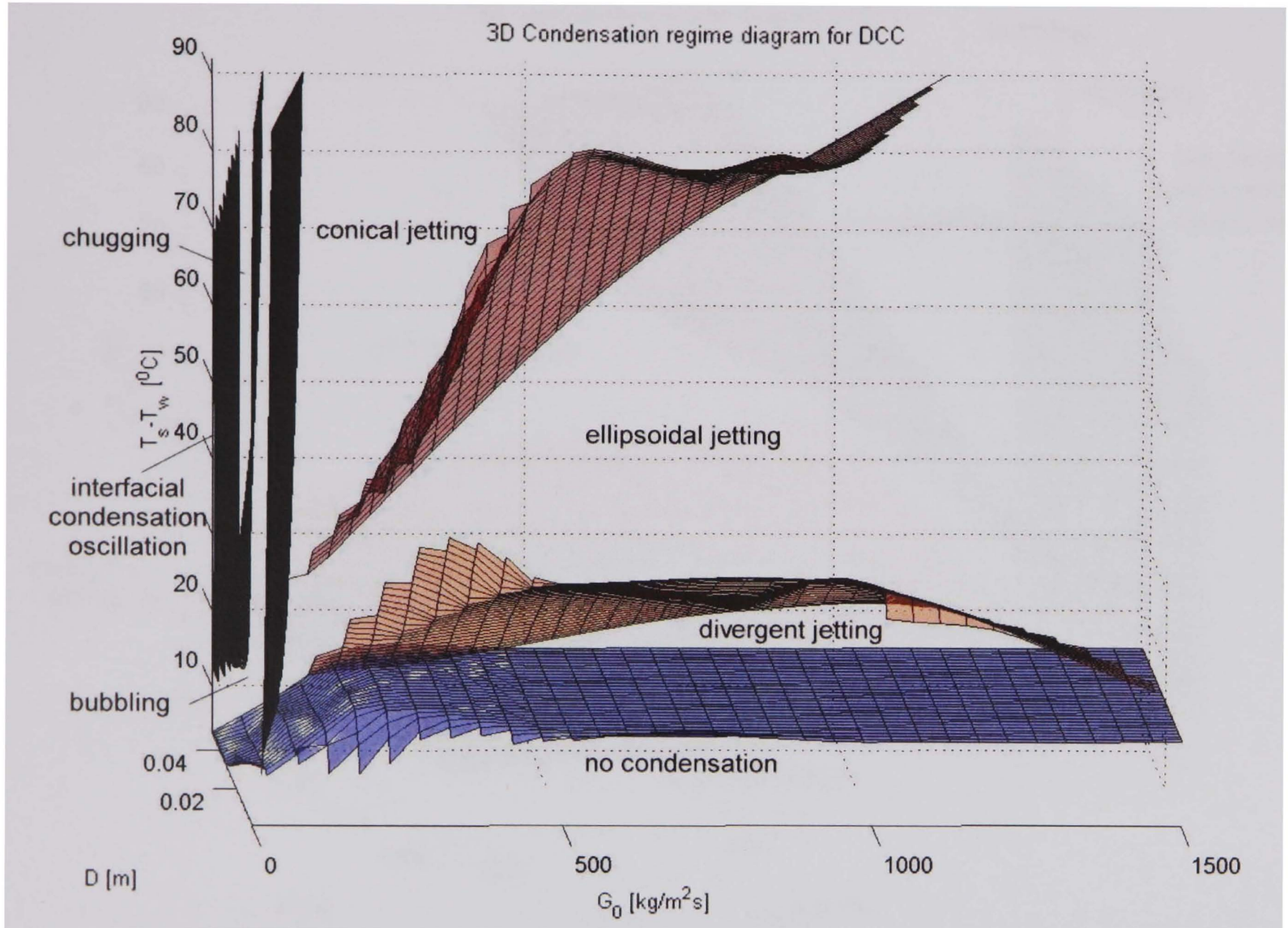

Figure 4.8: New 3DCR diagram viewed from a side with small steam injector diameters. Three different jetting regimes are clearly seen on the diagram. At small steam inflow rates, bubbling, chugging and interfacial condensation oscillation can be identified.

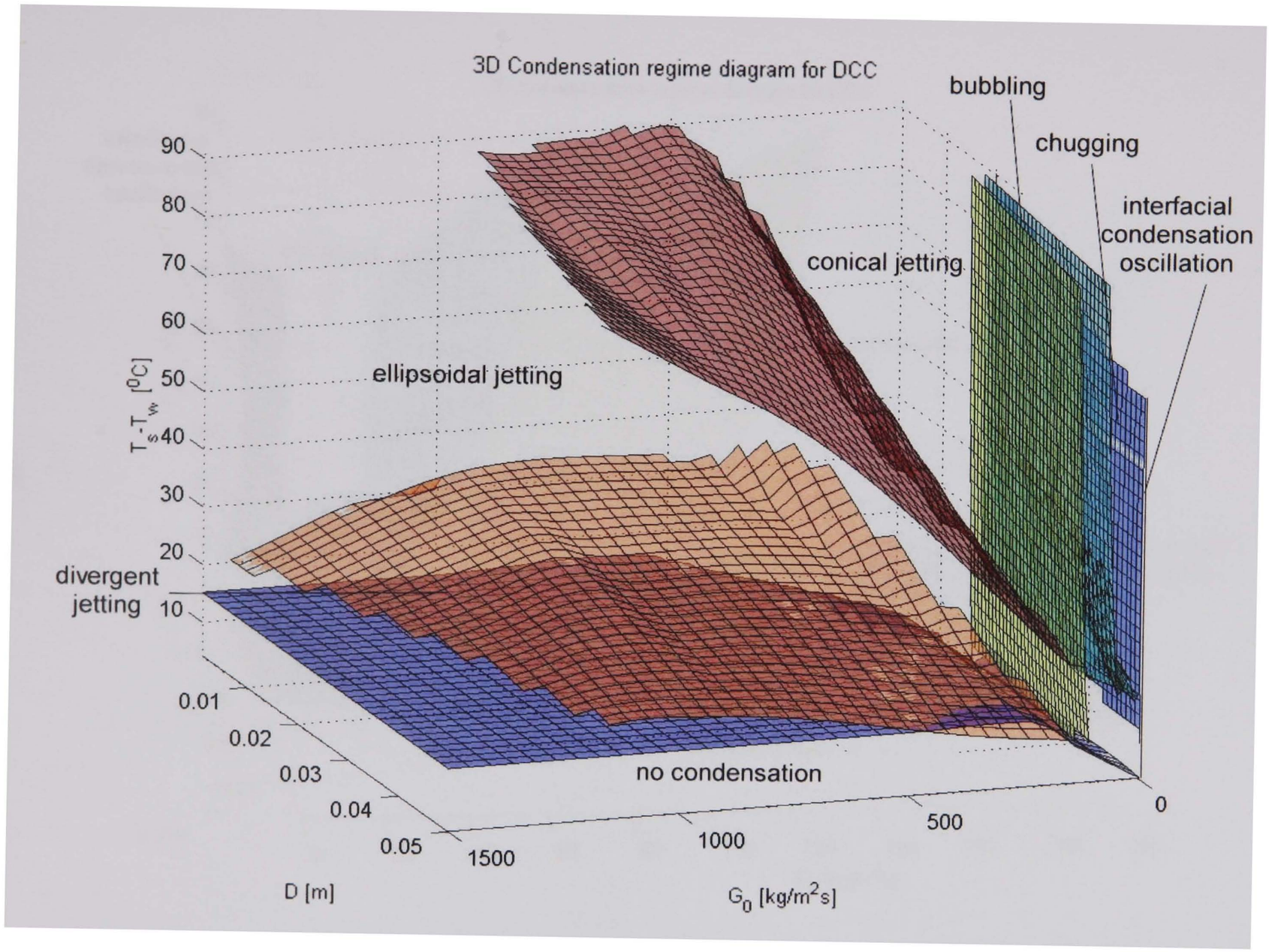

Figure 4.9: New 3DCR diagram viewed from a side with large steam injector diameters (opposite to view on Figure 4.8).

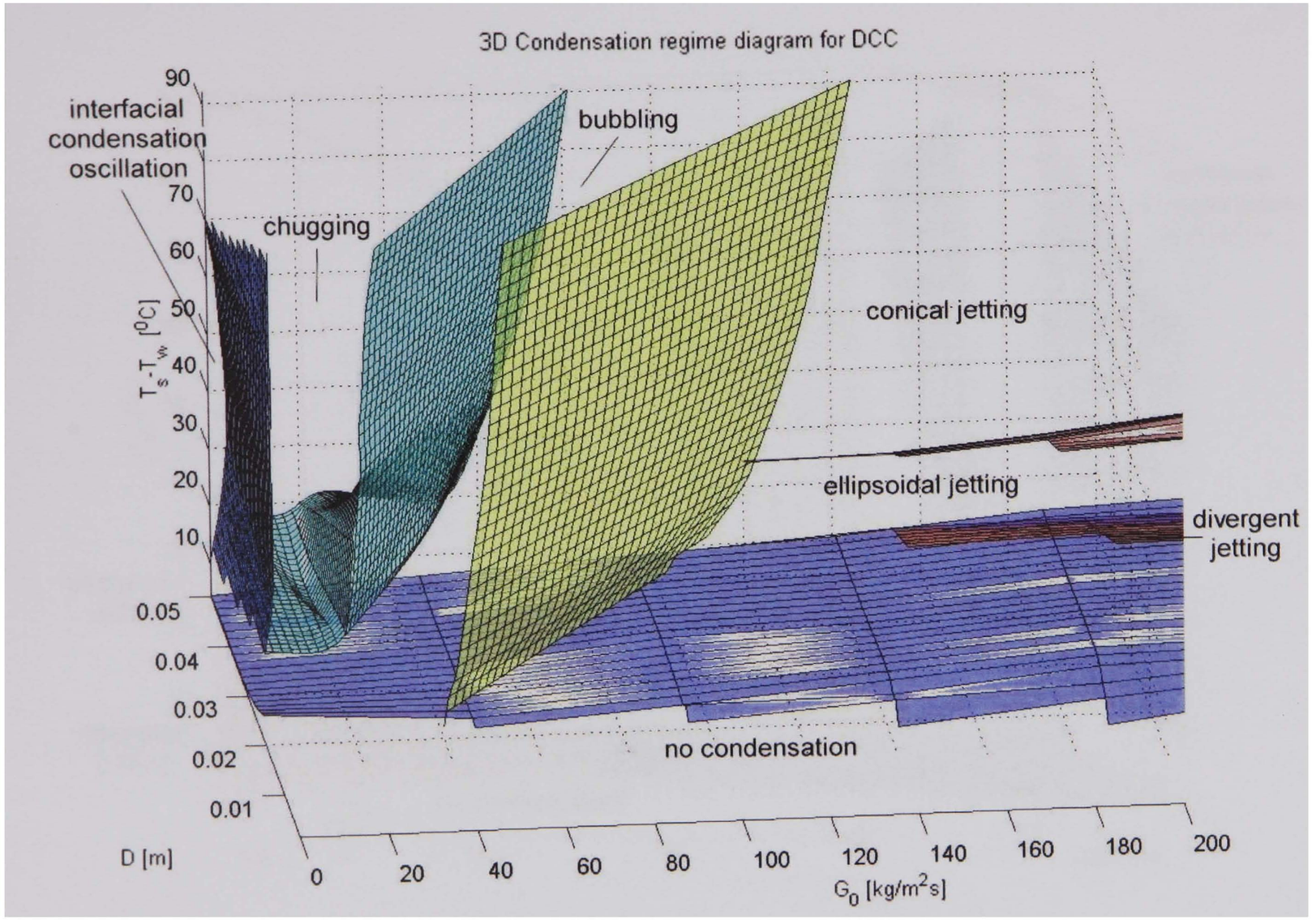

Figure 4.10: Side view of a section of the new 3DCR diagram at low steam inflow rates viewed from a side with small steam injector diameters. Chugging and bubbling regimes are clearly seen.

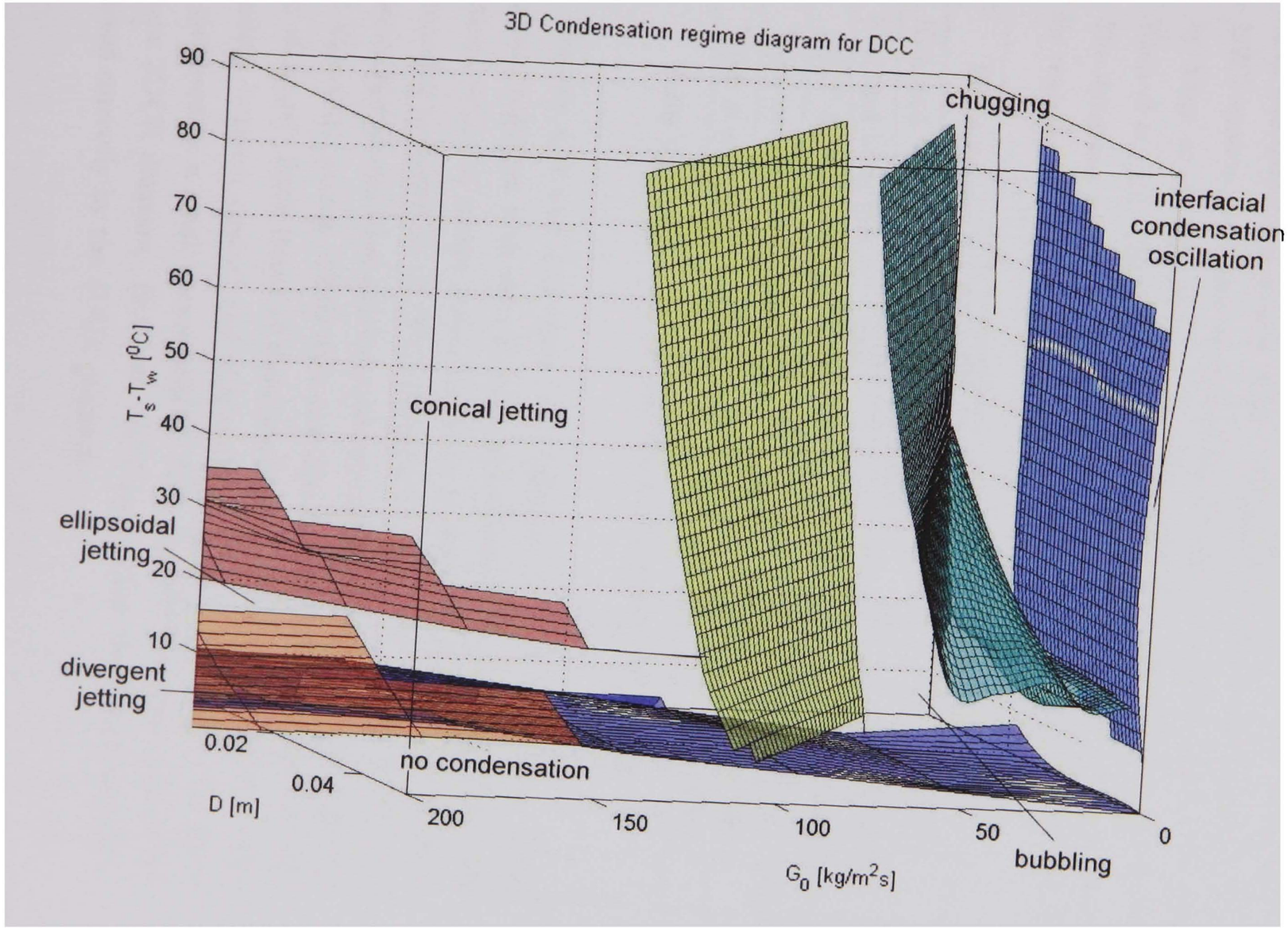

Figure 4.11: Side view of a section of the new 3DCR diagram at low steam inflow rates. View from a side with large steam injector diameters.

4.3 Validation of a 3D Condensation Regime Diagram

The new 3DCR diagram that has been developed might be validated using data about regimes which was not used during its creation. However, lack of available data resulted in majority of the data being used for development. Therefore, only a limited set of data was used for validation.

The 3DCR diagram was validated with data presented in Table 4.2. This includes two different data for a jetting regime, reported by Kim and Song [58], one data for a jetting regime, obtained during the development of the BWT system, one data reporting the transition between regimes, reported by Youn *et al.* [12], and one data for a bubbling regime, also reported by Youn *et al.* [12]. This data was not used during development of the diagram. The data was added to the 3DCR diagram and compared with predictions for regimes from the diagram (Figures 4.12 to 4.15).

Data from	$G_0 \left[\frac{kg}{m^2 s}\right]$	$D\,[m]$	$\Delta T\,[^0C]$	Regime
Kim and Song [58]	337	0.00765	78	conical jetting
Kim and Song [58]	468	0.00765	74	ellipsoidal jetting
BWT Experim.	1105	0.004	85	ellipsoidal jetting
Youn *et al.* [12]	60 to 80	0.02	> 30	transition
Youn *et al.* [12]	< 60	0.02	20	bubbling

Table 4.2: Data used for validation of the new 3DCR diagram.

Figures 4.12 and 4.13 show two different sections of the new 3DCR diagram together with data for validation from Kim and Song [58]. The sections relate to steam inflow rates up to $800 kg/\left(m^2 s\right)$ and for a water subcooling temperature of $78^0 C$ (Figure 4.12) and $74^0 C$ (Figure 4.13). For these temperatures Kim and Song [58] reported two regimes, conical jetting and ellipsoidal jetting. Their data is added to the graphs and given in the form of stars. Both items of data used for a validation are close to the boundary between conical and ellipsoidal jetting. Furthermore, the data was gathered at a small steam injector diameter which is just covered by the new 3DCR diagram. However, the Figures show that both stars are predicted correctly by the 3DCR diagram.

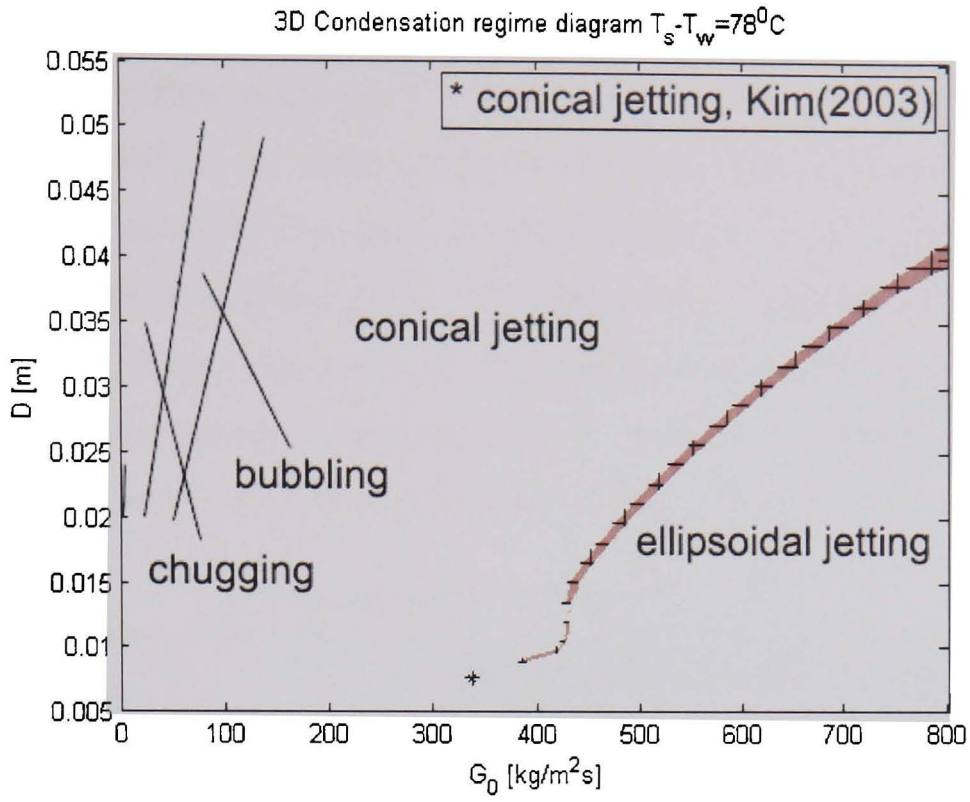

Figure 4.12: Comparison between the new 3DCR diagram and data for validation from Kim and Song [58]. Star relates to data for a conical jetting regime $G_0 = 337kg/\left(m^2s\right)$, $D = 0.00765m$, $\Delta T = 78^0C$.

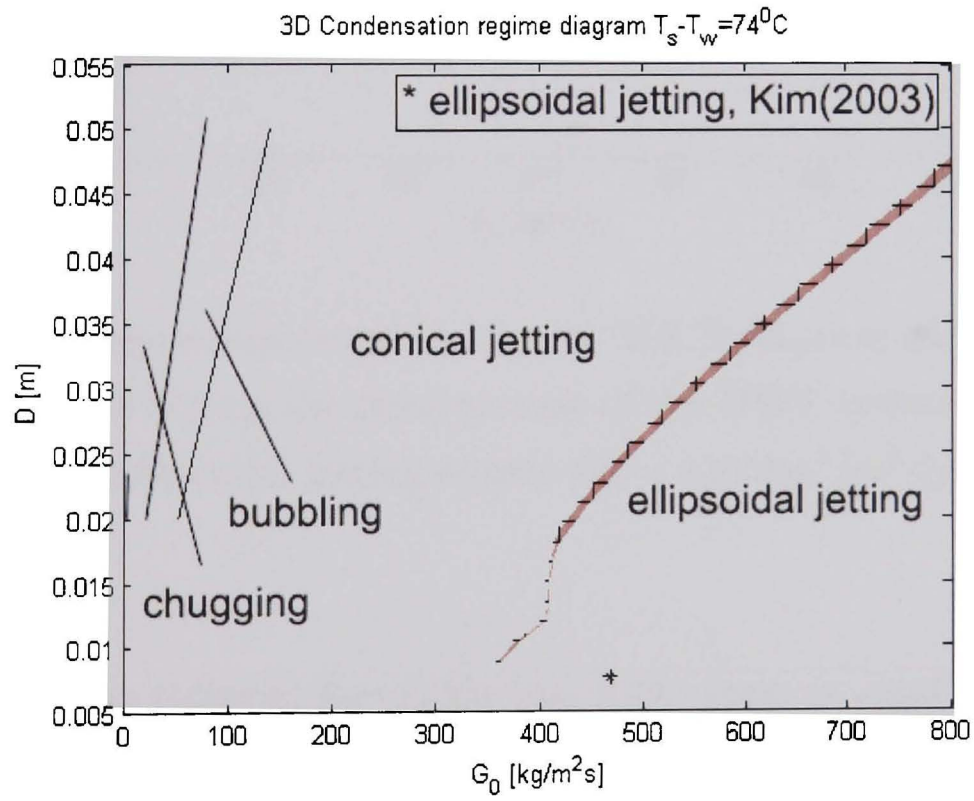

Figure 4.13: Comparison between the new 3DCR diagram and data for validation from Kim and Song [58]. Star relates to data for an ellipsoidal jetting regime $G_0 = 468kg/\left(m^2s\right)$, $D = 0.00765m$, $\Delta T = 74^0C$.

The graph in Figure 4.14 shows a cross section of the new 3DCR diagram for steam inflow rates up to $1200kg/\left(m^2s\right)$ and for a water subcooling temperature of 85^0C. An ellipsoidal jet observed during experiments for the development of the BWT system is represented by a star that is predicted accurately by the 3DCR diagram. The graph also suggests that with an extension of the conical-ellipsoidal jetting regimes boundary predicted by the 3DCR diagram to smaller injector sizes D, data will fall into the ellipsoidal jetting regime, which was also observed in the experiment.

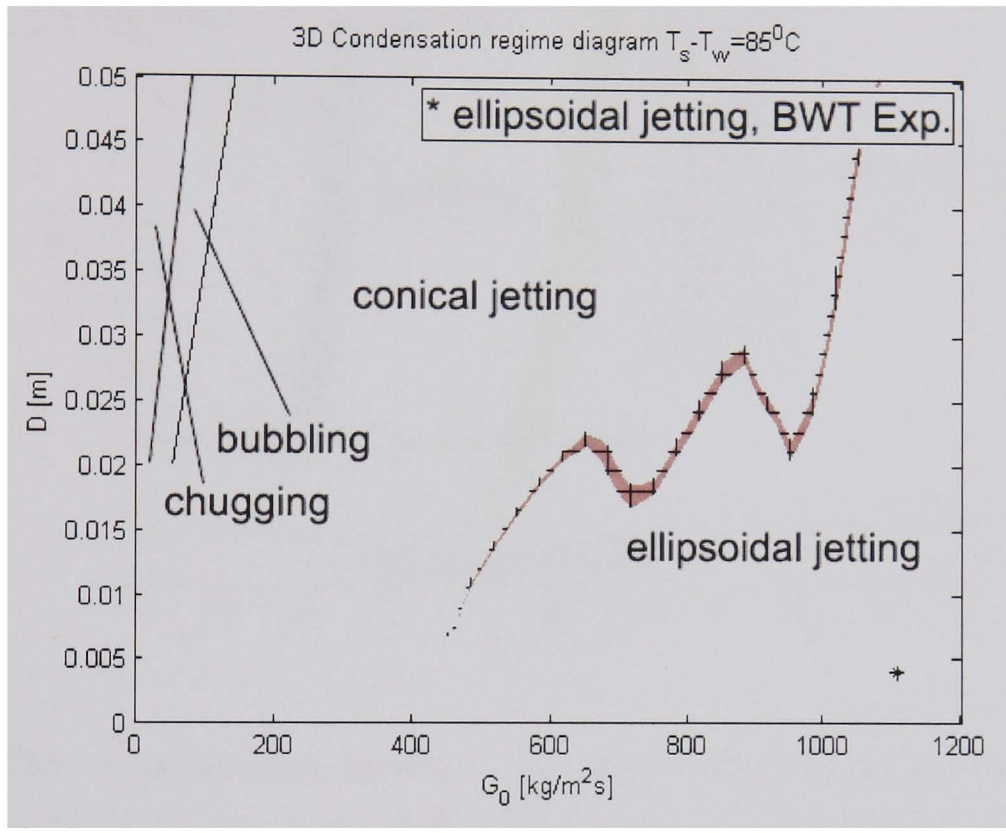

Figure 4.14: Comparison between the new 3DCR diagram and data for validation obtained during the development of the BWT system. Star relates to data for an ellipsoidal jetting regime $G_0 = 1105kg/\left(m^2s\right)$, $D = 0.004m$, $\Delta T = 85^0C$.

More data is required for validation of the map at small steam inflow rates. For this purpose, data from Youn *et al.* [12] has been used. These researchers detected regimes measurement of the pressure pulses in the surrounding water. For identification of regimes from measured pulses they used information about regimes from literature. Youn *et al.* [12] performed experiment with a steam injector with a diameter of $0.02m$. At a temperature of the water subcooling of $\Delta T = 20^0C$ they reported a bubbling regime for steam inflow rates up to $60kg/\left(m^2s\right)$. At the same steam injector but

at steam inflow rates from $60kg/(m^2s)$ to $80kg/(m^2s)$, workers detected a transition between regimes. The transition is defined as the change in observed pressure pulses indicating the change in a regime of condensation. Figure 4.15 shows a section of the new 3DCR diagram for steam inflow rates up to $100kg/(m^2s)$ and steam injector diameter of $0.02m$ compared with data from Youn *et al.* [12].

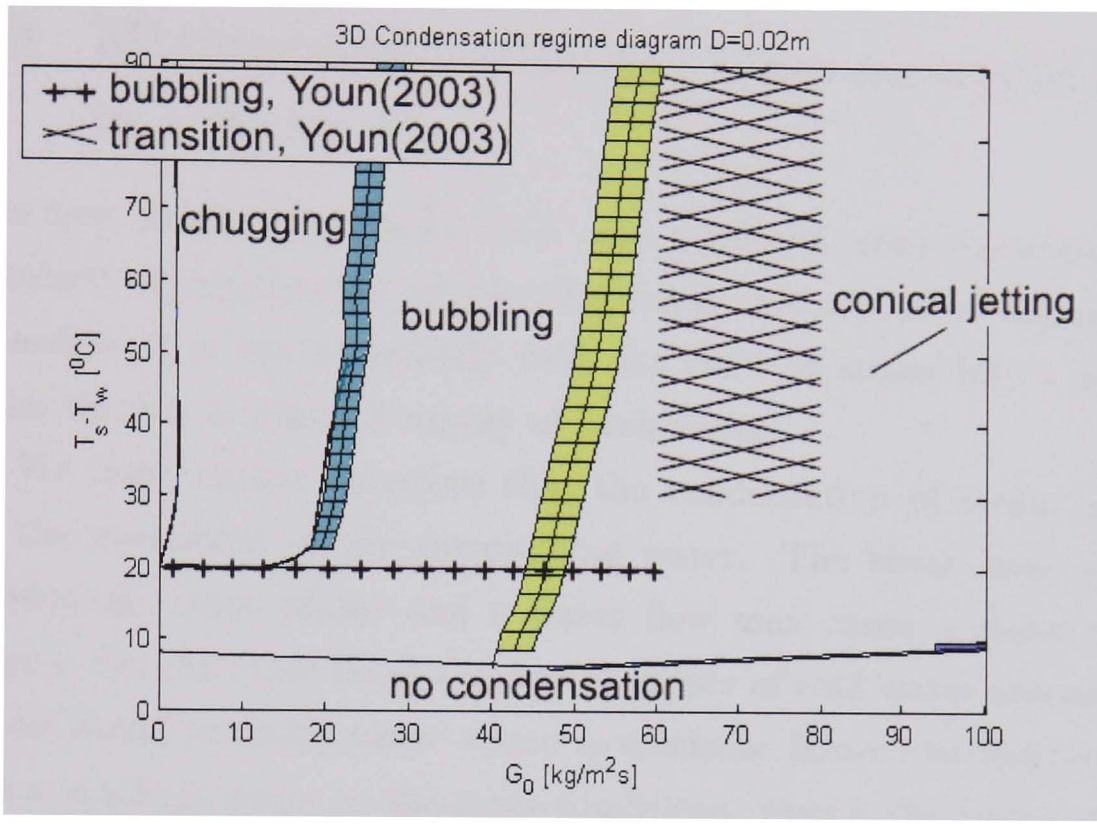

Figure 4.15: Comparison between the new 3DCR diagram and data for validation from Youn *et al.* [12]. Line with crosses relates to data for a bubbling regime $G_0 > 60kg/(m^2s)$, $D = 0.02m$, $\Delta T = 20^0C$. Shedded area relates to data for transition $G_0 \in (60, 80)\, kg/(m^2s)$, $D = 0.02m$, $\Delta T > 30^0C$.

The data from Youn *et al.* does not entirely correspond with data from the 3DCR diagram and the prediction of transition from bubbling to jetting regime is under-predicted by the diagram by approximately 15% as compared to data from Youn *et al.* [12]. Further data for bubbling regime show agreement, however, Youn *et al.* reported the bubbling regime to extend to slightly higher steam flow rates as compared to 3DCR diagram at reported flow conditions. Nevertheless, the results from the 3DCR diagram are in general agreement.

More data is needed for a solid proof, however this validation indicates

that the new 3DCR diagram is likely to be valid for steam inflow rates in the jetting regime and it can also be extended into a 'white' area of flow conditions. More experiments is also needed to validate the diagram in the chugging and bubbling regimes. However, validation showed, that there is a general agreement between the new 3DCR diagram and the data.

4.4 3D Condensation Regime Diagram Applied to DCC in a Water Flow

The new 3DCR diagram for DCC was generated using experimental data obtained at experiments of injecting steam into a pool of stagnant water. Therefore it is not necessarily valid for DCC of steam into a water flow when there is a constant supply of fresh water.

We must expect therefore that the condensation of steam is affected by the movement of the surrounding water. The shear layer between a developing steam plume and a water flow may cause a steam plume to extend. On the other hand a constant supply of cold water around a steam plume would probably cause steam to condense faster compared with DCC into a stagnant water at the same conditions. Hence, the regime of a DCC of steam into a water flow as well as shape of a steam plume is highly likely to be dependent on the velocity of the water flow.

Lack of published experimental data for DCC of steam into a water flow prevents the creation of a diagram predicting the regimes of DCC of steam into water flow. However, experiments performed during development of a BWT system have provided some indication of regimes at injection of steam into a water flow.

As part of the experiment, steam was injected in the centre of a water flow with a centreline velocity of $1.9m/s$ and a water subcooling of 85^0C. The water flow was guided through a pipe. The steam inflow rate was less then 5 percent of the water flow rate in the pipe to ensure blockage effects were negligible. Figure 4.16 shows a photograph taken during the experiments. It shows a pipe with a water flow and a steam nozzle through which steam was injected in the centre of the flow. Figure 4.17 shows a sketch of the experimental arrangements where directions of the water flow and of the injected steam are marked.

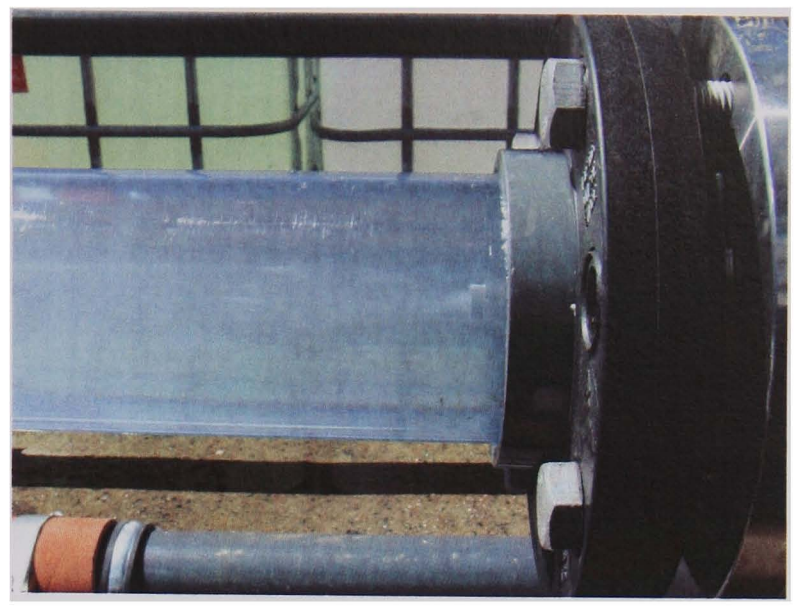

Figure 4.16: During the development of the system for ballast water treatment, steam was injected at the centre of a pipe with a steady flow of cold water.

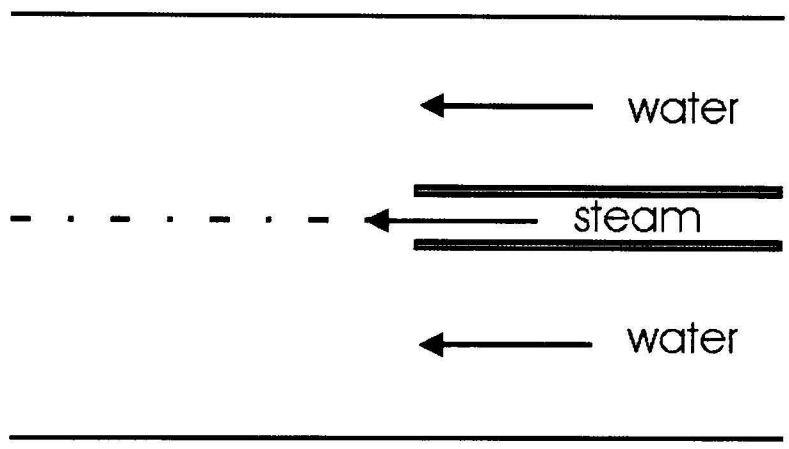

Figure 4.17: Sketch of the experimental arrangement.

Experiments were performed at different steam inflow rates using different steam injectors and a condensation behaviour was observed. Observations showed three different regimes of condensation. For a steam inflow rate of $424.4kg/\left(m^2s\right)$ and an injector with $5mm$ diameter, a hemispherical steam plume occurred at the exit of the injector. Photograph of the plume and the corresponding diagram are shown in Figure 4.18.

With steam injection rate of $663.1kg/\left(m^2s\right)$ of steam through an injector with $4mm$ diameter the steam plume extended slightly and it became conically shaped. Photograph of the plume and the corresponding diagram are presented in Figure 4.19.

Figure 4.18: Steam plume with a hemispherical shape developed at the injection of steam into a water flow with centreline velocity of $1.9m/s$ and temperature of 15^0C. Steam was injected through a $5mm$ injector with flow rate of $424.4kg/\left(m^2s\right)$.

Figure 4.19: Steam plume with conical shape developed at the injection of steam into a water flow with centreline velocity of $1.9m/s$ and temperature of 15^0C. Steam was injected through a $4mm$ injector with steam flow rate of $663.1kg/\left(m^2s\right)$.

For smaller steam injector with $2mm$ diameter and a steam inflow rate of $2652.6kg/\left(m^2s\right)$ the plume was extended even more and the ellipsoidal jetting regime was observed. Photograph of the ellipsoidal plume developed at the injector exit and the corresponding diagram are shown in Figure 4.20.

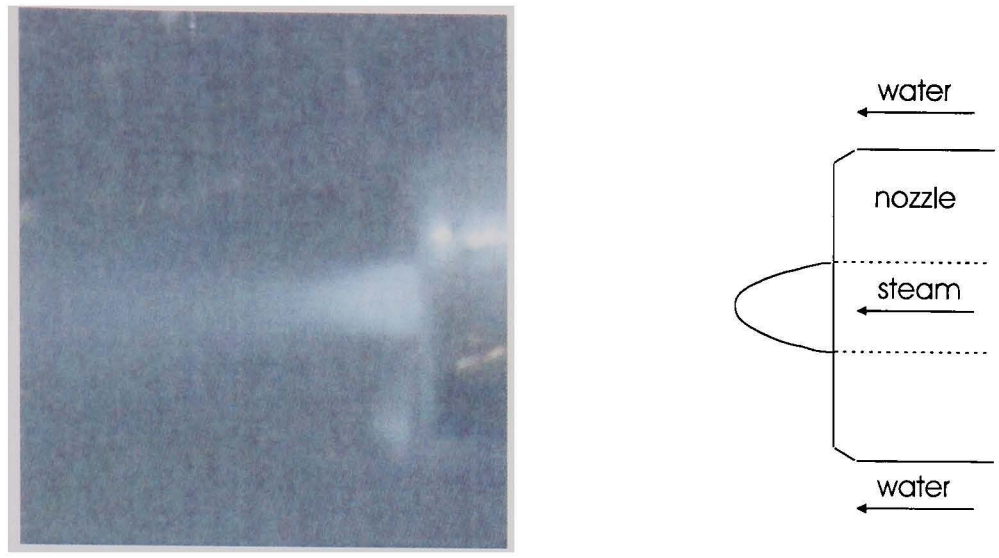

Figure 4.20: Steam plume with ellipsoidal shape developed at the injection of steam into a water flow with centreline velocity of $1.9m/s$ and temperature of 15^0C. Steam was injected through a $2mm$ injector with steam flow rate of $2652.6kg/\left(m^2s\right)$.

Data obtained at injection of steam into water flow and presented in Figures 4.18-4.20 is given in Table 4.3.

$G_0\ \left[\frac{kg}{m^2s}\right]$	$D\ [m]$	$\Delta T\ [^0C]$	Plume
424.4	0.005	85	hemispherical
663.1	0.004	85	conical
2652.6	0.002	85	ellipsoidal

Table 4.3: Steam plume shapes observed at injection of steam into water flow.

The observations from these experiments were compared with the new 3DCR diagram. Figure 4.21 shows a cross-section of the 3DCR diagram with a water subcooling temperature of 85^0C. The regime names are added to the graph and black markers representing the experimental observations are added. The circular marker relates to the data from a $5mm$ injector. This is located in the vicinity of the boundary between conical to ellipsoidal jetting. However, the experiments in a water flow suggested a hemispherical steam plume (Figure 4.18). Such a steam plume is expected to occur on the boundary between bubbling and conical jetting regimes. The square shaped marker relates to data from a $4mm$ injector. The marker is located

in the first part of the ellipsoidal jetting regime. However, the experiments showed that the jet was conical (Figure 4.19). The final diamond shaped marker relates to the data from a $2mm$ injector. The marker is located in the ellipsoidal jetting regime and an ellipsoidal jet was also found in the experiments (Figure 4.20).

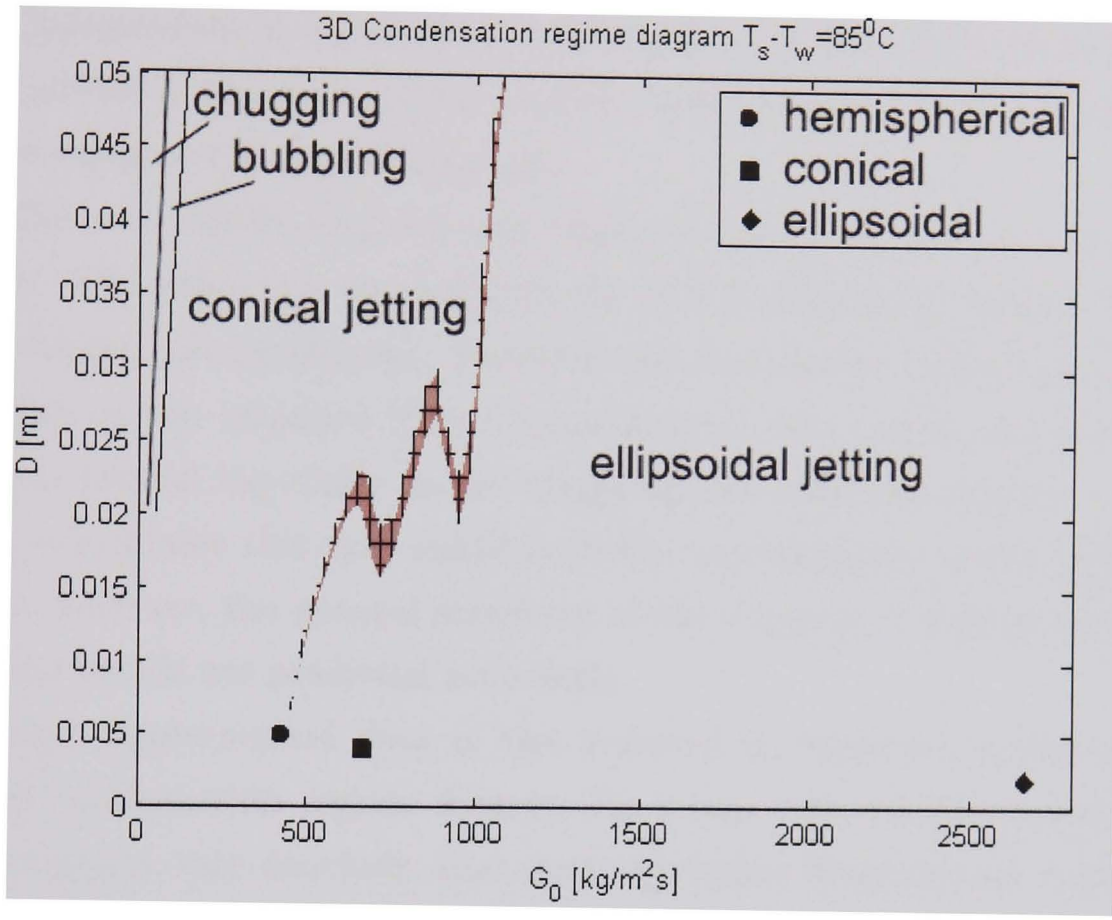

Figure 4.21: 3DCR diagram for DCC of steam into a stagnant water at $T_s - T_w = 85^0C$ with added data for DCC into a water flow, obtained at development of the BWT system.

It is concluded that a three dimensional condensation regime diagram for DCC of steam in a water flow has similar features to the condensation regime diagram for stagnant water that has just been developed. However, it is expected that the location of the various regimes in the diagram will differ. More experiments at different environmental conditions should be performed to make any conclusions more substantial.

4.5 Discussion

In this chapter, a new three dimensional condensation regime diagram for DCC of steam injected into a stagnant water has been created. We have seen

that this three dimensional diagram can predict the DCC regimes across a wide range of flow conditions and injector sizes. This is a considerable advance over the two dimensional regime maps found in the literature which are able to predict the regimes for one injector size only. The new 3DCR diagram was created from experimental data found in the literature. This data was independent and published over a period of more then three decades. The author is not aware of any further work published on this subject that could enhance the regime diagram.

The new 3DCR diagram was validated with data not used in its creation. The validation showed that the 3DCR diagram accurately predicts the various jetting regimes. Furthermore, boundaries between the various regimes can be extended if more experimental data can be provided. More data is needed especially in the chugging and bubbling regimes. If more data is available this may result in minor modifications to the 3DCR diagram, however, the general structure of the diagram is well established as general trends are predicted accurately.

More experimental data is also required to construct a three dimensional condensation regime diagram for steam injected into a water flow. Investigation may conclude, that separate regime diagrams are required for different velocities of the water flow.

5 Identification of the Steam Plume Length in DCC

In addition to the precise nature of the condensation regime, another important feature of DCC of steam into water is the length of a steam plume. In order to calculate the heat transfer coefficient and to model DCC of steam in water the length of the steam plume is needed for a series of flow conditions of the process. However, the length of a steam plume depends on the flow conditions of the process and is therefore difficult to predict.

Until now, researchers have performed experiments in which the steam plume length was measured. The data was used to derive correlations, predicting the dimensionless steam plume length. Correlations presented in literature have been derived empirically and are only valid for a narrow range of flow conditions. Therefore, there is a need for a more general correlation, capable of predicting plume lengths in a wide range of flow conditions.

This chapter aims to identify a new way of obtaining more general prediction of the plume length. To achieve this other physical parameters of the process which are related to the steam plume length are identify as compared to parameters used in correlations from literature.

5.1 Literature Review and Data Gathering

Data used in this work and gathered from literature is a collection of various information published in last three decades. It includes experimental data for steam plume length and correlations from literature.

Various researchers have performed experiments to obtain data for length of the plume. Kerney *et al.* [8] published experimental data for steam plume length when injecting steam into water through steam injectors with eight different diameters. The temperature of the water subcooling and the rate of steam injection covered a substantial range. Chun *et al.* [45] published data for one steam injector and one steam inflow rate. Kim & Park [11] presented photographic evidence from which lengths of a steam plume at two different conditions could be obtained. Kim *et al.* [14] and Kim *et al.* [13] presented experimental data for three different steam injectors. Table

5.1 shows flow conditions at which different researchers obtained their data.

Authors	$D\,[m]$	$\Delta T\,[^0C]$	$G_0\ \left[\frac{kg}{m^2 s}\right]$
Kerney *et al.* [8]	0.0004	20 to 80	250 to 2050
	0.00079		
	0.00158		
	0.00376		
	0.00635		
	0.0095		
	0.0101		
	0.0112		
Chun *et al.* [45]	0.00135	19 to 80	1488
Kim & Park [11]	0.01085	77	268
		57	439
Kim *et al.* [14]	0.0071	20 to 65	600
	0.005		870
			1045
			1188
Kim *et al.* [13]	0.01085	22 to 84	300
			400
			500
			268
			287

Table 5.1: Conditions at which data for steam plume length has been presented by different authors.

In addition to data for the steam plume length, researchers have also published empirical correlations for dimensionless plume length. These were obtained by fitting experimental data into a proposed correlation. An initial correlation for the steam plume length was derived by Kerney *et al.* [8]. Later studies giving further data for steam plume lengths, pointed to modifications to Kerney's original correlation.

Kerney *et al.* [8] derived a correlation using conservation of mass for an

axially symmetric steam plume with a smooth surface (Figure 5.1).

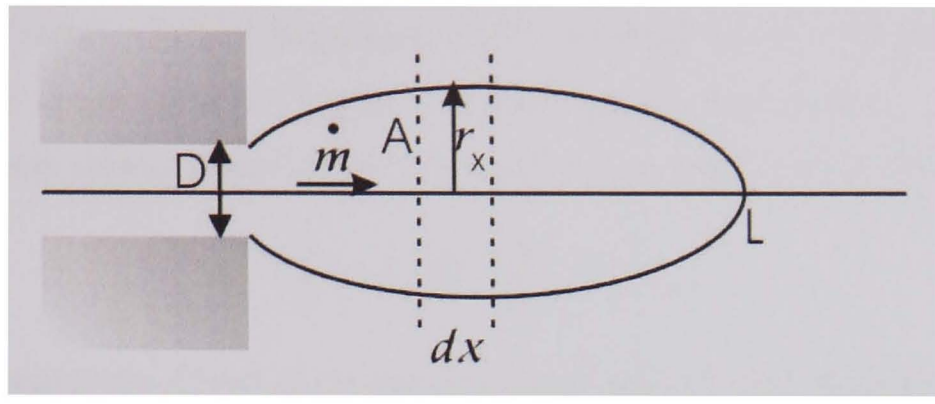

Figure 5.1: Kerney [8] assumed an axially symmetric steam plume in deriving a correlation for steam plume length.

Assuming that a change of a mass in a small section of a plume is equal to the mass of steam which condenses through a surface of a section, Kerney *et al.* [8] started with the equation

$$\dot{m}' \mathrm{d}x = \frac{h}{h_{fg}} \Delta T 2\pi r_x \mathrm{d}x \ , \tag{5.1}$$

where the rate of change of mass is

$$\dot{m} = \rho v A = G\pi r_x^2 \ . \tag{5.2}$$

Kerney *et al.* [8] further defined a dimensionless condensation potential

$$B = \frac{c_p}{h_{fg}} \Delta T \ , \tag{5.3}$$

and transport modulus

$$S = \frac{h}{c_p G} \ . \tag{5.4}$$

Substituting Equation (5.2) into Equation (5.1) and normalizing, Equation (5.1) can be rewritten as

$$\frac{\mathrm{d}\left(\frac{\dot{m}}{\dot{m}_0}\right)^{\frac{1}{2}}}{\mathrm{d}x} = -\left(\frac{G}{G_0}\right)^{\frac{1}{2}} SB \ . \tag{5.5}$$

The boundary conditions of Equation (5.5) are

$$x = 0 \ , \frac{\dot{m}}{\dot{m}_0} = 1 \ ; x = \frac{2L}{D} \ , \frac{\dot{m}}{\dot{m}_0} = 0 \ , \tag{5.6}$$

which gives the correlation derived by Kerney *et al.* [8]

$$\frac{L}{D} = 0.5 \frac{1}{B} \left(\frac{G_0}{G_m}\right)^{\frac{1}{2}} \frac{1}{S_m} \ . \tag{5.7}$$

The constant G_m was chosen by Kerney *et al.* [8] to normalize the data to $275kg/\left(m^2s\right)$. Using Equation (5.7), Kerney *et al.* [8] defined a dimensionless steam plume length as a function of condensation potential, a dimensionless steam mass inflow rate and mean transport modulus

$$\frac{L}{D} = f\left(B, \frac{G_0}{G_m}, S_m\right) . \tag{5.8}$$

Various researchers fitted their experimental data to the correlation (5.8) in order to obtain the functional relationship for a dimensionless steam plume length.

Kerney *et al.* [8] fitted part of the data obtained during experiments into correlation (5.7) giving

$$\frac{L}{D} = 0.2588B^{-1}\left(\frac{G_0}{G_m}\right)^{0.5} , \tag{5.9}$$

which was reported to have a 13.6% error. To decrease this error, the researchers repeated their work removing the restriction on powers implied by Equation (5.7). A slightly improved correlation was obtained (5.10).

$$\frac{L}{D} = 0.3583B^{-0.8311}\left(\frac{G_0}{G_m}\right)^{0.6446} \tag{5.10}$$

This correlation had an error of 11.7% with a steam injector with a diameter of $D = 0.00635m$.

Weimer *et al.* [56] proposed an improvement to the correlation (5.8). In their experiments these researchers injected steam, vapours of ethylene glycol and vapours of iso-octane into water. They observed a correlation between plume length and density ratio of the vapour and water. They then proposed a general correlation for the dimensionless plume length for the injection of various vapours into water by adding a density ratio to Equation (5.8)

$$\frac{L}{D} = f\left(B, \frac{G_0}{G_m}, \frac{\rho_s}{\rho_\infty}\right) . \tag{5.11}$$

Using the data they obtained during experiments the functional relationship was found to be

$$\frac{L}{D} = 17.75B^{-1}\left(\frac{G_0}{G_m}\right)^{0.5}\left(\frac{\rho s}{\rho_\infty}\right)^{0.5} . \tag{5.12}$$

Weimer *et al.* [56] reported 21.9% error using this proposed correlation. By removing the restriction on property powers they produced an improved correlation with a 13.0% error. Derived correlation is presented in Equation (5.13).

$$\frac{L}{D} = 10.285B^{-0.801}\left(\frac{G_0}{G_m}\right)^{0.713}\left(\frac{\rho s}{\rho_\infty}\right)^{0.384} \tag{5.13}$$

This correlation is valid for an injector with a diameter of $D = 0.00317m$. Validity of the equation here and further in this chapter refers to the conditions at which data used at generating the correlations was obtained. Authors of correlations did not report restrictions on validity of proposed correlations.

Chun *et al.* [45] and Kim *et al.* [14] both used the correlation in Equation (5.8) as proposed by Kerney *et al.* [8] and using their experimental data obtained correlations. The correlation

$$\frac{L}{D} = 0.5923B^{-0.66}\left(\frac{G_0}{G_m}\right)^{0.3444} \tag{5.14}$$

was published by Chun *et al.* [45] and is valid for a steam injector with diameter of $D = 0.00135m$. The correlation

$$\frac{L}{D} = 0.503B^{-0.70127}\left(\frac{G_0}{G_m}\right)^{0.47688} \tag{5.15}$$

was published by Kim *et al.* [14] and is valid for a steam injector with diameter of $D = 0.005m$.

All correlations for dimensionless steam plume length published in the literature are presented in Table 5.2. They have all been derived using the dimensionless equation as proposed by Kerney *et al.* [8]. All these predict the dimensionless steam plume length reasonably well for flow conditions at which data used to produce the individual functional relationships was obtained. However, they fail to predict steam plume length with any accuracy over a wide range of flow conditions. Therefore, there is a need for a new steam plume length prediction method, which is capable of predicting length over a wide range of flow conditions. During this research different approach from the one taken by researchers to date was taken in order to obtain a generalised prediction for a steam plume length.

Authors	Correlation	Error	Validity
Kerney *et al.* [8]	$L/D = 0.2588B^{-1}\left(G_0/G_m\right)^{0.5}$	13.6%	$D = 0.00495m$
	$L/D = 0.3583B^{-0.8311}\left(G_0/G_m\right)^{0.6446}$	11.7%	$G_0 \in (338, 1240)\, kg/\left(m^2 s\right)$
			$B \in (0.0028, 0.135)$
Weimer *et al.* [56]			$D = 0.00317m$
	$L/D = 17.75B^{-1}\left(G_0/G_m\right)^{0.5}\left(\rho_s/\rho_\infty\right)^{0.5}$	21.9%	$G_0 \in (321, 1136)\, kg/\left(m^2 s\right)$
	$L/D = 10.285B^{-0.801}\left(G_0/G_m\right)^{0.713}\left(\rho_s/\rho_\infty\right)^{0.384}$	13.0%	$B \in (0.0025, 0.063)$
			$\rho_\infty/\rho_s \in (3980, 27700)$
Chun *et al.* [45]	$L/D = 0.5923B^{-0.66}\left(G_0/G_m\right)^{0.3444}$		$D = 0.00135m$
			$G_0 = 1488kg/\left(m^2 s\right)$
			$B \in (0.035, 0.15)$
Kim *et al.* [14]	$L/D = 0.503B^{-0.70127}\left(G_0/G_m\right)^{0.47688}$		$D = 0.005m$
			$G_0 = 1188kg/\left(m^2 s\right)$
			$B \in (0.037, 0.12)$

Table 5.2: Different correlations for dimensionless steam plume length published in the literature.

5.2 Development of a 2D Steam Plume Length Diagram

In this study all the data for steam plume length available in literature was collected and used to construct the prediction unlike other researchers, who used only limited sets of data. Furthermore, correlation (5.8) was not used during this construction, but other ways of predicting steam plume length were discovered.

All collected data was plotted on single graphs in attempts to understand the underlying trends. First, the dimensionless steam plume length data was plotted in a graph (Figure 5.2) using condensation potential B and dimensionless steam mass inflow rate G_0/G_m as axes. This method of plotting has been used by other researchers to obtain their semi-empirical correlations. Therefore, if their correlations are generally valid, the generated graph should deliver a smooth, organised distribution of data.

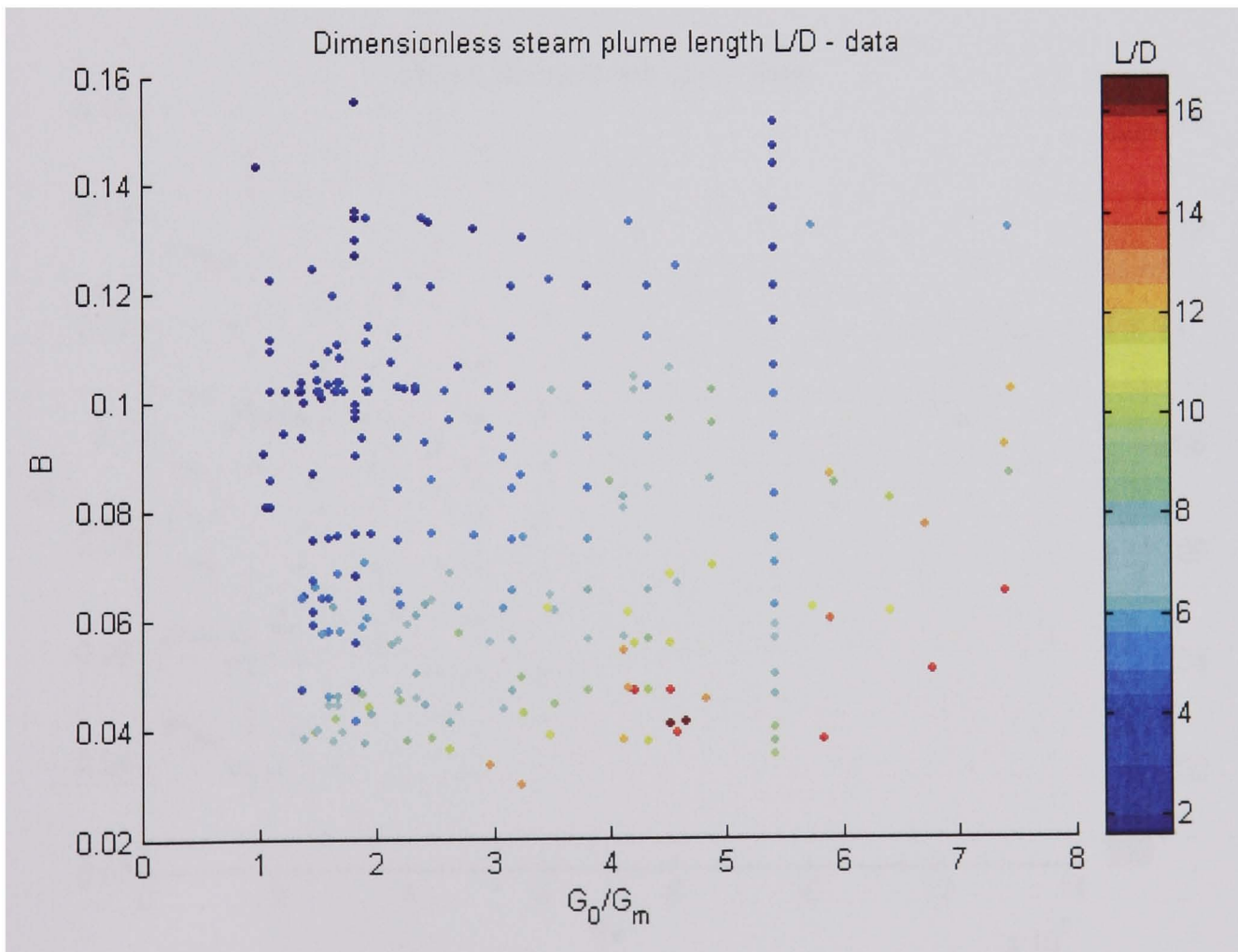

Figure 5.2: Dimensionless steam plume length data as a function of dimensionless steam mass inflow rate (G_0/G_m) and condensation potential (B).

The dots use colour to indicate dimensionless length of the steam plume. The results show some structure but generally no clearly defined trends. The dimensionless steam plume length tends to be small for high condensation potential and large for low condensation potential.

Further graphs were then generated where the dimensionless steam plume length (L/D) and the steam plume length (L) were presented as functions of steam mass inflow rate (G_0), condensation potential (B), injector diameter (D) and steam Reynolds number ($Re = DG_0/\eta$). In addition to physical parameters, known to affect the process of DCC, the Reynolds number was chosen as one of potential parameters. The Reynolds number is directly related to the inertia of injected steam and hence it should be related to the penetration length of the steam.

A much more coherent plot of the experimental data was found when using the steam plume length (L) as a function of Reynolds number (Re) and condensation potential (B) as shown in Figure 5.3.

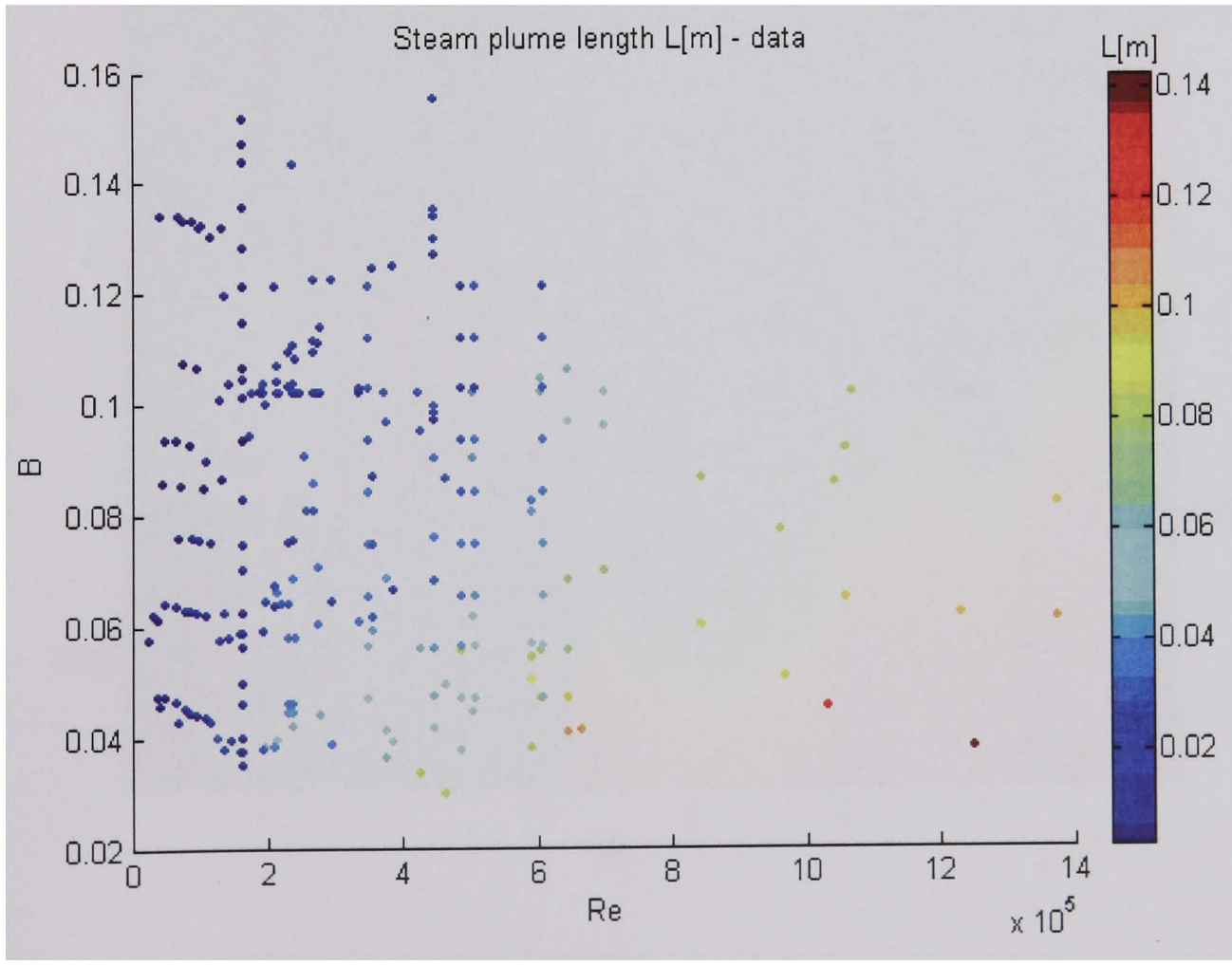

Figure 5.3: Steam plume length data as a function of a Reynolds number (Re) and a condensation potential (B).

Again, the dots use colour to indicate the different lengths of the plume. Figure 5.3 shows that the largest steam plume length occurs at high Reynolds numbers and low condensation potentials. The smallest lengths occur at low Reynolds numbers for all condensation potentials. The prediction is consistent with previous studies as it can be expected that the steam plume length is related to the condensation rate of steam and to the inertia of injected steam. In more detail, the steam plume extends with a higher inertia of the steam, but shortens at a higher rate of condensation. The pattern is also observed in Figure 5.3.

The steam plume length data as a function of Reynolds number and condensation potential was used to develop a two-dimensional steam plume length diagram. The diagram was produced through interpolation using existing data from literature to create generated surface shown in Figure 5.4.

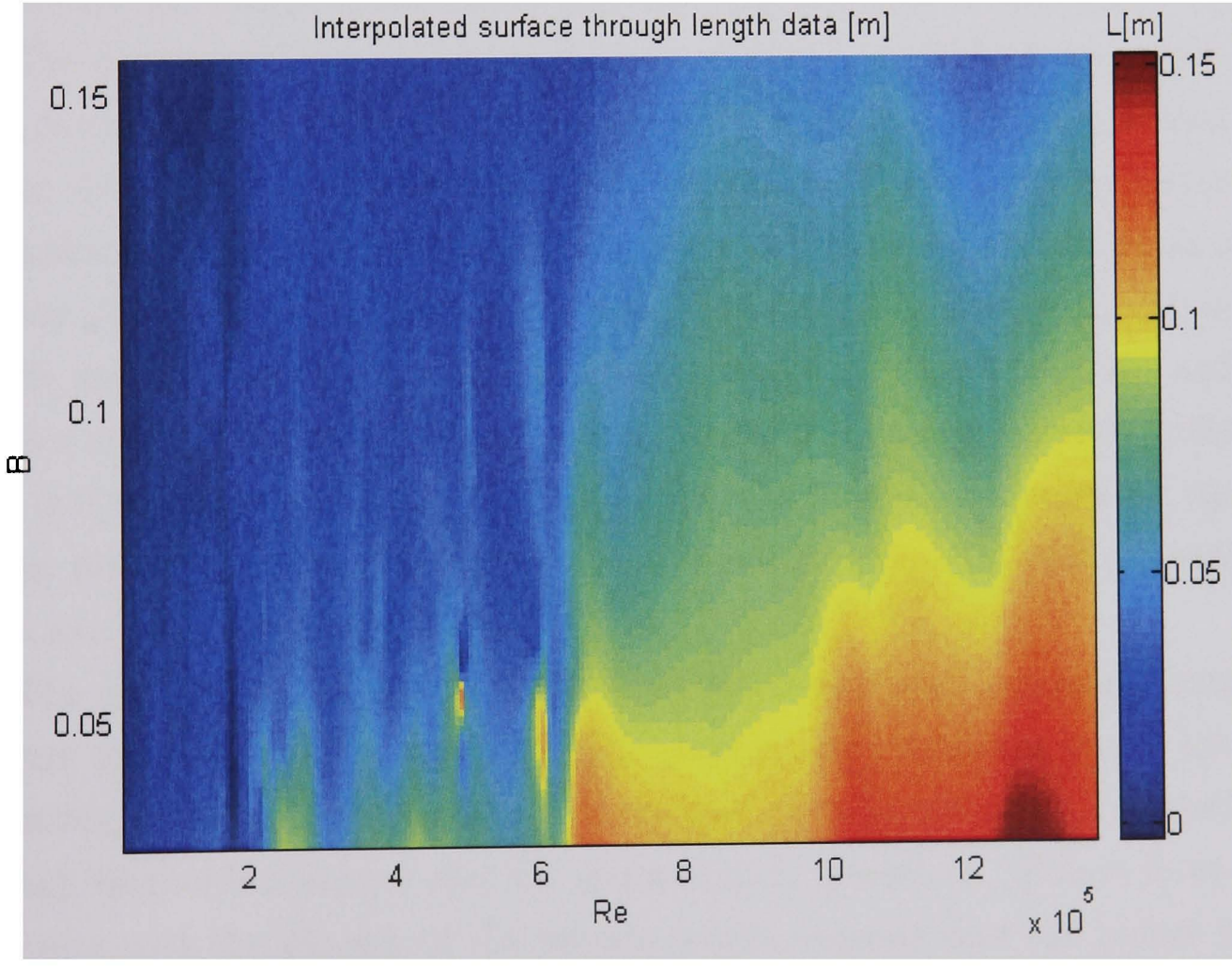

Figure 5.4: Steam plume length surface generated through existing data. Colours indicate length of the plume.

The interpolation technique used generates the surface using the method

documented in [59]. A fundamental criterion in this method is that the generated surface has to pass through all data that is provided. It is assumed that the large deviations in colours from the surrounding colours are the result of inaccuracies in the measurements, and variations in measurement techniques and setups during experiments. To produce a steam plume length diagram with better-defined trends, filtering was performed to the interpolation results which were stored in a matrix. The filtering technique used was derived by the author and includes a combination of two different filters. In the first filter a standard averaging method was applied to the neighbouring elements if these elements were dominated by scatter. In the second, a forth order polynomial was constructed for each column and each row of the matrix. Consequently, any given element of the matrix is described by its two corresponding polynomials. In the final stage of the filtering technique, the results from both polynomials were averaged, to provide the length of the steam plume at different flow conditions.

The developed Two-Dimensional Steam Plume Length diagram, generated from Figure 5.4 using the filter is given in Figure 5.5. In the pages that follow this diagram will be referred to as the "new 2DSPL diagram". It is a graphical representation of results for the steam plume length stored in a matrix. It shows the length of the steam plume in metres ($L[m]$) in relation to the steam Reynolds number (Re) in the range between 0.24×10^5 and 13.74×10^5, and the condensation potential (B) in the range between 0.029 and 0.155. Different colours on the diagram represent the length of the steam plume in metres. The error of the diagram compared with original data was calculated to be 13.7%.

The new 2DSPL diagram (Figure 5.5) shows that steam develops long plumes when injected at high Reynolds numbers and short plumes at low Reynolds numbers. Furthermore, the longest plumes are to be expected at high Reynolds numbers and low condensation potentials. This is in accordance with the physics of the process which suggests that the plume is longer if the inertia of the injected steam is higher, but is shortened with increasing condensation rate.

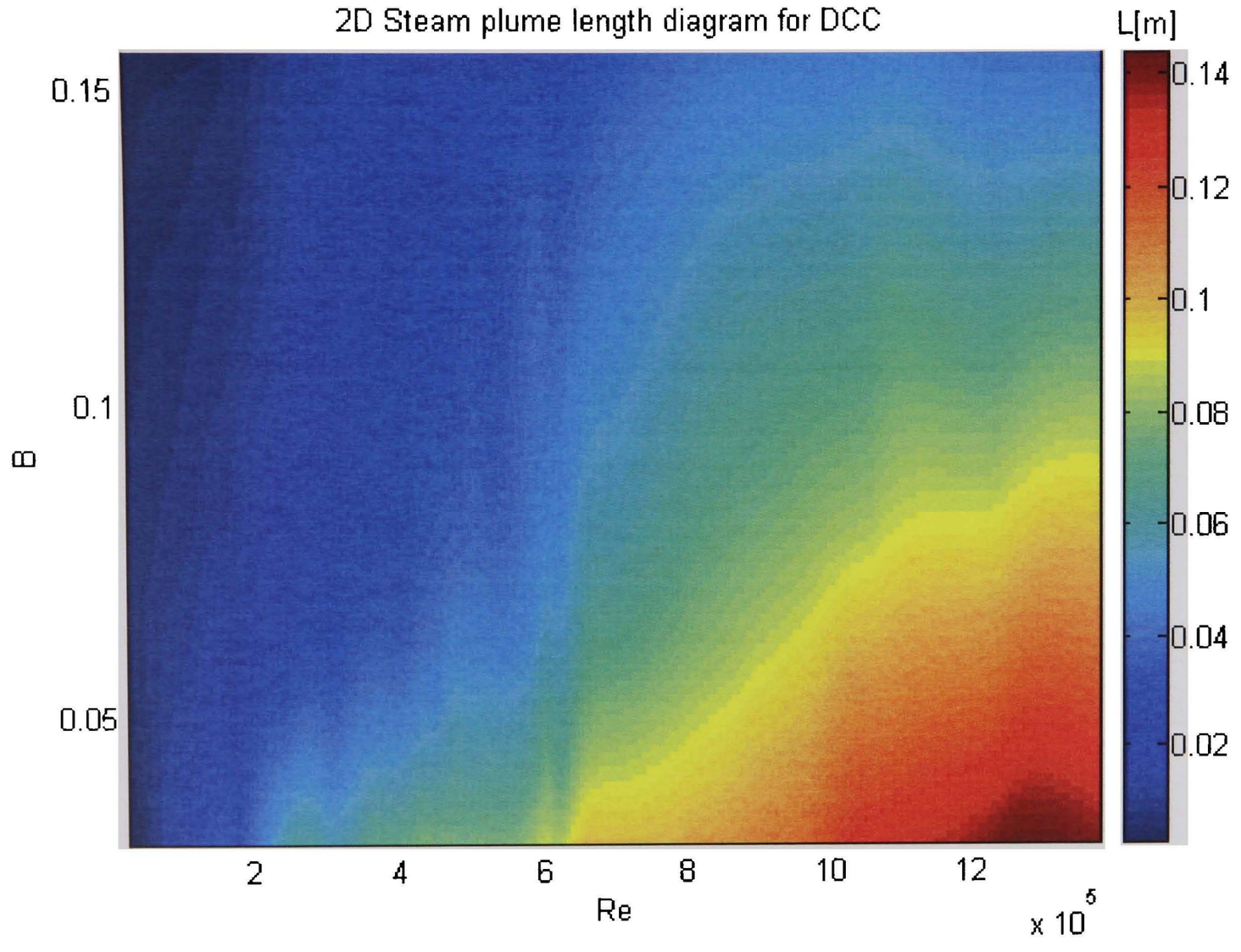

Figure 5.5: New 2DSPL diagram for DCC. Colours indicate predicted length of the steam plume in metres. The longest plumes are to be expected at high Reynolds numbers and low condensation potentials; short plumes at low Reynolds numbers.

5.3 Validation of a 2D Steam Plume Length Diagram

The new two-dimensional steam plume length diagram (Figure 5.5) developed, as described in previous section of this chapter, using data was evaluated using semi-empirical steam plume length correlations from the literature (Table. 5.2). These correlations are assumed to be valid only for specific limited conditions of flow. However, correlations were used by different researchers modelling the DCC process to predict the steam plume length also at flow conditions which differ from the specified ones [5], [6].

For the comparison with the new 2DSPL diagram, similar diagrams were generated from the correlations from literature and are presented in Figures 5.6 to 5.9. The colours represent the length of the plume in metres and the colour range of the four diagrams in Figures 5.6 to 5.9 was set to be the same as that in Figure 5.5.

Diagram generated from the correlation proposed by Kerney *et al.* [8] (Equation (5.10)) is presented in Figure 5.6.

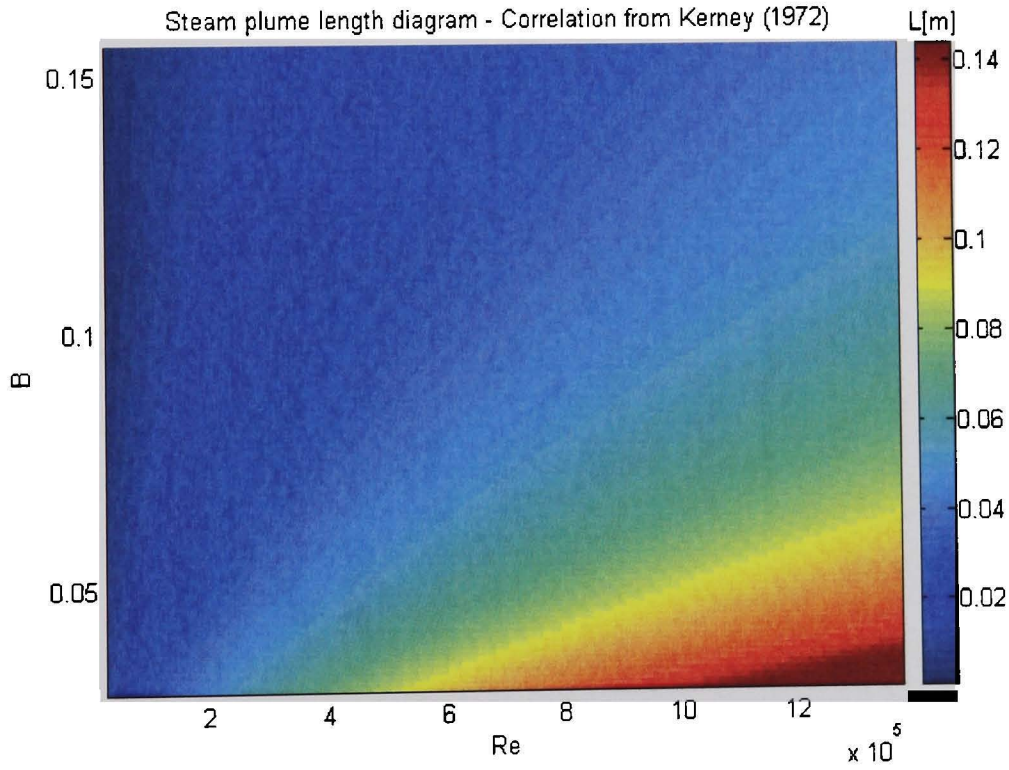

Figure 5.6: Steam plume length diagram from the correlation (5.10) proposed by Kerney *et al.* [8].

Figure 5.7 shows the diagram generated from the correlation (5.13) proposed by Weimer *et al.* [56].

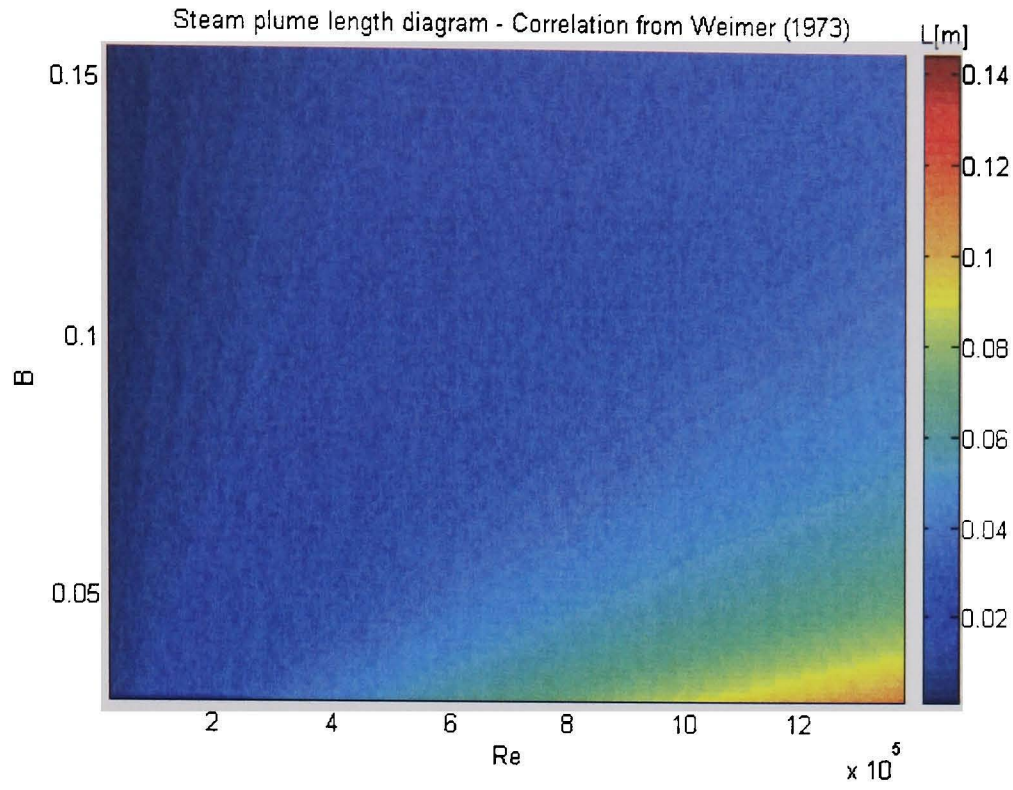

Figure 5.7: Steam plume length diagram from the correlation (5.13) proposed by Weimer *et al.* [56].

Diagram generated from the correlation (5.14) proposed by Chun *et al.* [45] is presented in Figure 5.8.

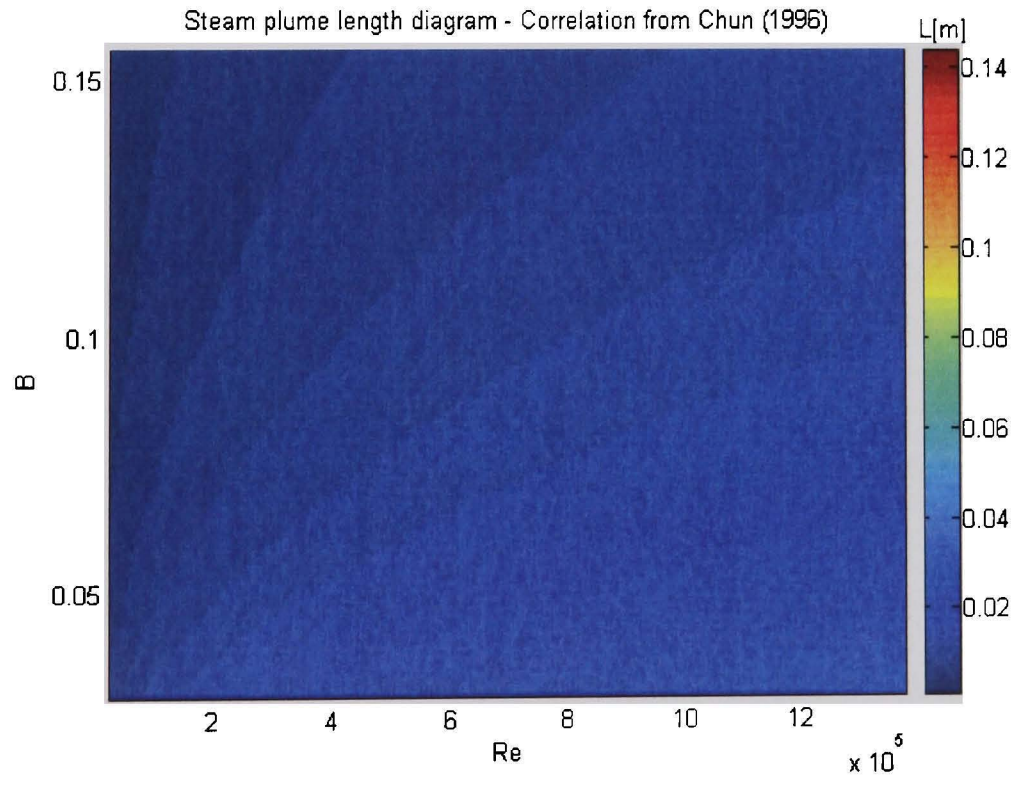

Figure 5.8: Steam plume length diagram from the correlation (5.14) proposed by Chun *et al.* [45].

In Figure 5.9 is a diagram generated using the correlation (5.15) proposed by Kim *et al.* [14].

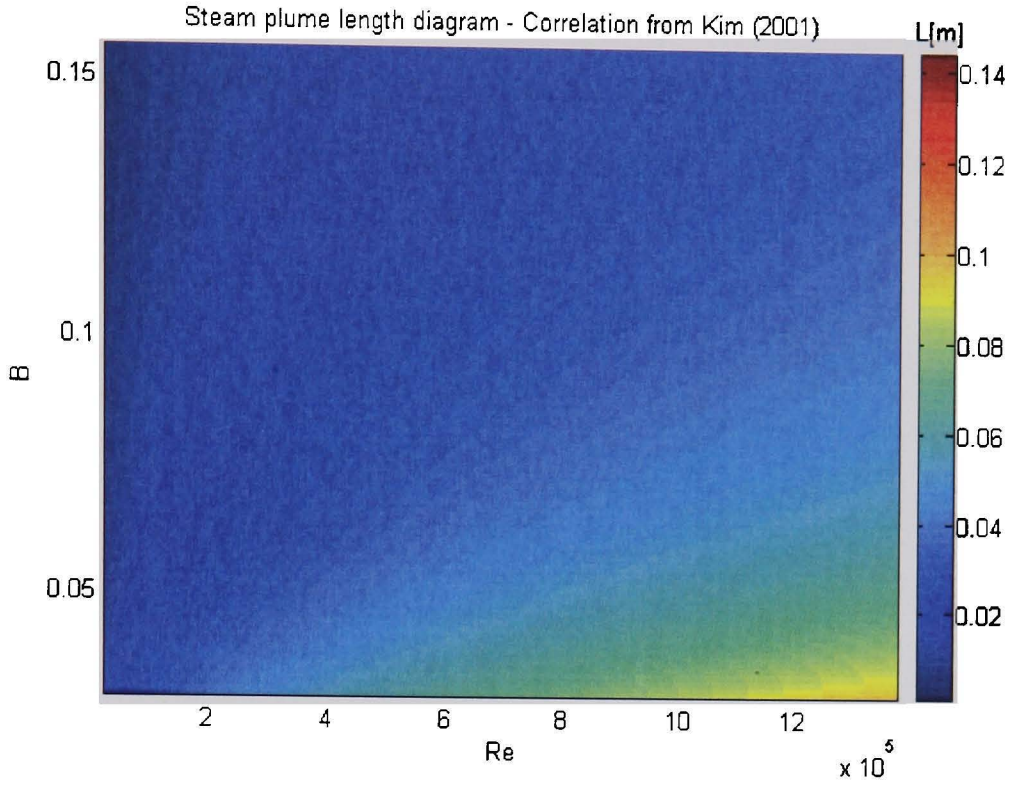

Figure 5.9: Steam plume length diagram from the correlation (5.15) proposed by Kim *et al.* [14].

The correlations proposed by Weimer *et al.* [56] (Equation (5.13)), Chun *et al.* [45] (Equation (5.14)) and Kim *et al.* [14] (Equation (5.15)) are all based on the original correlation proposed by Kerney *et al.* [8] (Equation (5.10)). Each author derived modifications to Kerney's correlation based on their newly performed experiments. For this reason each correlation provides similar trends with varying Re and B as seen on Figures 5.6-5.9. However, the length prediction differs as a result of the modification to the original correlation. The results in Figures 5.6-5.9 predict the longest plume at high Reynolds numbers and small condensation potential. The shortest plume lengths are predicted at low Reynolds numbers. The longest steam plumes are predicted by the correlation suggested by Kerney *et al.* [8] (Figure 5.6), whose correlation is also the most similar in prediction to the new 2DSPL diagram developed in this study. The shortest plumes are predicted by Chun *et al.* [45] (Figure 5.8) and these are much lower than those in the 2DSPL diagram. Correlations from Weimer *et al.* [56] (Figure 5.7) and Kim *et al.* [14] (Figure 5.9) give similar predictions.

The predicted steam plume lengths from correlations proposed by earlier workers were compared with the experimental data for the steam plume length gathered in this work and shown in Figure 5.3. Predictions by Kerney *et al.* [8] differ the least from the experimental data and predictions by Chun *et al.* [45] the most. The errors are presented on Table 5.3 plus that for the new 2DSPL diagram.

Authors	**Error [%]**
new 2DSPL diagram	13.7
Kerney *et al.* [8]	28
Weimer *et al.* [56]	40.5
Chun *et al.* [45]	70.4
Kim *et al.* [14]	43

Table 5.3: Calculated errors between data and plume length predictions from the new 2DSPL diagram (Figure 5.5) and diagrams from correlations from literature (Figures 5.6-5.9).

In addition, graphs have been produced, showing steam plume length predictions from the new 2DSPL diagram (Figure 5.5), correlations from the literature (Table 5.2, Figures 5.6-5.9) and data from literature. The Reynolds numbers at which graphs were produced were chosen to cover the whole range of conditions and were set where data is available. Results are given in Figures 5.10 to 5.12 for low Reynolds numbers and in Figures 5.13 and 5.14 for high Reynolds numbers.

Figure 5.10 shows the comparison at Reynolds number $Re = 164655$. Here the experimental data from Chun *et al.* [45] holds close agreement with the correlation he proposed. In contrast, the correlations proposed by other workers over-predict the steam plume length when compared with experimental data from Chun *et al.* [45]. Although the author is not aware of any fundamental flaw in Chun's experiments it is postulated that the experiments by Chun *et al.* [45] are not representative for the given flow conditions. The result of that is a correlation from Chun *et al.* [45] (Equation (5.14)), which is poorly dependent on the Reynolds number and which predicts lengths much lower than other correlations for a whole range of

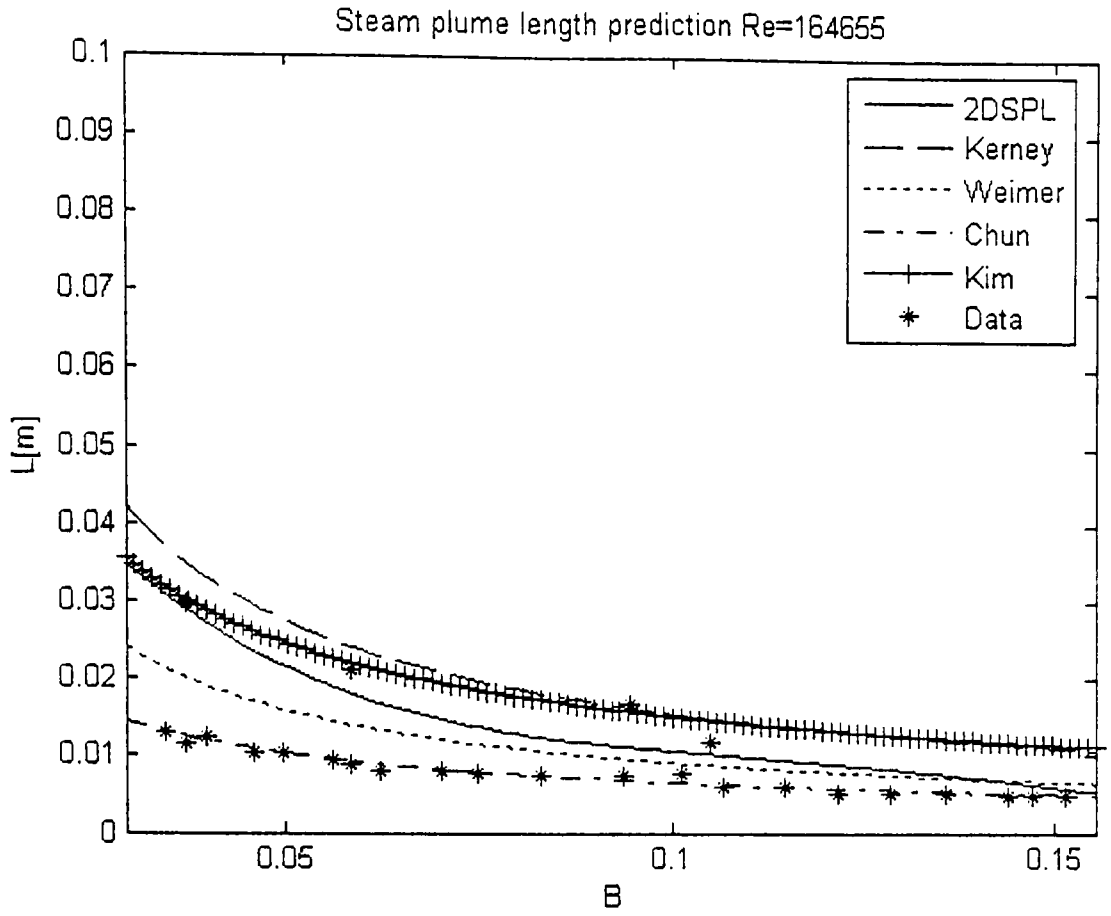

Figure 5.10: Comparison between steam plume length predictions from the new 2DSPL diagram, correlations from Kerney *et al.* [8], Weimer *et al.* [56], Chun *et al.* [45] and Kim *et al.* [14], and experimental data for $Re = 164655$.

flow conditions (Figure 5.8).

Figure 5.11 shows comparisons at Reynolds numbers $Re = 375000$ (Figure 5.11(a)) and $Re = 486885$ (Figure 5.11(b)). Here the correlation from Kerney *et al.* [8] (Equation 5.10) and the new 2DSPL diagram (Figure 5.5) show similar predictions for the steam plume length for the range of condensation potentials. These predictions also correspond well with experimental data. Other correlations under-predict steam plume lengths for the whole range of condensation potentials. However, the correlation by Kim *et al.* [14] (Equation 5.15) corresponds well with experimental data for some values of condensation potential.

(a)

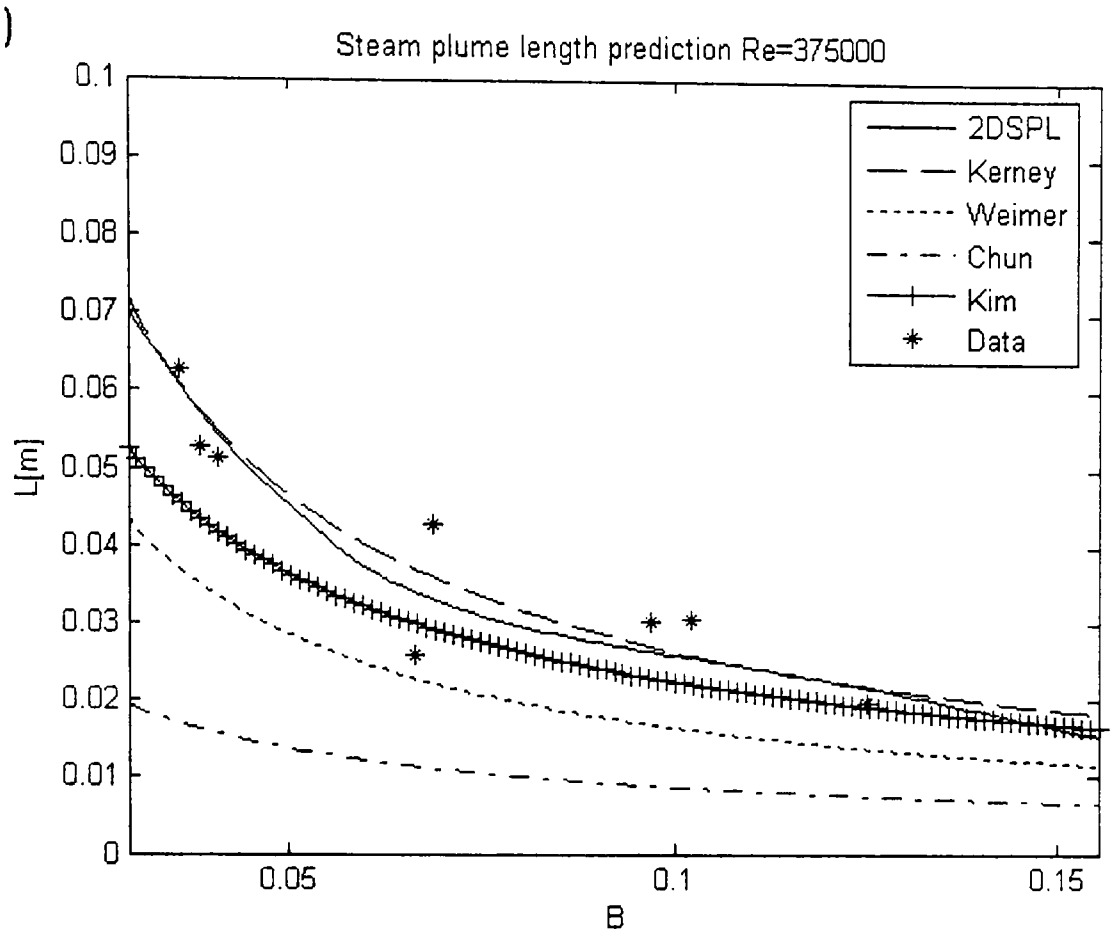

(b)

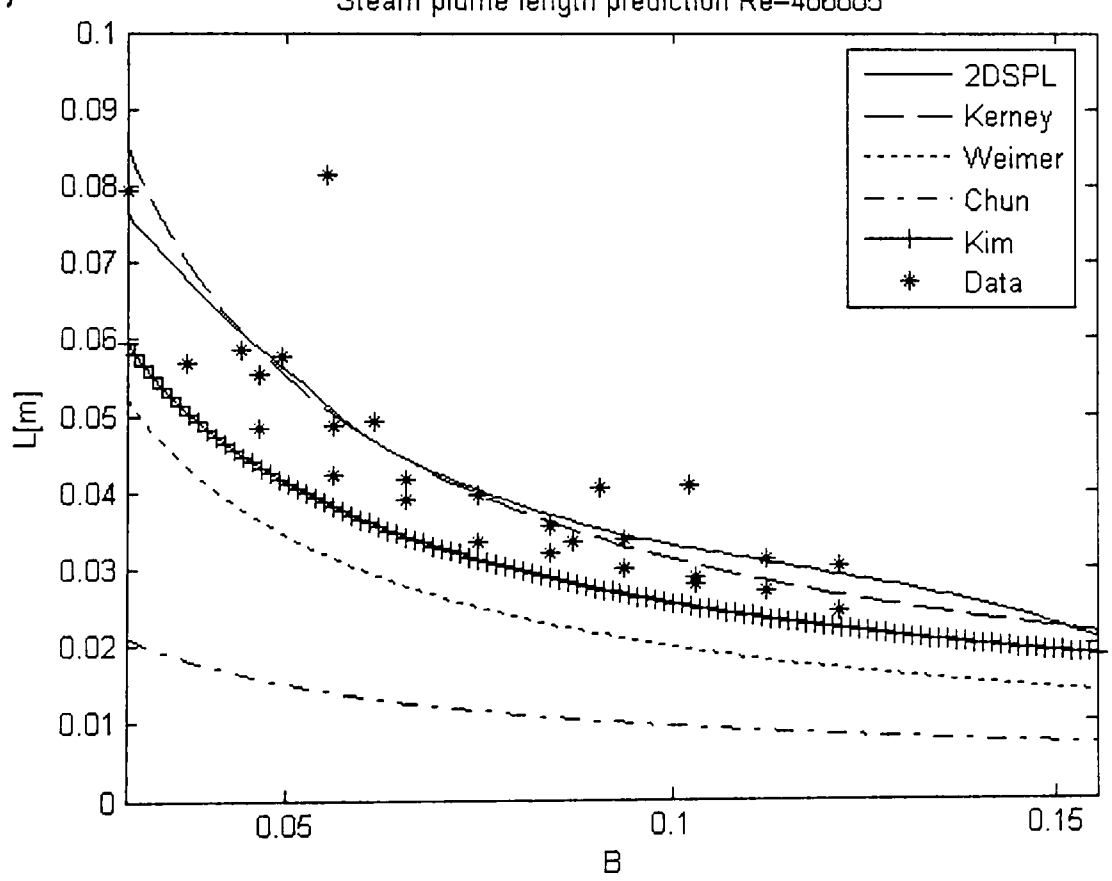

Figure 5.11: Comparison between steam plume length predictions from the new 2DSPL diagram, correlations from Kerney *et al.* [8], Weimer *et al.* [56], Chun *et al.* [45] and Kim *et al.* [14], and experimental data for (a) $Re = 375000$ and (b) $Re = 486885$.

Figure 5.12 shows the comparison between steam plume length predictions from the new 2DSPL diagram, correlations from Kerney *et al.* [8], Weimer *et al.* [56], Chun *et al.* [45] and Kim *et al.* [14], and experimental data for $Re = 650000$. Here steam plume lengths predicted by the new 2DSPL diagram correspond best with experimental data. All semi-empirical correlations from literature under-predict plume lengths for all values of condensation potential.

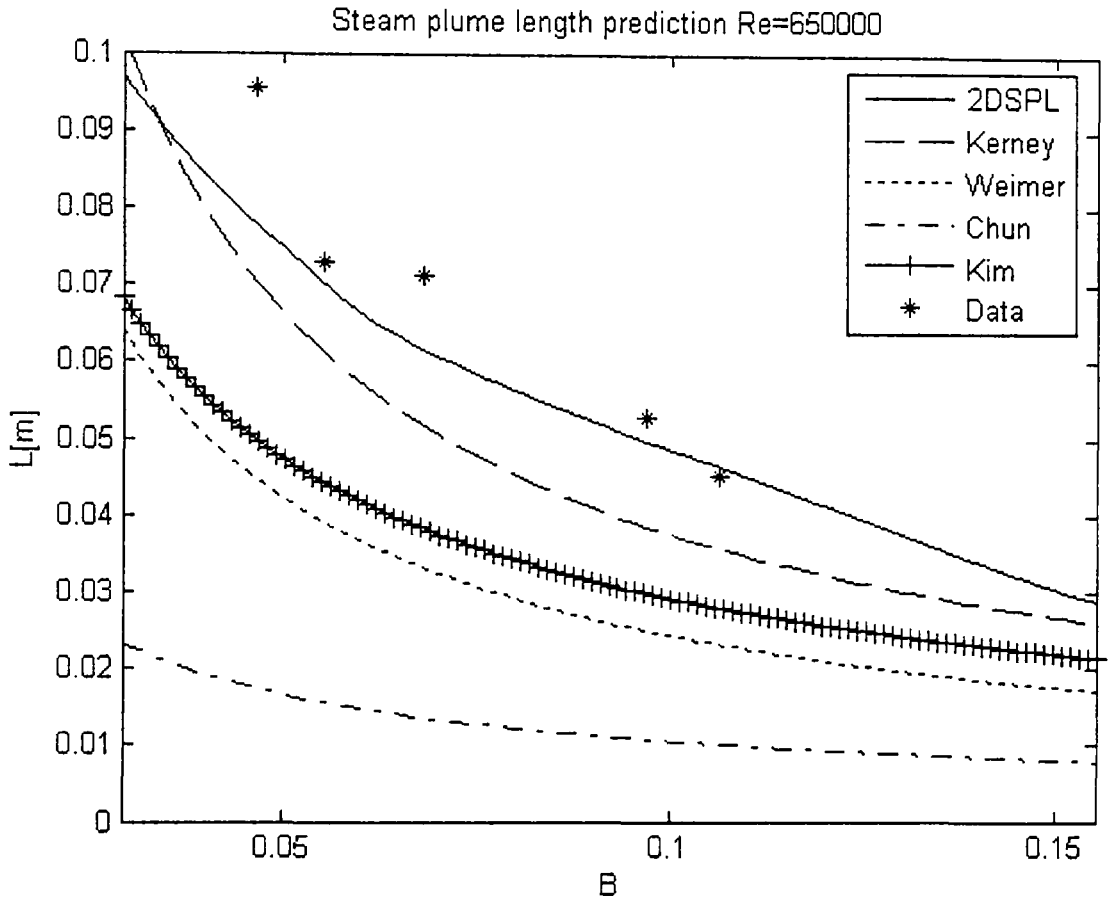

Figure 5.12: Comparison between steam plume length predictions from the new 2DSPL diagram, correlations from Kerney *et al.* [8], Weimer *et al.* [56], Chun *et al.* [45] and Kim *et al.* [14], and experimental data for $Re = 650000$.

At high Reynolds numbers less experimental data is available but a comparison between predictions could still be performed and this is presented in Figures 5.13 and 5.14. Because the predicted steam plume lengths for these flow conditions are longer, note that the vertical axis of these Figures have a greater range than that of Figures 5.10 to 5.12.

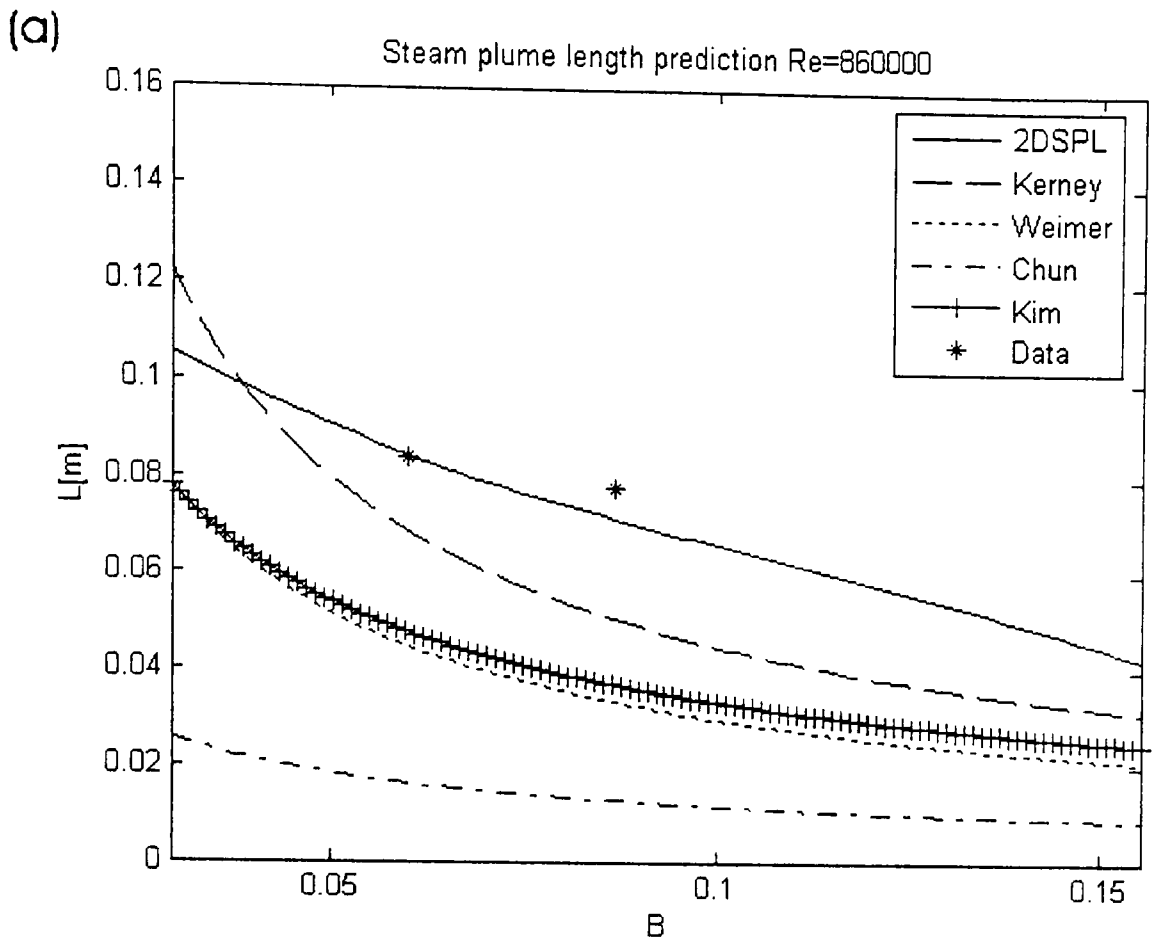

Figure 5.13: Comparison between steam plume length predictions from the new 2DSPL diagram, correlations from Kerney *et al.* [8], Weimer *et al.* [56], Chun *et al.* [45] and Kim *et al.* [14], and experimental data for (a) $Re = 860000$ and (b) $Re = 1050000$.

(a)

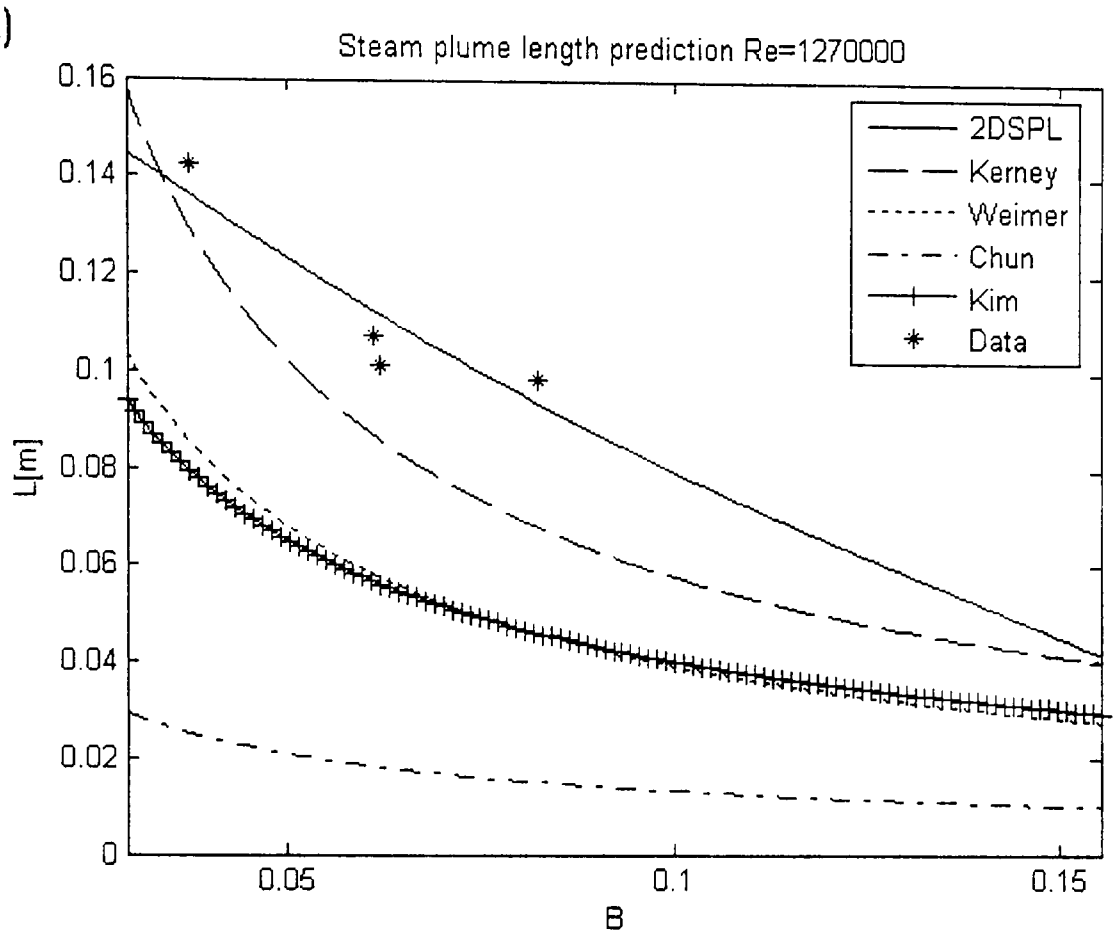

(b)

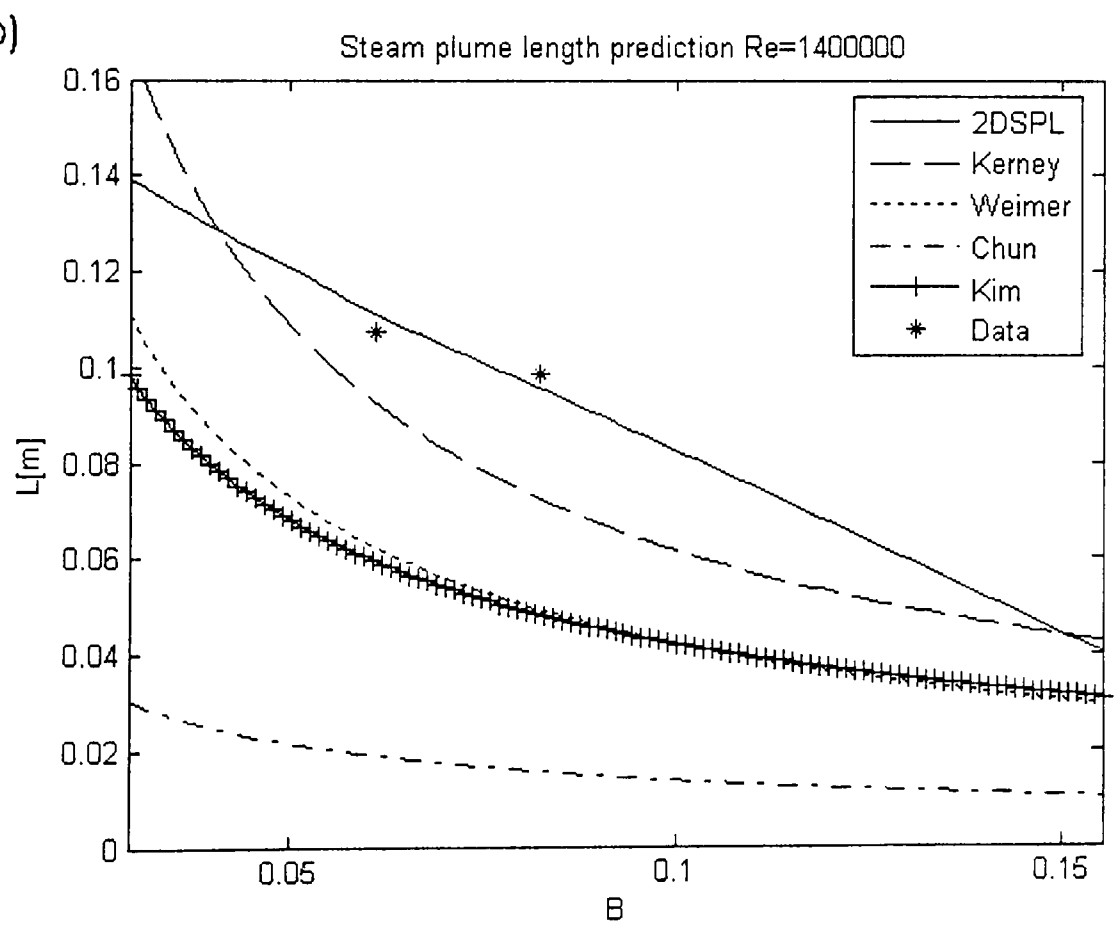

Figure 5.14: Comparison between steam plume length predictions from the new 2DSPL diagram, correlations from Kerney *et al.* [8], Weimer *et al.* [56], Chun *et al.* [45] and Kim *et al.* [14], and experimental data for (a) $Re = 1270000$ and (b) $Re = 1400000$.

Figures 5.13 and 5.14 show, the new 2DSPL diagram gives the best prediction for all chosen Reynolds numbers. The next best is the prediction by Kerney *et al.* [8]. Predictions by Weimer *et al.* [56], Chun *et al.* [45] and Kim *et al.* [14] under predict lengths, where prediction by Chun *et al.* [45] under-predicts the most. Lengths predicted by Weimer *et al.* [56] and Kim *et al.* [14] are similar for all values of condensation potential.

Compared with the plume lengths at low Reynolds numbers (Figures 5.10-5.12), the lengths at high Reynolds numbers (Figures 5.13-5.14) are more linearly dependent on the condensation potential. This is also predicted by the new 2DSPL diagram (Figure 5.5), but the semi-empirical correlations from the literature (Table 5.2) fail to show this difference.

The deviations of measured lengths were calculated for the eight cases presented in Figures 5.10 to 5.14. The average errors are given in Table 5.4.

	% Error in prediction				
Re	2DSPL	Kerney [8]	Weimer [56]	Chun [45]	Kim [14]
164,655	69.7	131.3	46	13.2	119.2
375,000	14.3	14.8	35.7	68	20
486,885	11.8	11.1	35.1	70.3	29.4
650,000	12.2	23.6	51.2	80.3	44.3
860,000	4.1	26.4	51.9	82.1	47.8
1,050,000	6.3	22.5	48.7	82.4	47
1,270,000	6	18.4	45.5	83	47.2
1,400,000	3	19.8	45.8	83.2	47.6

Table 5.4: Calculated errors [%] between data and plume length predictions from the new 2DSPL diagram and semi-empirical correlations from literature for different Reynolds numbers.

Table 5.4 shows that the new 2DSPL diagram gives predictions much closer to data for high Reynolds numbers compared with correlations from the literature. At Reynolds numbers below $500,000 kg/(m^2 s)$ the correlation from Kerney *et al.* [8] gives similar error to that of the new diagram. The error from other correlations is higher for these conditions. At

$Re = 164,655 kg/(m^2 s)$ only the correlation by Chun *et al.* [45] gives a prediction close to experimental results, but the error using correlation by Chun *et al.* [45] is very high for all other Reynolds numbers. This confirms that Chun's work is a little suspect.

To summarize, the developed two-dimensional steam plume length diagram (Figure 5.5) outperforms the semi-empirical correlations from the literature (Table 5.2) for a wide range of flow conditions. The new 2DSPL diagram could still be improved when new experimental data becomes available. This would be of special benefit at high Reynolds numbers.

5.4 2D Steam Plume Length Diagram Applied to DCC in a Water Flow

As seen in the previous section of this chapter, the developed 2DSPL diagram gives good predictions for the injection of steam into a stagnant water. Now the predictions will be compared with experimental observations of steam injected into a water flow. For this purpose the experimental data obtained during the development of the BWT system is used.

When steam is injected into a water flow, the plume is affected by the combined momentum of the injected steam and the water flow. Furthermore, the plume is also affected by the constant suppy of cold water around the steam plume causing the steam to condense faster. Hence, the 2DSPL diagram for an injection of steam into a water flow will probably differ from the 2DSPL diagram for stagnant water.

During the development of the BWT system, experiments were performed in which steam was injected at the centre of a pipe with a steady flow of cold water. The centreline velocity of the water flow just upstream of the point of steam injection was $1.9 m/s$ and temperature difference between injected steam and water flow was $85^0 C$. The diameter of the pipe was much larger than the generated steam plumes. A photograph taken during the experiments and a sketch of the experimental arrangements have already been presented in Figures 4.16 and 4.17. Steam was injected at three different Reynolds numbers through steam injectors with three different diameters $5mm$, $4mm$ and $3mm$. Figures 4.18, 4.19, 4.20 have already shown some plumes generated.

The experiments were repeated several times for each flow condition. Table 5.5 gives average observed plume lengths at different Reynolds numbers. In addition to measuring the plume length with water flow with $4mm$ injector diameter, measurements were also made under the same conditions but with the water flow temporarily stopped to give the stagnant state. A significant increase in a length of a steam plume was observed when there was no flow.

B	Re	$L[m]$	
0.158815	173,934	0.003	water flow
0.158815	217,409	0.0035	water flow
0.158815	434,852	0.007	water flow
0.158815	217,409	0.01	stagnant water

Table 5.5: Observed lengths of steam plume with injection into a water flow. Note the observed length of plume with injection into stagnant water.

The lengths of steam plume given in this Table are compared with predictions using the new 2DSPL diagram in Figure 5.15.

Figure 5.15 shows that the plume lengths are here much shorter when steam is injected into a water flow instead of stagnant water. However, with stagnant water the plume extends and the length is in good agreement with the length proposed by the new 2DSPL diagram.

Calculations show that the length of the steam plume decreased by 60 to 65% for all three Reynolds numbers when steam was injected into a water flow. This shows that the effect of increased condensation due to the constant supply of fresh water is much larger than the momentum effect of the water flow. Hence, heat and mass transfer due to condensation seem to affect the steam plume more than the momentum of the injected steam. This agrees with previous observations where it was found that more steam is needed to achieve jetting in a water flow than in stagnant water.

It is likely that different centreline velocities of water flow would cause different decreases of the steam plume length. Therefore, it is desirable that more experiments should be performed at various condensation potentials, Reynolds numbers and velocities of water flow.

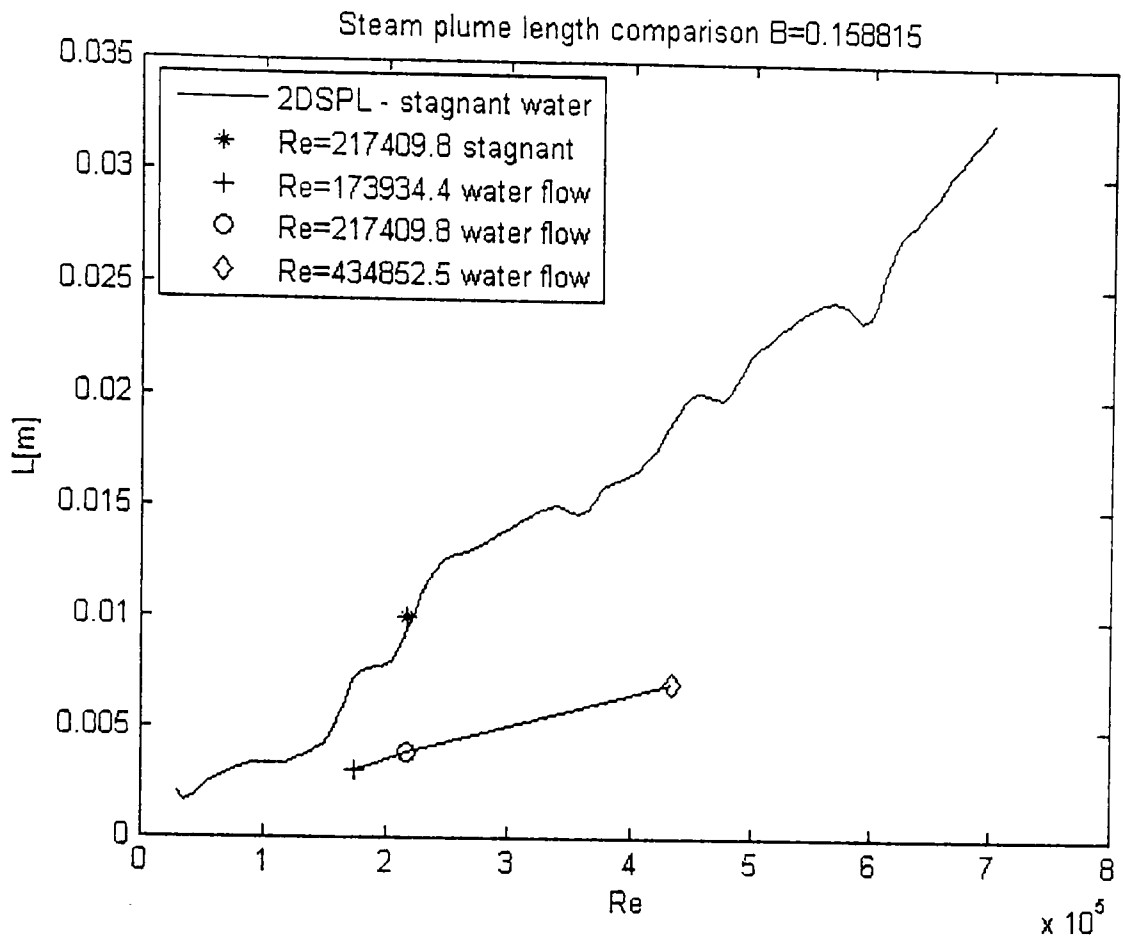

Figure 5.15: Comparison between plume length predictions from new 2DSPL diagram for stagnant water and experimental data for injection into a water flow. Added is also data from experiments for injection into stagnant water.

5.5 Discussion

In this chapter, a new two-dimensional steam plume length diagram for DCC of steam injected into stagnant water has been developed. The diagram is incorporating all steam plume experimental data available to date and is capable of predicting plume length with good accuracy for a wide range of flow conditions. This gives an advantage over the correlations for dimensionless plume length found in literature which can only predict lengths correctly for limited conditions.

The predictions from the new 2DSPL diagram have been compared with those from semi-empirical correlations from the literature. The comparison shows that the 2DSPL diagram accurately predicts lengths at both high and low Reynolds numbers. The semi-empirical correlations were derived from experiments performed at low Reynolds numbers and therefore are

not capable of predicting accurately lengths at high Reynolds numbers. More experimental data to more firmly establish the soundness of the new 2DSPL diagram at high Reynolds numbers would be useful but this would be unlikely to change the general structure of the diagram.

Data for DCC of steam into a water flow showed that the length of the plume decreases in comparison with the no-flow conditions. For a water flow with a centreline velocity of $1.9m/s$ the length decreased by around 60 to 65% for three different Reynolds numbers. Predictions of length using the new 2DSPL diagram over-estimated the plume length by this amount. More experiments should be performed to fully understand the effect of water flow on a steam plume.

6 Modelling of the Steam-Water Interface

One of the most crucial factors in the heat and mass transfer in steam-liquid flows is the shape of the interface which determines the shape of the steam plume in the process of DCC. As discussed in previous chapters, the shape of the steam plume is dependent on the steam and water conditions. For some conditions, the interface evolves smoothly, being of an approximately regular shape throughout as for example in conical and ellipsoidal jetting regimes. For others, the interface consists of small structures which resemble sine waves or irregular fractals superimposed on a regular surface. These plumes are observed in divergent jetting regime and at some conditions in bubbling regime.

This chapter aims to propose a model which can be used for the calculation of the heat transfer coefficient. The model proposed is a mass conservation model for a steam plume. The basic mass conservation model was proposed by Kerney *et al.* [8] and is presented in the Chapter 5 of this thesis. Another aspect of the model is developed in this work.

Furthermore, this chapter also aims to propose various models of the steam-water interface. These models can be used during calculation of the flow characteristics of the process of DCC.

6.1 Literature Review and Data Gathering

Structures of the interface of multiphase flows have been thoroughly investigated in last fifty years [60]-[62]. However, the lack of knowledge about DCC has resulted in very limited information about the steam-water interface and structures occurring on the interface of condensing steam being available.

In order to solve this latter problem, researchers started to investigate the process by introducing steam onto the surface of stagnant [63], slowly moving [47], [64], [65] and turbulent water [66], and onto the liquid film surface [67]-[69]. In some cases, steam was injected at the top of the experimental chamber slowly falling onto the water surface. In other cases, steam was injected on the top of the water surface through the injector positioned parallel to the water surface. In both cases, the velocity of steam in con-

tact with water was very slow reaching a maximum of $0.1m/s$. The mass flow rate of water used during these experiments was up to $250kg/h$. These studies provide some knowledge about the steam-water interface, however they do not provide the information about the interface shape when steam is injected directly into water. In this process, the velocity of the steam is in most cases higher. Moreover, when steam is injected onto the top of the water surface, only part of the steam is condensed in direct contact with the water and the rest condenses in the surrounding air.

Fewer studies were performed for the investigation of the interface at the injection of steam into water. Meier and Yadigaroglu [70] and Yadigaroglu [71] performed an experiment with the injection of steam/air bubbles into water and investigated the possibilities of modelling the bubble interface. However, they assumed that all of the injected steam condenses in the close proximity of the injector and therefore neglected the mass transfer between different phases involved in the process and modelled only air bubble injection into the water.

The most relevant information about the steam-water interface structures can be found in papers by Chun *et al.* [45] and Eden *et al.* [72]. Both papers contain sketches of divergent steam plumes observed during experiments of injection of steam into water but do not give detailed information about the interface structures. However, they show a common trend of structures which form on the interface of a plume in the divergent jetting regime. Figure 6.1 shows two interface shapes presented by Eden *et al.* [72].

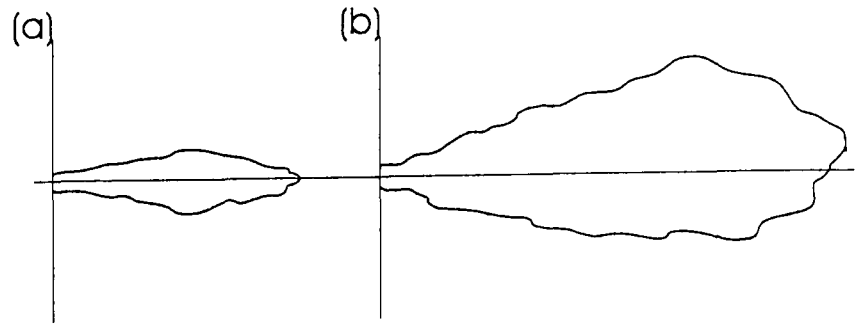

Figure 6.1: Two different divergent plume shapes by Eden *et al.* [72]. (a) $\Delta T = 24^0C$, (b) $\Delta T = 10^0C$

Quite often it is not necessary to retain the full details of the shape of

the interface in order to describe the gross physics and the average geometrical properties are sufficient [4], [73]. The approximated shapes of the steam plume, observed during experiments, have been reported in the form of two-dimensional regime maps [9], [10], [51], [52], [55]. Researchers have reported spherical, hemispherical and ellipsoidal bubbles developed in chugging and bubbling regimes. Conical, ellipsoidal and divergent plumes have been reported to form in jetting regimes. Aya and Nariai [52] proposed cylindrical, spherical and hemispherical shapes as representing shapes of bubbles in the bubbling regime of DCC. Weimer *et al.* [56] reported a possible two-part plume which could develop under some conditions. Here, the first part of the plume is an external steam expansion region, which develops soon after the exit of an injector. It is a narrow region and forms the basis for the second part of the plume which usually takes an ellipsoidal shape.

Some data for a steam plume expansion ratio, which is a ratio between the maximum diameter of the plume and the diameter of the injector, can also be found in the literature such as that published by Simpson & Chan [46] for jetting and bubbling regimes and by Kim *et al.* [14] for the jetting regime only. Arebi and Dempster [57], [74] investigated bubbling of steam into water at low steam inflow rates through multiple injectors $1mm$ in diameter. They measured the radius of developing bubbles and reported that bubbles grow in $15ms$ to a size 3 to $4mm$ in radius when they detach from the injector.

6.2 Development of a Mass Conservation Model for a Steam Plume

When steam is injected into a water a steam plume is generated. Assuming an axially symmetric flow and approximating an unstable interface with a smooth steady surface, a schematic diagram of steam plume is proposed (Figure 6.2). In order to account for conservation of mass, all of the steam injected into the water must condense on and pass through the steam - water interface. Therefore the change of the mass of steam in a plume volume must be equal to the mass of steam which condenses on and passes

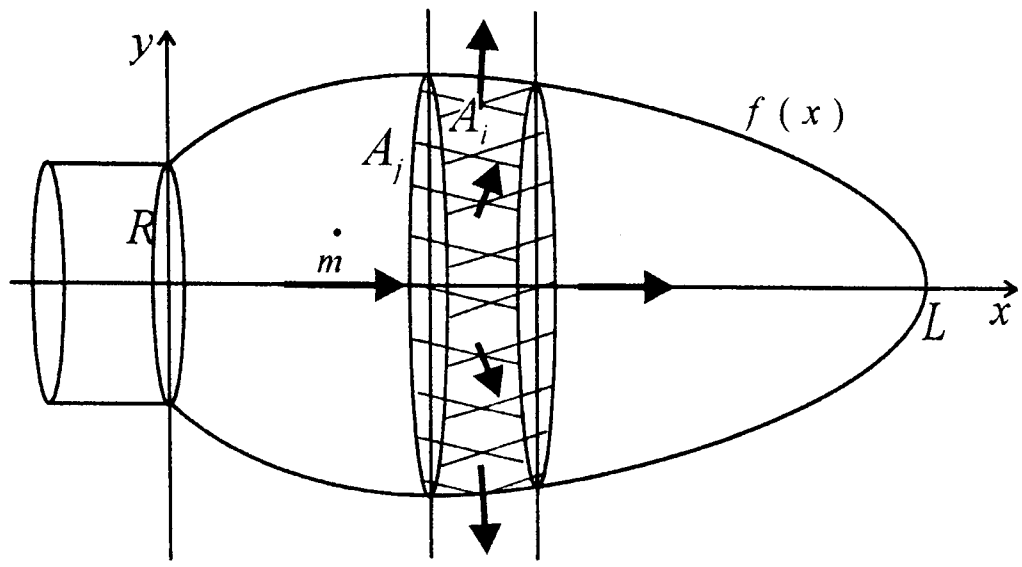

Figure 6.2: Schematic diagram of a steam plume of DCC of steam injected into water. If all the steam condenses through the interface, the change of mass of steam in the volume is equal to the mass of steam, which is condensed through the surface of the same volume.

through a surface of the same volume

$$\rho v\left(x\right) A_j\left(x\right) - \rho v\left(x+\mathrm{d}x\right) A_j\left(x+\mathrm{d}x\right) = \frac{h}{h_{fg}} \Delta T A_i\left(x\right) \ . \tag{6.1}$$

The left hand side of Equation (6.1) can be rewritten using the expression for the rate of change of mass $\dot{m} = \rho v A$

$$\rho v\left(x\right) A_j\left(x\right) - \rho v\left(x+\mathrm{d}x\right) A_j\left(x+\mathrm{d}x\right) = -\dot{m}^{'} \mathrm{d}x \ . \tag{6.2}$$

Furthermore, assuming an axially symmetric steam plume (Figure 6.2), the surface of the volume through which condensation occurs, is calculated as

$$A_i\left(x\right) = 2\pi f\left(x\right) \sqrt{1+f^{'2}\left(x\right)} \mathrm{d}x \ . \tag{6.3}$$

Here the surface of condensation is calculated correctly using the declination of the function. This is in contrast with models used to date [45], [52] which discretised the plume into small cylinders as an approximation of the area.

Assuming a constant temperature difference between steam and water and substituting Equations (6.2) and (6.3) into Equation (6.1), Equation (6.1) can be transformed into an integral equation

$$\int_{\dot{m}_0}^{0} \mathrm{d}\dot{m} = -\frac{h}{h_{fg}} \Delta T 2\pi \int_0^L f\left(x\right) \sqrt{1+f^{'2}\left(x\right)} \mathrm{d}x \ . \tag{6.4}$$

Integration of the integral on the left side of Equation (6.4) and replacing $\dot{m}_0$ with $G_0 \pi D^2/4$ gives

$$G_0 \pi \frac{D^2}{4} = \frac{h}{h_{fg}} \Delta T 2\pi \int_0^L f(x) \sqrt{1 + f'^2(x)} \mathrm{d}x \, . \tag{6.5}$$

Using Equation (6.5), the heat transfer coefficient depends on flow properties as follows

$$h = \frac{G_0 D^2 h_{fg}}{8 \Delta T \int_0^L f(x) \sqrt{1 + f'^2(x)} \mathrm{d}x} \, . \tag{6.6}$$

Following (6.6) the heat transfer coefficient is a function of steam mass inflow rate, size of the injector, temperature difference and size of a plume surface area (6.7).

$$h(h_{fg}, G_0, D, \Delta T, A) = \frac{h_{fg} \pi}{4} \frac{G_0 D^2}{\Delta T A} \tag{6.7}$$

The heat transfer coefficient will decrease inversely with respect to surface area of the plume. Furthermore, Equation (6.7) shows that the heat transfer coefficient is dependent on the diameter of steam injector, which correlations for the heat transfer coefficient from literature fail to predict.

The form of Equation (6.6) is such that it can be easily used for different steam plume shapes defined by function $f(x)$. However, the integral for a plume's surface area can only be found analytically for certain functions. For others, usually more complicated shapes, the surface area can be discretised for calculations on small sections y_v of a function $f(x)$, where

$$y_v = \frac{f(x_{i+1}) - f(x_i)}{(x_{i+1} - x_i)} x + f(x_i) - \frac{f(x_{i+1}) - f(x_i)}{(x_{i+1} - x_i)} x_i \, . \tag{6.8}$$

The surface area of a small section described with y_v is calculated as

$$A_i = 2\pi \int_{x_i}^{x_{i+1}} y_v \sqrt{1 + y_v'^2} \mathrm{d}x \, , \tag{6.9}$$

and the surface area of the whole plume is a sum of small surface areas

$$A = 2\pi \sum_{i=0}^{n-1} I_i \, . \tag{6.10}$$

The single integral I_i is calculated as

$$I_i = \frac{1}{2} (x_{i+1} - x_i) (f(x_{i+1}) + f(x_i)) \sqrt{1 + \frac{(f(x_{i+1}) - f(x_i))^2}{(x_{i+1} - x_i)^2}} \, . \tag{6.11}$$

In Equation (6.10) the declination of the surface is considered while calculating the plume's surface area.

The proposed mass conservation model for a steam plume used to calculate the heat transfer coefficient will give different results for the heat transfer coefficient with different shapes of a steam plume. Different functions describing the shape of a steam plume and corresponding equations for the heat transfer coefficient are listed in the next section. These models for a steam plume shape may also be used in the conjunction with the two-phase system of equations for DCC (Equations (2.10)-(2.15)) for determining the position of the interface.

6.3 Models for Interface with a Smooth Surface

Until now two different shapes of the steam plume have been used by other researchers for calculations. The ellipsoidal shape was used by Chun *et al.* [45] and Simpson & Chan [46], and spherical shape was used by Arebi and Dempster [57]. However, also other steam plume shapes like spherical, hemispherical, conical and divergent have been observed and now for the first time several of such shapes are investigated.

Steam injector surface area

For some conditions in the chugging regime, the steam condenses immediately at the steam injector exit. Therefore, for these conditions, the steam plume can be approximated by a steam injector exit surface area. Using Equation (6.7), corresponding heat transfer coefficient is

$$h = \frac{h_{fg} G_0}{\Delta T} \,. \tag{6.12}$$

Conical steam plume

The conical steam plume is expected in the jetting regime of DCC. The conical shape (Figure 6.3) of a steam plume suggests that condensation along plume is rapid as the shape of a bubble is not formed and the cross-section of the plume is the largest at the pipe exit. The function describing conical steam plume is

$$f(x) = -\frac{R}{L} x + R \,. \tag{6.13}$$

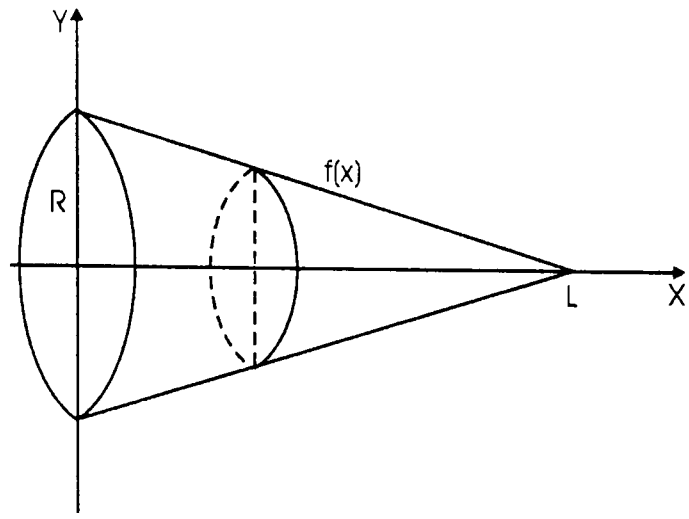

Figure 6.3: Schematic diagram of a conical steam plume.

The corresponding heat transfer coefficient is

$$h = \frac{h_{fg} G_0 D}{2\Delta T L \sqrt{1 + \frac{D^2}{4L^2}}} \,. \tag{6.14}$$

Parabolic Steam Plume

The parabolic shape of a steam plume is expected in the bubbling and jetting regimes. Similarly, as in the conical regime, the cross-section of the plume which is parabolic in shape is the largest at the pipe exit. However, condensation along the plume is not as fast as in a conical plume (Figure 6.4).

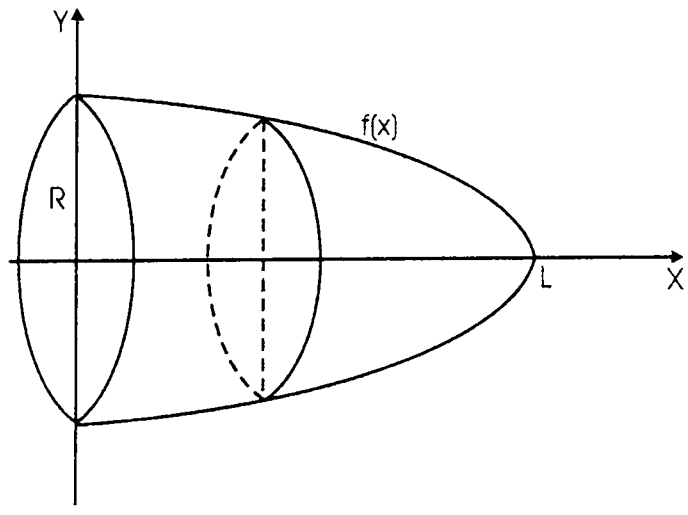

Figure 6.4: Schematic diagram of a parabolic steam plume.

The function describing the parabolic steam plume is

$$f\left(x\right) = R\sqrt{1 - \frac{x}{L}} \tag{6.15}$$

and a heat transfer coefficient

$$h = \frac{24 h_{fg} G_0 D L^2}{\Delta T \left[-D^3 + (D^2 + 16L^2)^{3/2} \right]} . \tag{6.16}$$

Sinusoidal steam plume

The sinusoidal shape may be used to describe the steam plume in the jetting regime. Condensation along the plume is slower than with the parabolic or conical shapes and the plume expands after the injection into water.

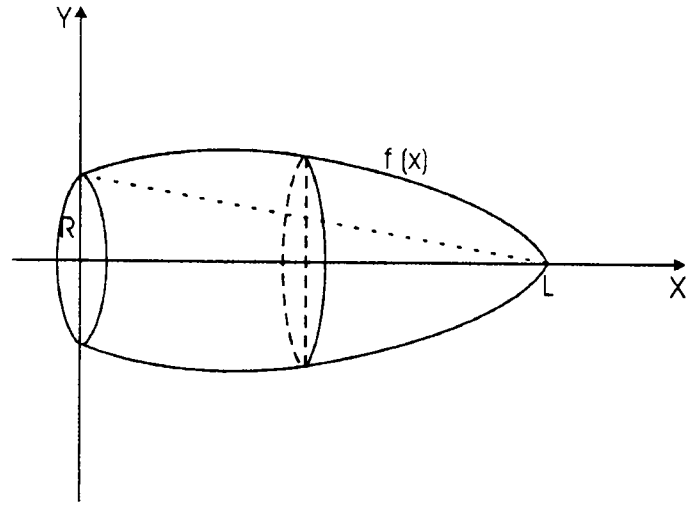

Figure 6.5: Schematic diagram of a sinusoidal steam plume.

The function, describing the plume's shape is

$$f(x) = -\frac{R}{L} x + R + a \sin\left[\frac{\pi x}{L}\right] \tag{6.17}$$

and it is presented in Figure 6.5. The heat transfer coefficient can be calculated using the equations for the discretization of the plume (Equations (6.8)-(6.11)).

Spherical steam plume

The spherical steam plume is expected in the chugging and bubbling regime, if only a small part of a sphere is formed at the injector exit. When half of the sphere or more is formed, condensation is likely to be on the boundary between the bubbling and jetting regimes. A complete spherical bubble is formed behind the injector exit in the bubbling regime. To account for all these different cases, a general function for the spherical plume is considered

$$f(x) = \sqrt{(L-a)^2 - (x-a)^2} , \tag{6.18}$$

where the centre of the sphere can be moved along the x-axis in and out of the injector by a distance a (Figure 6.6).

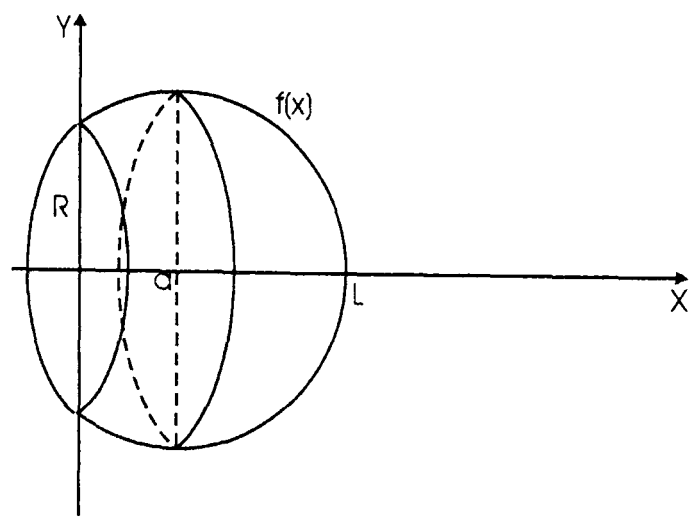

Figure 6.6: Schematic diagram of a spherical steam plume. Centre of the sphere is moved along the x-axis by a distance a.

The heat transfer coefficient for a general spherical bubble is

$$h = \frac{h_{fg} G_0 D^2}{8 \Delta T L \left(L - a\right)} \,. \tag{6.19}$$

Three different cases may occur:

half sphere	$a = 0 \,, L = D/2 \,,$	$h = \frac{h_{fg} G_0}{2 \Delta T} \,,$
section of the sphere	$a \neq 0 \wedge \mid a \mid < R_{sp} \,,$	$h = \frac{h_{fg} G_0 D^2}{\Delta T \left(4L^2 + D^2\right)} \,,$
sphere	$a \geq R_{sp} \,,$	$h = \frac{h_{fg} G_0 D^2}{4 \Delta T L^2} \,.$

The equation for the heat transfer coefficient for a spherical bubble is only valid at an instant when the complete sphere is formed at the injector exit and the amount of steam in the bubble is still dependent on the steam injected through an injector. When bubble detaches from the injector, the heat transfer coefficient should be calculated differently.

Ellipsoidal steam plume

Similar to a spherical steam plume, the ellipsoidal steam plume is observed in the chugging, bubbling and jetting regimes. If only a small part of the ellipsoidal plume is formed at the injector exit, condensation is in the chugging

or bubbling regime. If half of the ellipsoidal or more is formed, condensation is in the jetting regime. If the complete ellipsoid is formed behind the injector exit, condensation is in the bubbling regime. Condensation along the plume is slower than with conical and parabolic plume shape. To account for all these different cases, a general function for an ellipsoidal plume is considered

$$f(x) = y_m \sqrt{1 - \frac{(L-a)^2}{(x-a)^2}}\,, \tag{6.20}$$

where the centre of the ellipsoid can be moved along the x-axis in and out of the injector exit by a distance a

$$a = \frac{D^2 L - 4y_m^2 L \pm 2y_m L\sqrt{4y_m^2 - D^2}}{D^2}\,.$$

Parameter $y_m = r_p R$ represents the maximum radius of the ellipsoid (Figure 6.7).

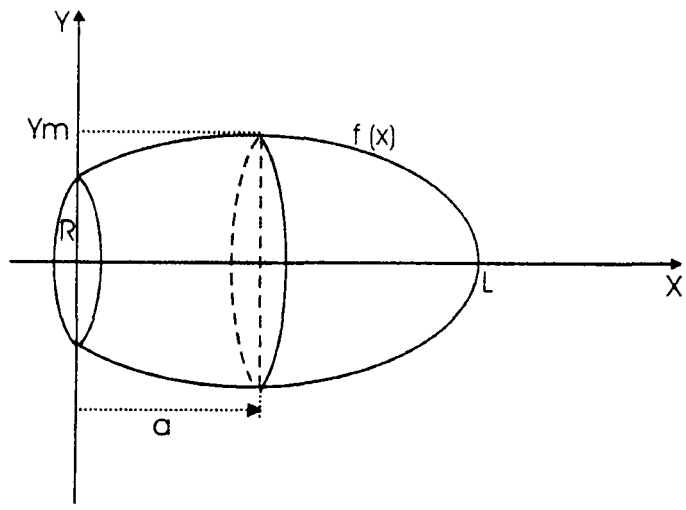

Figure 6.7: Schematic diagram of an ellipsoidal steam plume. Centre of the ellipsoid is moved along the x-axis by a distance a.

The heat transfer coefficient can be calculated using the equations for the discretization of the plume (Equations (6.8)-(6.11)).

Divergent steam plume

The divergent steam plume is observed in the divergent jetting regime. If the surface of the plume is approximated by a smooth surface (Figure 6.8), the divergent steam plume can be described by two linear functions

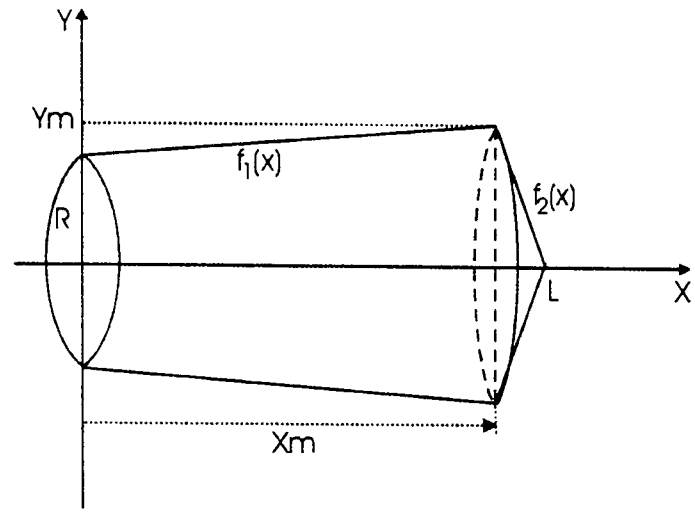

Figure 6.8: Schematic diagram of a divergent steam plume.

$$\begin{aligned} f_1 &= \frac{y_m - R}{x_m} x + R \,; & x &\in (0, x_m) \\ f_2 &= \frac{y_m}{x_m - L} x - \frac{y_m L}{x_m - L} \,; & x &\in (x_m, L) \end{aligned} \tag{6.21}$$

where $y_m = r_p R$ is the maximum radius of the plume and $x_m = l_p L$ is the distance from the injector, where the plume converges toward the centreline. The heat transfer coefficient for a divergent plume is

$$h = \frac{h_{fg} G_0 D^2}{4\Delta T \left[(y_m + R) \sqrt{x_m^2 + (y_m - R)^2} + y_m \sqrt{y_m^2 + (L - x_m)^2} \right]} \,. \tag{6.22}$$

Two-part steam plume

During the development of the plume in the bubbling or jetting regime, the plume sometimes takes a two-part shape, where the first part of the plume can be approximated by a cylinder or a cone and the second part of the plume by an ellipsoidal or sinusoidal bubble. Figure 6.9 shows two possible two-part steam plumes. The plume is described by equations

$$\begin{aligned} f_1 &= \frac{y_m - R}{x_m} x + R \,; & x &\in (0, x_m) \\ f_2 &= \frac{y_m}{x_m - L} (x - L) + a \sin \left[\frac{\pi x}{L - x_m} - \frac{\pi x_m}{L - x_m} \right] \,; & x &\in (x_m, L) \end{aligned} \tag{6.23}$$

for a sinusoidal second part, or by equations

$$\begin{aligned} f_1 &= \frac{y_m - R}{x_m} x + R \,; & x &\in (0, x_m) \\ f_2 &= r_m \sqrt{1 - \frac{(x - x_m - a)^2}{(L - x_m - a)^2}} \,; & x &\in (x_m, L) \end{aligned} \tag{6.24}$$

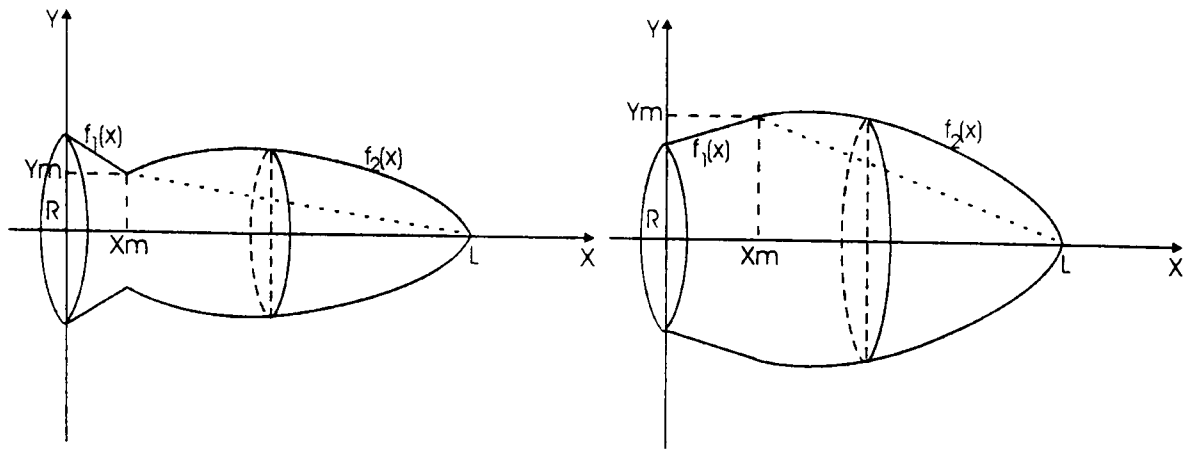

Figure 6.9: Schematic diagrams of two possible two-part steam plume.

for an ellipsoidal second part. The heat transfer coefficient can be calculated using the equations for the discretization of the plume (Equations (6.8)-(6.11)).

6.4 Models for Interface with Irregular Structures

Irregular steam plume shapes occur at certain inflow conditions. The most noticeable of these occur in the divergent jetting regime. When only an approximation of a flow field is needed, the numerical calculation of the two-phase equations for DCC (Equations 2.10- 2.15) can be performed using an approximation of the divergent plume (Equation (6.21)). From Equation (6.7) it can be seen that the heat transfer coefficient is inversely dependent on the steam plume surface area. Any additional small structures superimposed on the original surface would increase the surface area. Therefore, the heat transfer coefficient of the plume with additional structures would be smaller than the coefficient of the original plume. On the other hand, the formation of small structures and bubbles would act as a two-phase blanket around the interface and hinder the resupply of a cold liquid to the surface. This would reduce the efficiency of the heat transfer process. From the point of view of analysing the process, quite often it is not necessary to retain the full details of the shape of the interface in order to describe the gross physics and the average geometrical properties are sufficient [4]. Therefore, the averaged surface of the plume used during calculations is likely to give better approximation of the heat transfer coefficient than the irregular wavy surface and detailed modelling of the small structures of the

interface in order to calculate the heat transfer coefficient is not necessary [73]. However, for a more detailed calculation of the two-phase system of equations for DCC (Equations 2.10- 2.15), wavy structures should be added onto the surface of the plume in order to simulate the shape irregularities [72].

In this section a way of modelling interfacial structures will be discussed. In general, modelling of complex forms is performed in order to construct formations with appropriate statistical features [75]. Due to the lack of knowledge about the interface developed in DCC, construction of the model for interfacial structures is not possible. Therefore, this section is aimed to demonstrate a method for the creation of structures by presenting examples of possible irregular steam plume shapes.

To simulate a periodic oscillation of the interface, different periodic signals can be superimposed on the function defining the steady state plume surface. Some of the possible periodic signals are a square signal, a triangular signal, a saw-tooth signal and a sinusoidal signal. The one that is closest to the shape of the divergent plume observed during experiments and presented in the literature [72] is the sinusoidal signal. The choice for a sinusoidal signal allows construction of any arbitrary flow structure. Nevertheless, it is the selection of a suitable series of sinus signal which will determine if the superimposed waves hold close agreement with experimental observations.

The steady state plume surface was chosen to be divergent in shape and was constructed using data from the literature and correlations for the divergent plume given in Equations (7.8) and (7.9) with $D = 0.01m$, $L = 0.135m$, $x_m = 0.11m$ and $y_m = 0.021m$. Different functions may now be superimposed on the steady state surface using a rotation and translation of data [76], [77].

The first is a basic sine function as for example one presented in Equation (6.25).

$$f(x) = \frac{R}{3} \sin\left(\frac{7\pi x}{L_1 + L_2}\right) \tag{6.25}$$

Parameters L_1 and L_2 represent lengths of the two linear functions describing the steady state plume surface between the points $(0, R)$ and (x_m, y_m), and (x_m, y_m) and $(L, 0)$ (Figure 6.8).

Figure 6.10 shows the constructed steam plume using the Equation (6.25). Added to the Figure is a graph of the corresponding absolute value of the fluctuation Δ, where

$$\Delta(x) = |y_s(x) - y_a(x)|. \tag{6.26}$$

In Equation (6.26), $y_s(x)$ represents the value of a sine function after the translation and rotation and $y_a(x)$ the value of linear functions describing the steady state plume surface.

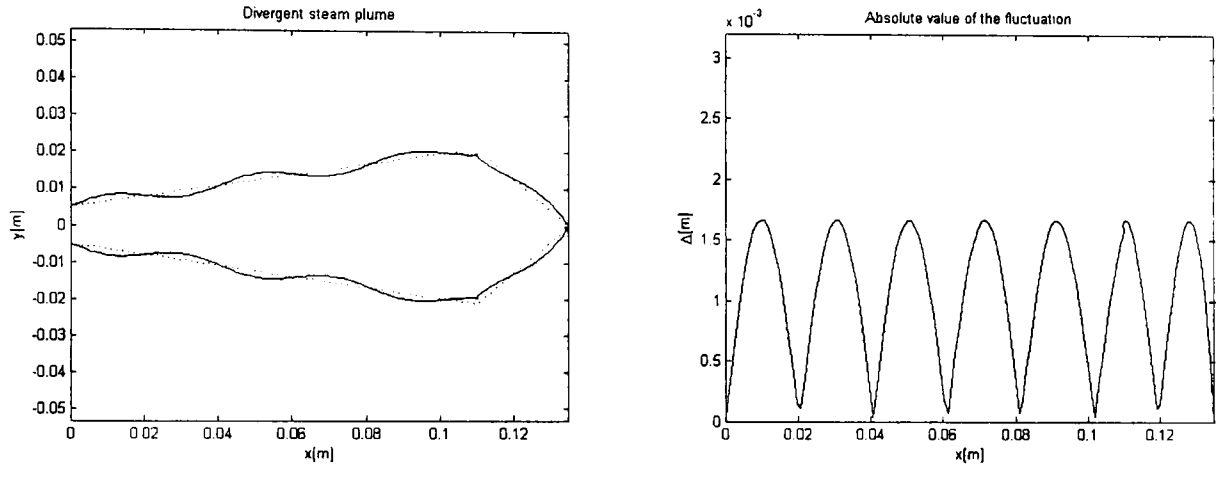

Figure 6.10: Left: Divergent steam plume shape with periodic structures generated by using the Equation (6.25). Right: The corresponding absolute value of the fluctuation.

With increased complexity of the sinus signal a more complicated interface can be constructed. Figures 6.11 and 6.12 show two different steam plume shapes generated by superimposing two combinations of two different sine functions.
Steam plume shape in Figure 6.11 was generated using the Equation (6.27)

$$f(x) = \frac{R}{3}\sin\left(\frac{7x\pi}{L_1 + L_2}\right) + \frac{R}{5}\sin\left(\frac{15x\pi}{L_1 + L_2}\right) \tag{6.27}$$

and Equation (6.28) was used to construct the plume presented in Figure 6.12.

$$f(x) = \frac{R}{3}\sin\left(\frac{7x\pi}{L_1 + L_2}\right) + \frac{R}{5}\sin\left(\frac{5x\pi}{L_1 + L_2}\right) \tag{6.28}$$

The first part of functions in both combinations (6.27) and (6.28) is the

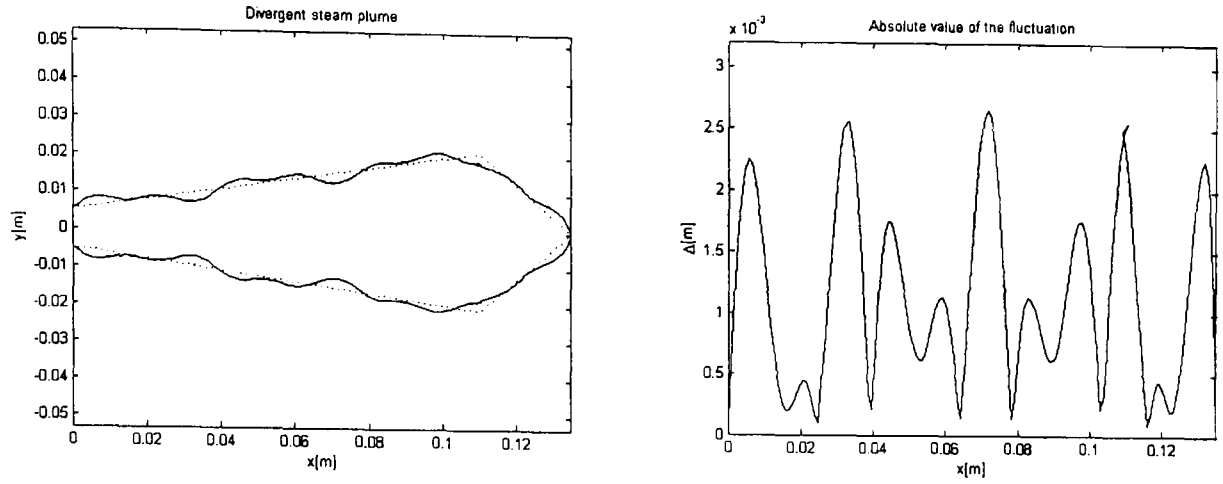

Figure 6.11: Left: Divergent steam plume shape with periodic structures generated by using the Equation (6.27). Right: The corresponding absolute value of the fluctuation.

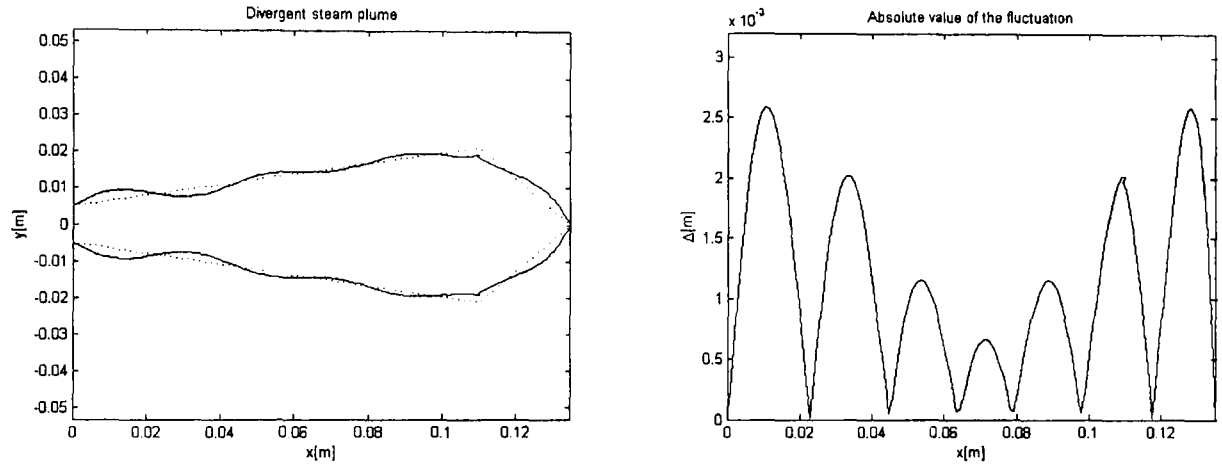

Figure 6.12: Left: Divergent steam plume shape with periodic structures generated by using the Equation 6.28. Right: The corresponding absolute value of the fluctuation.

same as the function in Equation (6.25). The second parts of Equations (6.27) and (6.28) have equal amplitudes but different wave lengths.

To achieve an even greater complexity of fluctuation, a series of three or more sine functions can be superimposed on the steady state steam plume shape. An example of a function using the sum of three sine functions is presented in Equation (6.29).

$$f(x) = \frac{R}{3}\sin\left(\frac{7x\pi}{L_1 + L_2}\right) + \frac{R}{5}\sin\left(\frac{30x\pi}{L_1 + L_2}\right) + \frac{R}{7}\sin\left(\frac{50x\pi}{L_1 + L_2}\right) \quad (6.29)$$

Figure 6.13 shows a divergent steam plume shape with structures generated using Equation (6.29). The corresponding absolute value of the fluctuation.

graph of which is added to the Figure 6.13, resembles a chaotic fluctuation.

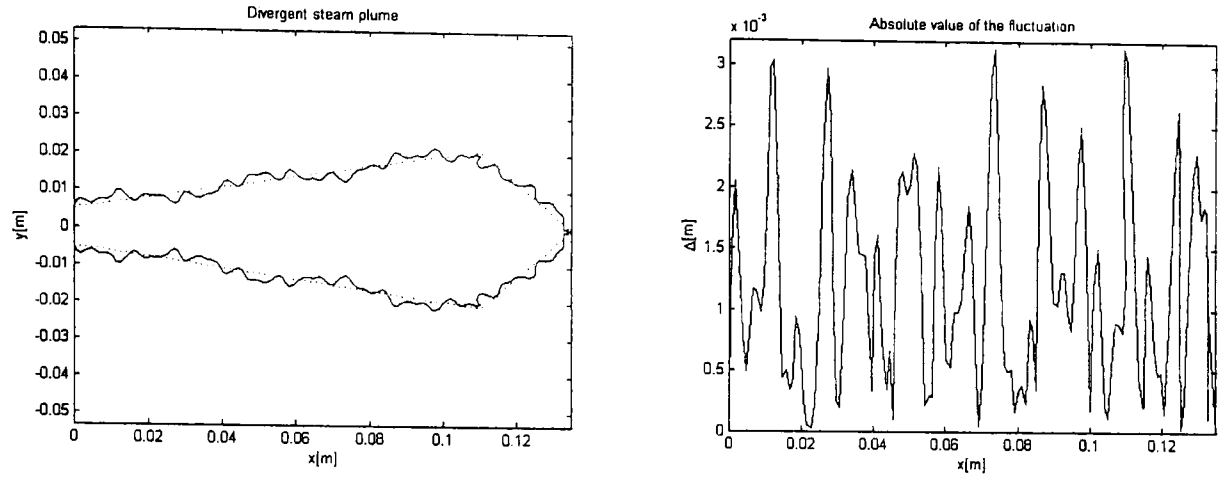

Figure 6.13: Left: Divergent steam plume shape with periodic structures generated by using the Equation 6.29. Right: The corresponding absolute value of the fluctuation.

An infinite number of different functions constructed using sinusoidal signal is available. Here, four different examples were chosen (Equations 6.25-6.29) in order to demonstrate the method of using sinusoidal signal for the construction of the steam plume shape which resembles the shapes observed at experiments.

To simulate a non-periodic oscillation imposed on the interface, a non-periodic function can be superimposed on the original divergent function representing the steady state plume. One can be a random signal, which is the simplest means of generating a non-periodic shape [75]. This signal can be superimposed on the function over a chosen interval of the original function. The width of the interval defines the maximum amplitude of the generated fluctuation.

Figure 6.14 shows an example of a generated divergent steam plume shape with a non-periodic structure and the corresponding absolute value of the fluctuation. The steady state steam plume shape has been made equal to the one used to generate periodic structures.

Non-periodic structures may also be added to the periodic structures on the interface. The steam plume shape in Figure 6.15 was generated by adding a non-periodic signal over a chosen interval around the steam plume

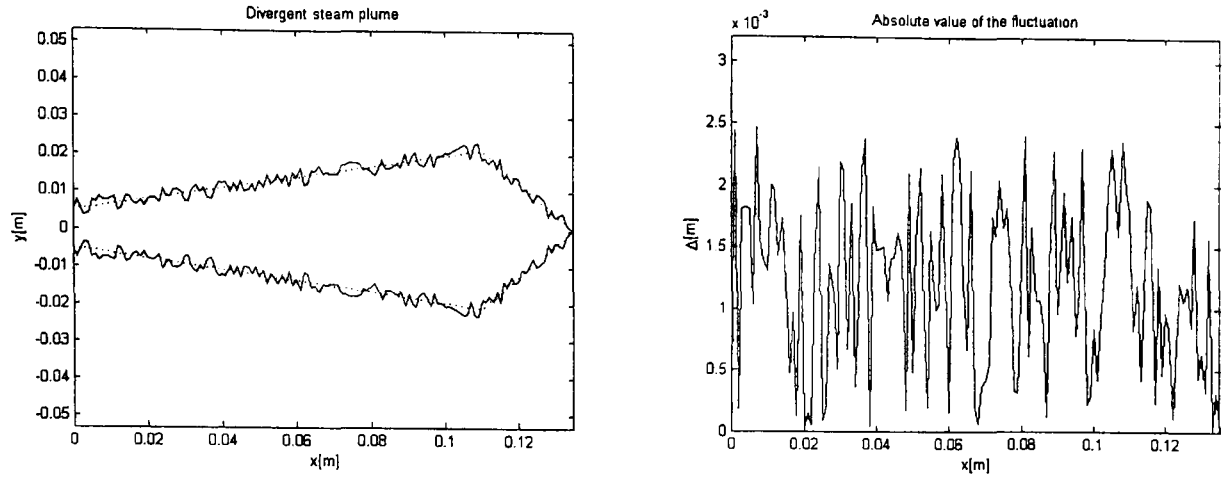

Figure 6.14: Left: Divergent steam plume shape with non-periodic structures. Right: The corresponding absolute value of the fluctuation.

shape presented in Figure 6.10. A graph of the corresponding absolute value of the fluctuation has been added to the Figure.

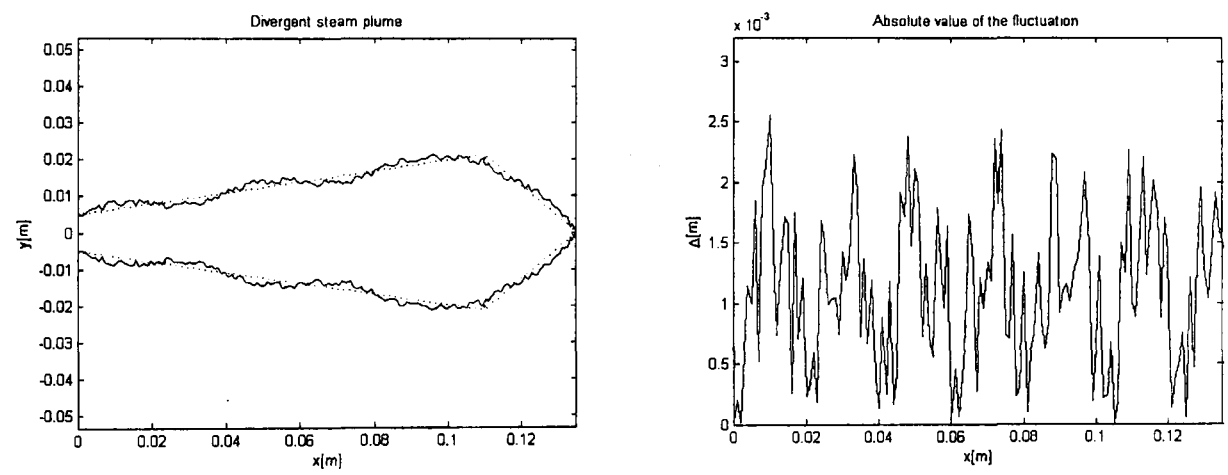

Figure 6.15: Left: Divergent steam plume shape with non-periodic structures superimposed on periodic structures. Right: The corresponding absolute value of the fluctuation.

6.5 Discussion

In this chapter a mass conservation model for a steam plume was proposed. The model can be used for the calculation of the heat transfer coefficient if the geometry of the plume is known.

In addition a number of different models for an interface with a smooth surface was proposed. These can be used in a mass conservation model

for calculation of the heat transfer coefficient. Furthermore, models can be used for the identification of the position of the interface when the system of equations for a two-phase flow is applied to model the process of DCC.

Irregular interfacial structures have been observed at certain inflow conditions. These are dominated by turbulence and can vary from large-scale structures to small-scale structures. Detailed turbulence modelling is required to model these structures, which is beyond the work presented in this thesis. Therefore, this chapter was aimed to find an alternative way of presenting the steam plume shape with irregular structures on the interface.

Irregular shape of the interface can be modelled by superimposing fluctuations on a smooth surface. The method for creation of the interface with irregular structures was discussed. Some possible examples of created plumes were presented. These show some similarities with the observed divergent steam plumes. Lack of information about the steam-water interface structures prevents the formation of a reliable model describing these structures. However, the present section shows, that by adding appropriate periodic and non-periodic signals to the initial shape of the interface, a wavy shape of the interface could be simulated. The experimental data is needed which would configure this method.

7 Identification of the Heat Transfer Coefficient in DCC

The new 3DCR diagram and the new 2DSPL diagram are essential when modelling the DCC process; however, they are not sufficient. In addition, a heat transfer coefficient, the criterion controlling the rate of heat transfer from steam to water, is needed.

The heat transfer coefficient is difficult to detect and measure during experiments and therefore only a limited amount of information about the heat transfer coefficient is provided in the literature. The difficulty of calculating the heat transfer coefficient is that it depends in a complicated way on many variables, including the fluid properties, the flow velocity, the value of the characteristic temperature difference, and the surface temperature distribution [78]. For example, adding non-condensable gases to the steam reduces the rate of condensation of steam by DCC, but a higher velocity of the steam relative to the water velocity increases the rate of condensation. Also, many variables which affect the heat transfer coefficient lead to a space and time dependent heat transfer coefficient. Therefore, ways of predicting the over-all heat transfer coefficient, which combines the influence of different effects, must be proposed.

This chapter aims to identify a new way of obtaining the heat transfer coefficient in order to propose the prediction for the coefficient for a wide range of environmental conditions. To achieve this the new 3DCR and 2DSPL diagrams, and the mass conservation model developed in this work will be used.

7.1 Literature Review and Data Gathering

The heat transfer coefficient is a ratio between a heat flow rate and the product of a characteristic area and a characteristic temperature difference. The difficulty here is to determine the heat transfer coefficient of the process. The available information about the coefficient has been gathered from the literature.

The heat transfer coefficient during condensation on the water interface can be calculated from the rate of molecules arriving onto and departing

from the interface (Equation (2.3)). However, Equation (2.3) can only predict the local heat transfer. Furthermore, the value of the heat transfer coefficient falls to lower values than predicted by the Equation (2.3) in a few milliseconds of the start of the process due to the increase in the local temperature of the surrounding water in close vicinity of the interface [19].

Researchers until now have used different approaches to find the heat transfer coefficient for different conditions of DCC. In 1991, Aya and Nariai [55] collected information about the heat transfer coefficient available in the literature which were presented by Young *et al.* [79], Tsai [80], Kozeki [81] and Fukuda [82]. Using this information Aya and Nariai [55] presented a diagram of heat transfer coefficient for different types of DCC that is given in Figure 7.1. From this diagram it can be seen that a heat transfer coefficient for DCC of steam injected into water is higher than that for other types of DCC.

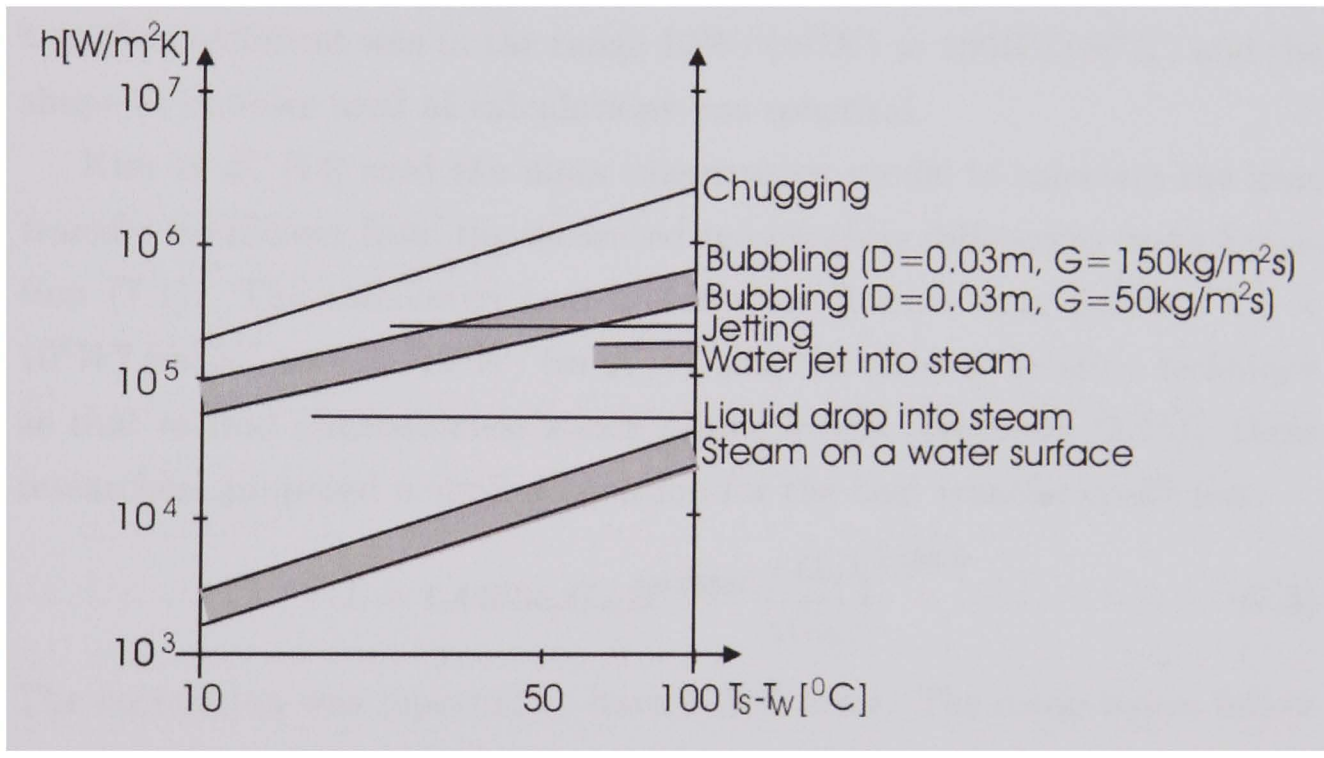

Figure 7.1: Diagram for the heat transfer coefficient for different types of DCC presented by Aya and Nariai [55].

Other researchers derived correlations for the heat transfer coefficient. Kim and Song [58] used the kinetic theory of molecules to describe the heat transfer coefficient taking into account a wavy interface surface, which enhances heat transfer. Simpson and Chan [46] calculated the heat transfer

coefficient from conservation of mass equation

$$h = \frac{\dot{m} h_{fg} A_0}{\Delta T A_p} , \tag{7.1}$$

where A_0 represents the surface area of the injector exit and A_p the surface area of the plume. They used Equation (7.1) to calculate the heat transfer coefficient from temperature differences measured during experiment. The shape of the plume, used during their calculations was assumed to be ellipsoidal. Calculated heat transfer coefficients ranged between $15 \times 10^4 W/(m^2 K)$ and $70 \times 10^4 W/(m^2 K)$.

The same approach was used by Arebi and Dempster [57], who presented a time dependent heat transfer coefficient for observed growing bubbles

$$h = \frac{\Delta V \rho_s h_{fg}}{\Delta T \Delta t A_b} , \tag{7.2}$$

where A_b represents time dependent surface area of a bubble. The heat transfer coefficient was in the range $10 W/(m^2 K)$ to $100 W/(m^2 K)$ and the shape of bubbles used at calculations was spherical.

Kim *et al.* [14] used the mass conservation model to calculate the heat transfer coefficient from the measured temperature differences using Equation (7.1). The calculated heat transfer coefficients were between $1.5 \times 10^6 W/(m^2 K)$ and $2 \times 10^6 W/(m^2 K)$. Using the same correlation technique as that to find dimensionless steam plume length (Equation (5.15)), these researchers proposed a similar equation for the heat transfer coefficient.

$$h = 1.4453 c_p G_m B^{0.03587} \left(\frac{G_0}{G_m} \right)^{0.13315} . \tag{7.3}$$

The correlation was reported to have a 20% error. The mean steam inflow rate was $G_m = 275 kg/(m^2 s)$.

The same approach was taken by Chun *et al.* [45]. Their heat transfer coefficients range between $1 \times 10^6 W/(m^2 K)$ and $3.5 \times 10^6 W/(m^2 K)$, and their correlation for the heat transfer coefficient, which has a 30% error, was based on the equation

$$h = 1.3583 c_p G_m B^{0.0405} \left(\frac{G_0}{G_m} \right)^{0.3714} . \tag{7.4}$$

Kim *et al.* [13] wanted to improve the correlation from Equation (7.3) and reported that the heat transfer coefficient is a function of the eddy size

and the steam plume shape. To account for an unstable interface, they used a theory of single phase jets and presented the improved correlation for the heat transfer coefficient

$$h = 0.1409 \left(\frac{k_w}{\nu_w} \frac{c_p}{\rho_s} \frac{1}{4 - 2\eta} \right)^{0.5} B^{0.33} \left(\frac{G_0}{G_m} \right)^{0.8278} . \tag{7.5}$$

Parameters k_w and ν_w represent thermal conductivity and kinematic viscosity of water respectively. Parameter η represents a plume shape factor defined by researchers which is 1 for a conical plume and 0.8 for an ellipsoidal plume. The measured heat transfer coefficient reported by Kim *et al.* [13] ranged between $1 \times 10^6 W/(m^2 K)$ and $2 \times 10^6 W/(m^2 K)$.

The heat transfer coefficient cannot be measured directly during experiments so it must be calculated from measurements of parameters such as water subcooling and steam plume size and shape. Until now, different methods of calculation have been used in combination with approximated shapes of plume. Despite there being many different shapes that have been observed, only two approximated shapes have been used in calculations for various inflow conditions. Therefore, the proposed correlations can only predict the heat transfer coefficient accurately for a limited range of flow conditions.

7.2 Development of a 3D Heat Transfer Coefficient Diagram

Only a small amount of data for the heat transfer coefficient exists in the literature and for this study practically all has been collected. In spite of this, no correlation similar to the correlation for a plume length data (Figure 5.3) has been found to be possible so other means of predicting the heat transfer coefficient must be used.

As part of this study, the heat transfer coefficient has been calculated using the mass conservation model (Equation (6.6)) for a wide range of flow conditions. Different interfacial shape models proposed in Chapter 6 are used in the model and specific shapes can be allocated to different regimes. Conditions at which different shapes are used, can be read from the new 3DCR diagram. In addition, the new 2DSPL diagram and data for steam plume radius expansion can be used to obtain the length and the maximum

radius of the plume needed for the calculation. By using the corresponding geometry of the plumes at specific flow conditions (G_0, D, ΔT) in the mass conservation model (Equation (6.6)), the heat transfer coefficients can be calculated for a wide range of flow conditions and presented as a three-dimensional diagram. Different regimes of condensation are expected to have different heat transfer coefficients so the heat transfer coefficient diagram has the same axes as the 3DCR diagram. These are the extent of water subcooling, the steam inflow rate and the diameter of the injector.

Interfacial condensation oscillation occurs at very low steam inflow rates ($G_0 < 5kg/\left(m^2s\right)$). The steam water interface is pushed forwards and backwards in the steam injector and changes its shape from the circular shape of the steam injector exit area to an irregular shape, where water penetrates into the steam area. Therefore, here the heat transfer coefficient is strongly time dependent. However, the averaged interface shape is considered to be the shape of the steam injector exit area. This is also the shape used in the mass conservation model, to calculate the heat transfer coefficient of the interfacial condensation oscillation (Equation (6.12)).

At steam inflow rates up to $200kg/\left(m^2s\right)$, chugging and bubbling regimes occur. In these two regimes, the steam plume also constantly changes its shape. Also, in the bubbling regime the surface of the interface is not smooth. An unstable interface results in the breaking off of bubbles from the main plume. All this suggests a time dependent heat transfer coefficient which does not converge towards a certain value in time, but continues to change during the process. However, an average steam plume shape can be identified and an average heat transfer coefficient calculated for both regimes. For the chugging regime, an average steam plume shape is a small section of a sphere and the heat transfer coefficient can be calculated using the second variation of Equation (6.19).

An average steam plume shape for the bubbling regime is a section of an ellipsoid (Equation (6.20)). The expansion or maximum radius of the ellipsoidal (y_m) is dependent on conditions of the process, like steam inflow rate and water subcooling. Data from Simpson & Chan [46] for the expansion rate was used to identify the dependance. The correlation

obtained for the expansion of the plume is

$$y_m = 120.3DG_0^{0.4}\Delta T^{-1.5} \,. \tag{7.6}$$

This correlation has been used for the calculation of the heat transfer coefficient of the bubbling regime.

On the boundary between bubbling and jetting regimes, a plume of half the sphere is expected. To test this expectation, flow conditions at which the length of the steam plume is the same as one half of the steam injector diameter were identified from the two-dimensional steam plume length diagram. Data for the identified conditions was added to the three-dimensional condensation regime diagram in a form of the surface that runs through all of the identified conditions. Figure 7.2 shows the diagram with the half-sphere surface added in a grey colour.

From the Figure 7.2 it can be seen that the generated surface almost exactly covers the surface representing the boundary between the bubbling and jetting regimes, shown on the diagram in the yellow colour. This confirms that the assumption of a semi-spherical steam plume on this border is correct. Furthermore, Figure 7.2 also confirms that the new three-dimensional condensation regime diagram and the new two-dimensional steam plume length diagram are compatible. Therefore, combining information from them for the purpose of calculating the heat transfer coefficient using the mass conservation model is valid.

In the conical and ellipsoidal jetting regimes, the steam plume takes on its final shape with an almost smooth surface within the first milliseconds of the process. With these regimes, the heat transfer coefficient converges quickly towards its final value and it can be calculated using the observed shapes of the plume. For conditions on the boundary between bubbling and jetting, a half sphere shape was used in a mass conservation model (the first variation of Equation (6.19)). Under conditions for conical jetting, a conical shape was used in the model and the heat transfer coefficient was calculated using the Equation (6.14).

Under conditions for ellipsoidal jetting, a section of the ellipsoid (Equation (6.20)) was used in the mass conservation model for calculating the heat transfer coefficient. Similar to the bubbling regime, the expansion of a plume at ellipsoidal jetting regime depends on water subcooling and steam

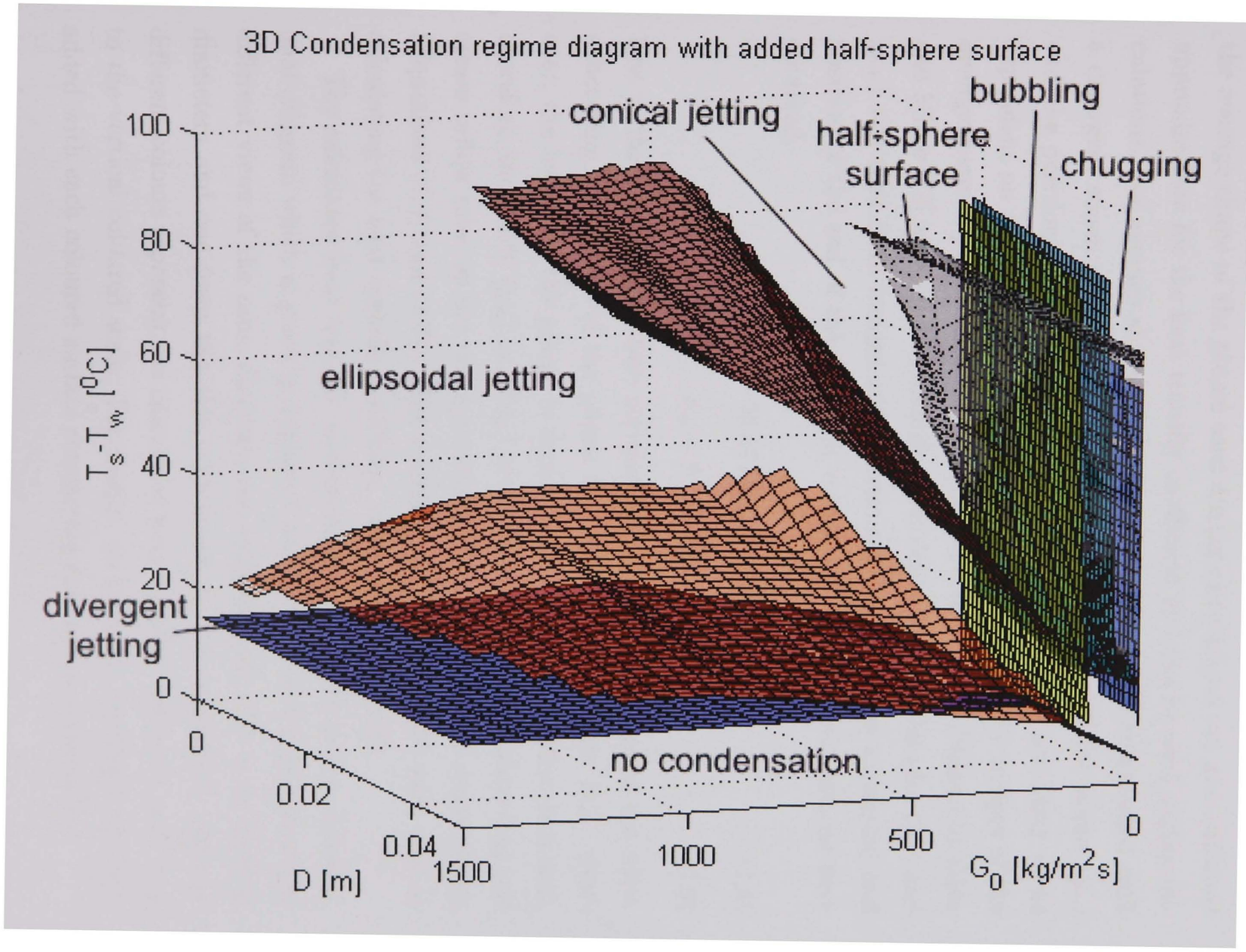

Figure 7.2: Three-dimensional condensation regime diagram with added surface, where a steam plume with the shape of a half-sphere is predicted by the 2DSPL diagram.

inflow rate. Data from Kim *et al.* [14] was used to obtain the correlation

$$y_m = 0.165 D G_0^{0.36} \Delta T^{-0.23} , \tag{7.7}$$

which has been used during calculations.

Also in the divergent jetting regime, the final shape of the plume is formed within the first milliseconds of the process. However, the interface of the divergent jet is not smooth but wavy. As discussed in Chapter 6 the average shape of the plume used during calculations can give sufficient approximation for the heat transfer coefficient and can be used during calculations. An average shape of the steam plume can be represented with a divergent steam plume (Figure 6.8). Here, expansion of the plume (y_m) and the position of the end of the divergent region (x_m) are likely to be dependent on the flow conditions of the process. Schematic images of the divergent steam plume, observed at different conditions, published by Eden and Miller [72] were used to identify these dependencies. Data for (y_m) and (x_m) was read from images and correlations for the plume expansion and position of the end of the divergent region, the following correlations were obtained.

$$y_m = 25.877 D L^{0.8} \Delta T^{-0.3} \tag{7.8}$$

$$x_m = 0.58 L^{0.83} \tag{7.9}$$

Due to the lack of data, these correlations show dependencies on the water subcooling and length of the plume but not the steam inflow rate. However, the length of the plume is dependent on the steam inflow rate and, therefore, indirectly (y_m) and (x_m) are dependent on water subcooling and steam inflow rate- as are other correlations for expansion of steam plume (Equations (7.6) and (7.7)). The correlations (7.8) and (7.9) were used in calculating the heat transfer coefficient using Equation (6.22).

The calculated heat transfer coefficients are plotted on a three-dimensional diagram which is given in Figures 7.3 and 7.4. The Figures show two different views of the same diagram, one from the side with large injector diameters and one from the side with small injector diameters. Dots of different colours represent the calculated heat transfer coefficient according to the vertical coloured scale. For clarity, six different surfaces have been added with each coloured surface connecting dots of the same colour.

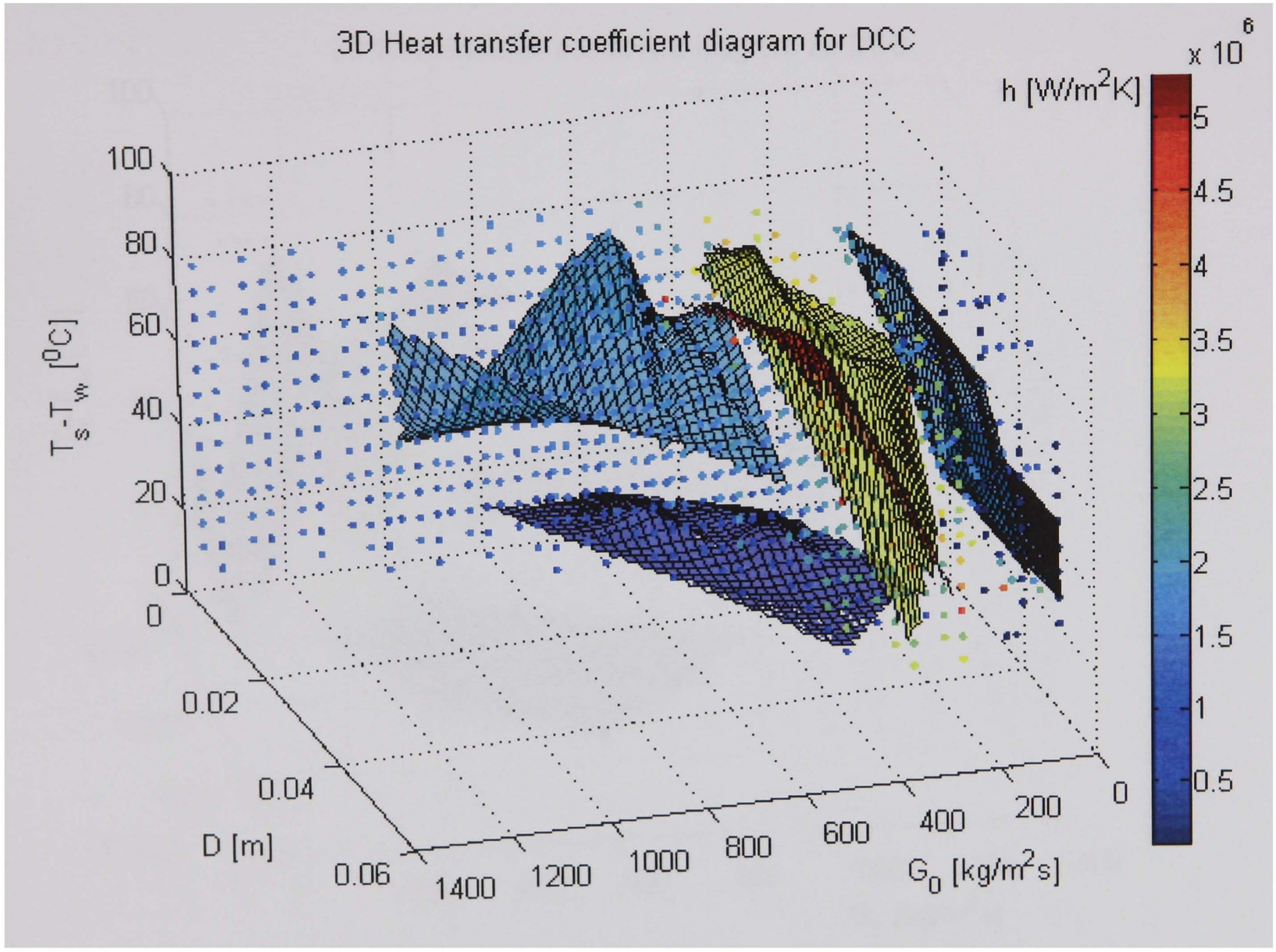

Figure 7.3: Three-dimensional heat transfer coefficient as a function of water subcooling, diameter of steam injector and steam inflow rate. The diagram is viewed from the side with large injector diameters. Colours represent calculated heat transfer coefficient $h[W/(m^2K)]$.

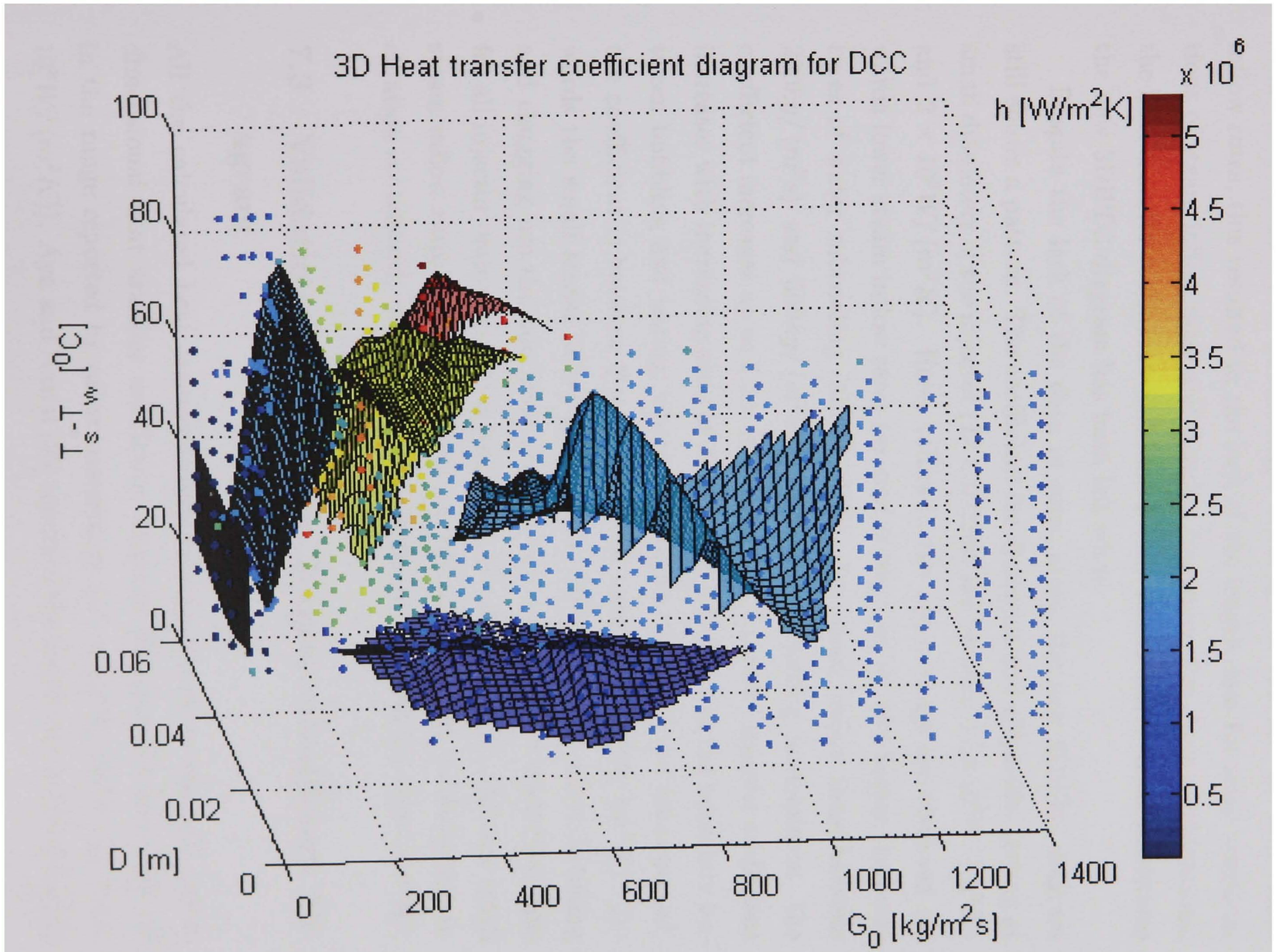

Figure 7.4: Three-dimensional heat transfer coefficient diagram viewed from the side with small injector diameters. Colours represent calculated heat transfer coefficient $h[W/(m^2K)]$.

The diagram developed in this work and shown in Figures 7.3 and 7.4 was named the Three-Dimensional Heat Transfer Coefficient Diagram. Further in the thesis this diagram will be referred to as the new "3DHTC" diagram.

The lengths of the plume used in the calculation were taken from the new 2DSPL diagram, which gives specific lengths at different water subcoolings and Reynolds numbers. Because the heat transfer coefficients were calculated at different water subcoolings, diameters of the injector and steam inflow rates, this resulted in the lack of the length data for some combinations of steam inflow rates and injector diameters. For these combinations, the heat transfer coefficient could not be calculated and at these conditions the new 3DHTC diagram has been left white.

Despite the lack of the data in some areas, the new 3DHTC diagram still shows a pattern. The coefficient for divergent and ellipsoidal jetting at small diameters of the injector ($D < 0.02m$) are between $0.5 \times 10^6 W/\left(m^2 K\right)$ and $2 \times 10^6 W/\left(m^2 K\right)$. Here, values in the upper range are observed towards lower steam inflow rates (around $500 kg/\left(m^2 s\right)$) and higher temperatures of water subcooling (above $50^0 C$). For steam inflow rates between $200 kg/\left(m^2 s\right)$ and $500 kg/\left(m^2 s\right)$, where conical jetting is dominant, the coefficient increases up to $5.3 \times 10^6 W/\left(m^2 K\right)$. The heat transfer coefficient increases with increasing sizes of diameter of injector. On the boundary between bubbling and jetting, where half sphere steam plumes are expected, the coefficient is between $2 \times 10^6 W/\left(m^2 K\right)$ and $2.5 \times 10^6 W/\left(m^2 K\right)$. Towards the small steam inflow rates ($G_0 < 200 kg/\left(m^2 s\right)$), where bubbling and chugging are the dominant regimes, the heat transfer coefficient falls for all injector diameters and is less than $1.5 \times 10^6 W/\left(m^2 K\right)$. At very small steam inflow rates ($G_0 < 10 kg/\left(m^2 s\right)$), where interfacial condensation oscillation is observed, the heat transfer coefficient is about $2 \times 10^5 W/\left(m^2 K\right)$.

7.3 Validation of a 3D Heat Transfer Coefficient Diagram

All the calculated heat transfer coefficients presented in the new three-dimensional heat transfer coefficient diagram (Figures 7.3 and 7.4) are in the range reported by other researchers ($2.7 \times 10^4 W/\left(m^2 K\right)$ to $5.3 \times 10^6 W/\left(m^2 K\right)$). Aya and Nariai [55] reported the coefficient in the chugging

regime to be higher than in other regimes, which differs from the prediction from the 3DHTC diagram. However, it has been reported that a lower velocity of steam relative to the velocity of water decreases the heat transfer coefficient ([20], [78], [83]). Therefore, the coefficient in the chugging regime, which occurs at low steam inflow rates, should be lower than in the bubbling and jetting regimes, which is also predicted by the new 3DHTC diagram.

The diagram also shows that the heat transfer coefficient is dependent on water subcooling, steam inflow rate and diameter of injector, which is in contrast with the semi-empirical correlations for the coefficient published in the literature until now (Equations (7.3)-(7.5)).

For the comparison with the new 3DHTC diagram two-dimensional diagrams were generated where the coefficient was calculated using correlations from the literature (Equations (7.3)-(7.5)). Diagrams are presented in Figures 7.5 to 7.7. Different colours represent different values of the heat transfer coefficient and have been made the same as those used in the new 3DHTC diagram. Figure 7.5 shows the heat transfer coefficient diagram created using correlation (7.3) proposed by Kim *et al.* [14].

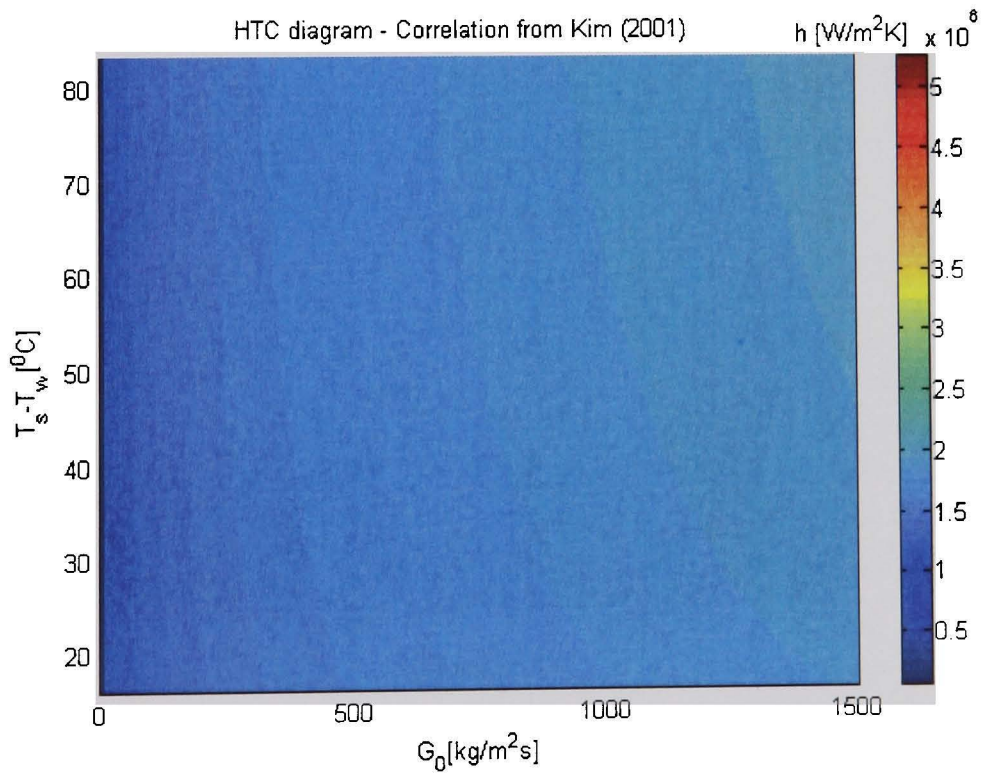

Figure 7.5: Heat transfer coefficient diagram from the correlation (7.3) proposed by Kim *et al.* [14].

Figure 7.6 shows the heat transfer coefficient diagrams created using correlation (7.5) proposed by Kim *et al.* [13]. The plume shape factor (η) used during calculations was 0.8, which corresponds to the ellipsoidal shape (Figure 7.6(a)) and 1, which corresponds to the conical shape (Figure 7.6(b)).

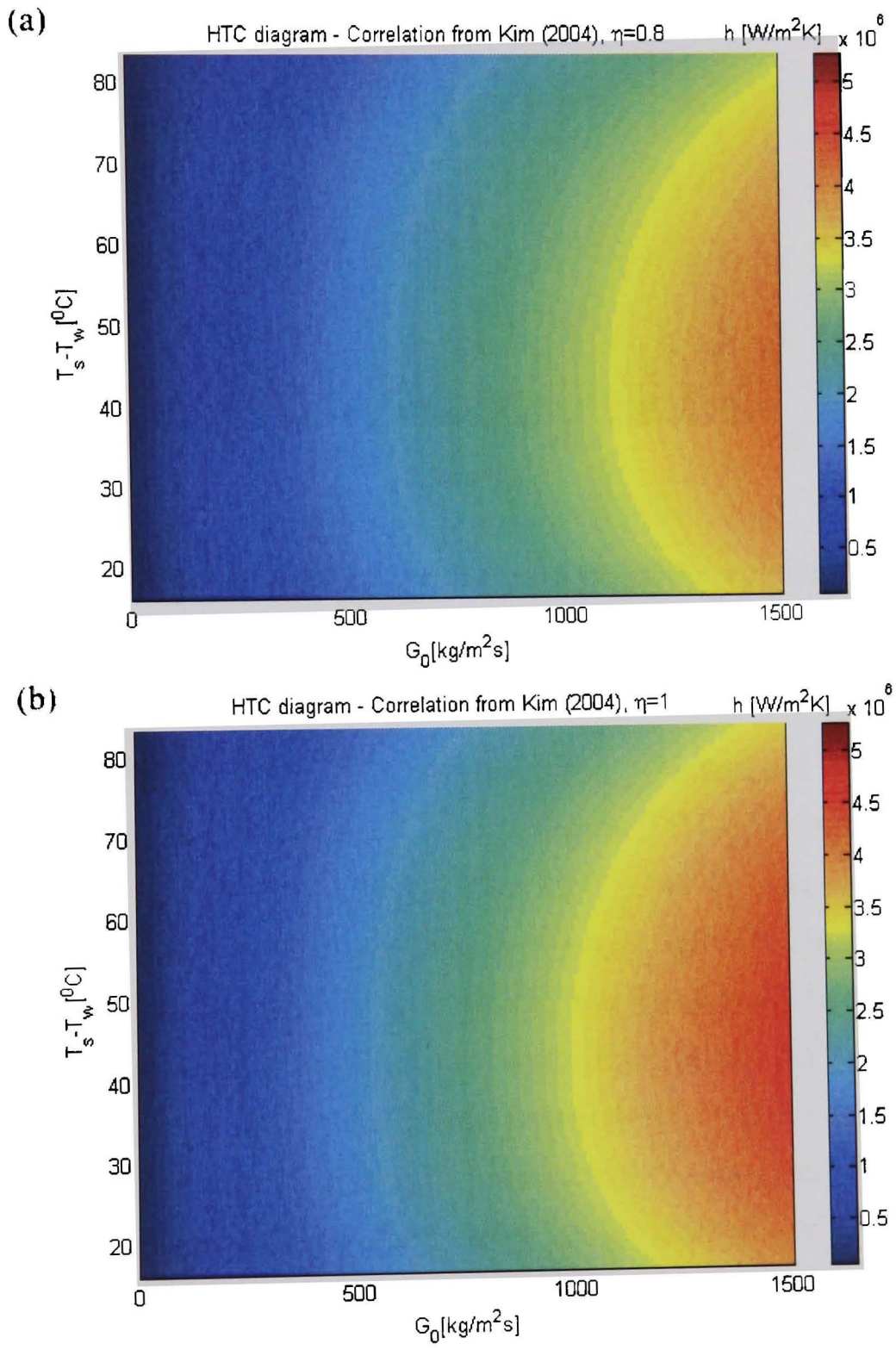

Figure 7.6: Heat transfer coefficient diagram from the correlation (7.5) proposed by Kim *et al.* [13]. The plume shape factor on diagrams is; (a) $\eta = 0.8$ corresponding to ellipsoidal shape and (b) $\eta = 1$ corresponding to conical shape.

Figure 7.7 shows the heat transfer coefficient diagram created using correlation (7.4) proposed by Chun *et al.* [45].

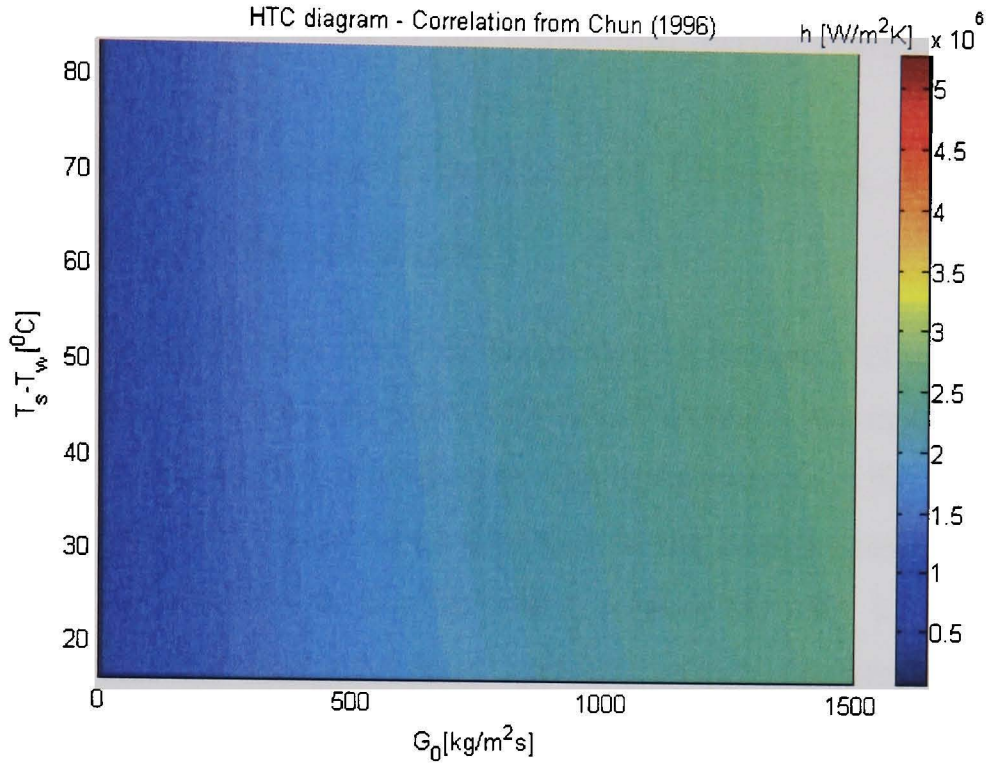

Figure 7.7: Heat transfer coefficient diagram from the correlation (7.4) proposed by Chun *et al.* [45].

In Figures 7.5 to 7.7 it can be seen that correlations by Kim *et al.* [14] (Figure 7.5) and Chun *et al.* [45] (Figure 7.7) predict heat transfer coefficients up to $2\times10^6 W/\left(m^2K\right)$ and $3\times10^6 W/\left(m^2K\right)$ respectively. These values are comparable with those given in the new 3DHTC diagram for small diameters of steam injector ($D = 0.01m$). Furthermore, the heat transfer coefficient predicted by Kim *et al.* [14] and Chun *et al.* [45] increases with increasing water subcooling and steam inflow rates. Values in the 3DHTC diagram also increase with increasing water subcooling, but increase with steam inflow rates only for inflow rates up to $200kg/\left(m^2s\right)$. For steam inflow rates between 200 and $1500kg/\left(m^2s\right)$ they decrease.

The correlation by Kim *et al.* [13] (Figure 7.6(a) and 7.6(b)) predicts higher values of heat transfer coefficient than those of Kim *et al.* [14] and Chun *et al.* [45]. Also, the heat transfer coefficient predicted by Kim *et al.* [13] increases with increasing steam inflow rate, which differs from the trend in the new 3DHTC diagram; however, the correlation for a conical plume with $\eta = 1$ (Figure 7.6(b)) gives higher values of coefficient than that for an

ellipsoidal plume with $\eta = 0.8$ (Figure 7.6(a)). This agrees with the form of the new 3DHTC diagram, where heat transfer coefficients are higher in the conical jetting regime than in the ellipsoidal jetting regime.

7.4 3D Heat Transfer Coefficient Diagram Applied to DCC in a Water Flow

The heat transfer coefficient depends significantly on the turbulent activity at the interface and the temperature difference between steam and water. If the turbulent activity at the interface or the temperature difference is comparatively high this may result in an increase in the heat transfer coefficient.

The turbulent activity at the interface relates directly to the velocity difference between the injected steam and the ambient water flow. Therefore, it is postulated that there is a decrease in turbulent activity when the steam is injected into a water flow, resulting into a reduced heat transfer coefficient. In contrast, if steam is injected into a water flow, there is a constant source of cold water; hence, there will be an increase in heat transfer coefficient.

Experimental observations from the development of the BWT system are used to identify the effect of water flow on the heat transfer coefficient. The heat transfer coefficient is calculated using the steam plume shapes and lengths found during observations. That provides data for DCC into a water flow of $1.9m/s$ centerline velocity as well as into stagnant water.

In the previous Chapters it has been shown, that the length of the steam plume decreases as a result of the water flow. Furthermore, as a result of the water flow more steam had to be injected to achieve the same condensation behaviour.

The experimental data used for calculation of the heat transfer coefficient is found in the Tables 4.3 and 5.5. The data was used to calculate the heat transfer coefficient using the mass conservation model presented in Chapter 6. Different interface shape models were used for the calculation and these corresponded to the plume shapes observed during experiments. The calculated heat transfer coefficients are presented in Table 7.1.

The heat transfer coefficients presented in Table 7.1 were added to the developed 3DHTC diagram and presented in Figures 7.8 and 7.9.

$G_0 \left[\frac{kg}{m^2 s}\right]$	$D\,[m]$	$\Delta T\,[^0C]$	$h \left[\frac{W}{m^2 K}\right]$	
424.4	0.005	85	5.6345×10^6	water flow
663.1	0.004	85	8.7356×10^6	water flow
2652.6	0.002	85	2.8167×10^6	water flow
663.1	0.004	85	1.6378×10^6	stagnant water

Table 7.1: Calculated heat transfer coefficient of generated steam plume at injection of steam into a water flow. Added is calculated heat transfer coefficient of a plume at injection into a stagnant water.

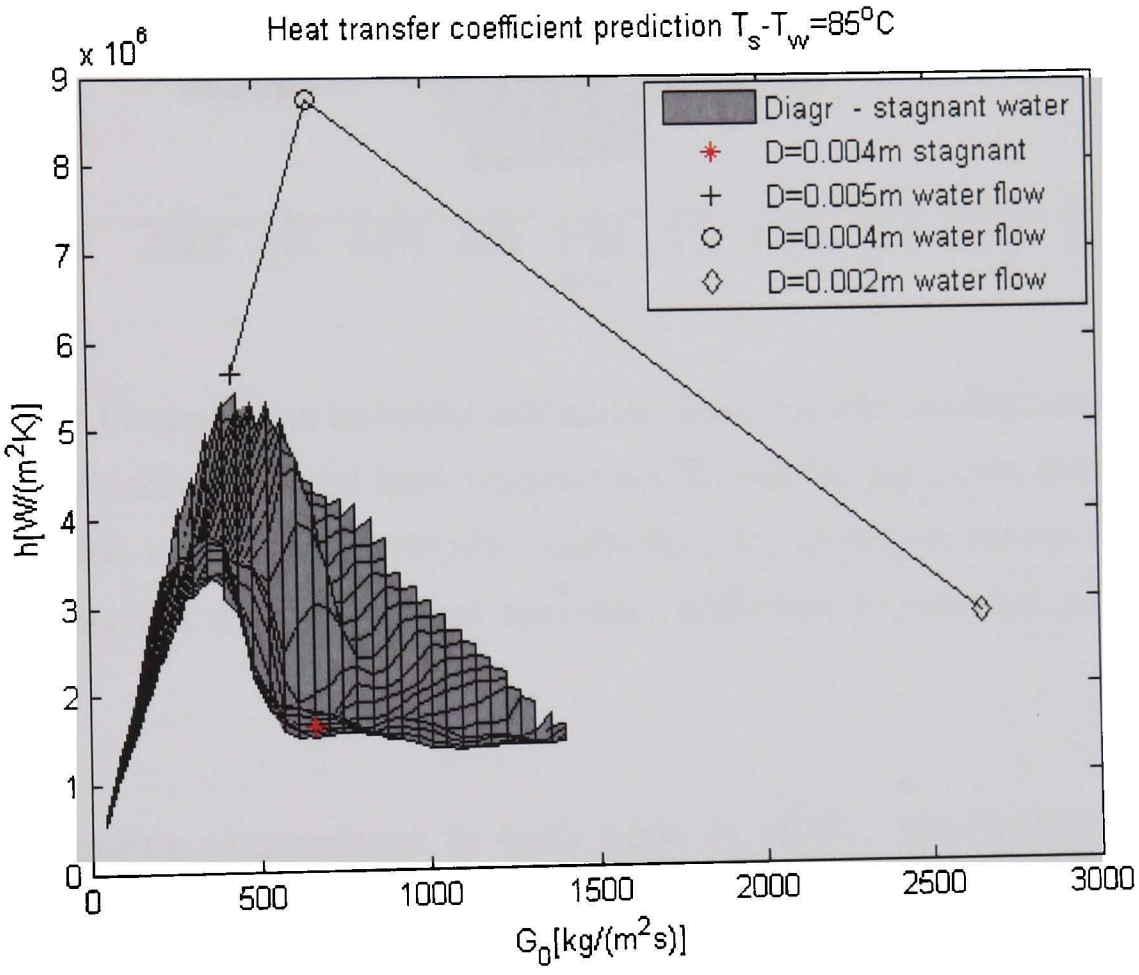

Figure 7.8: Comparison between calculated heat transfer coefficient for stagnant water and calculated heat transfer coefficient for injection into a water flow. Added is also heat transfer coefficient for injection into a stagnant water. Diagram shows the heat transfer coefficient in relation to steam inflow rate.

Figures 7.8 and 7.9 show two different plane views of the 3DHTC diagram presenting the heat transfer coefficient at different steam inflow rates (Figure 7.8) and diameters of the steam injector (Figure 7.9). The water

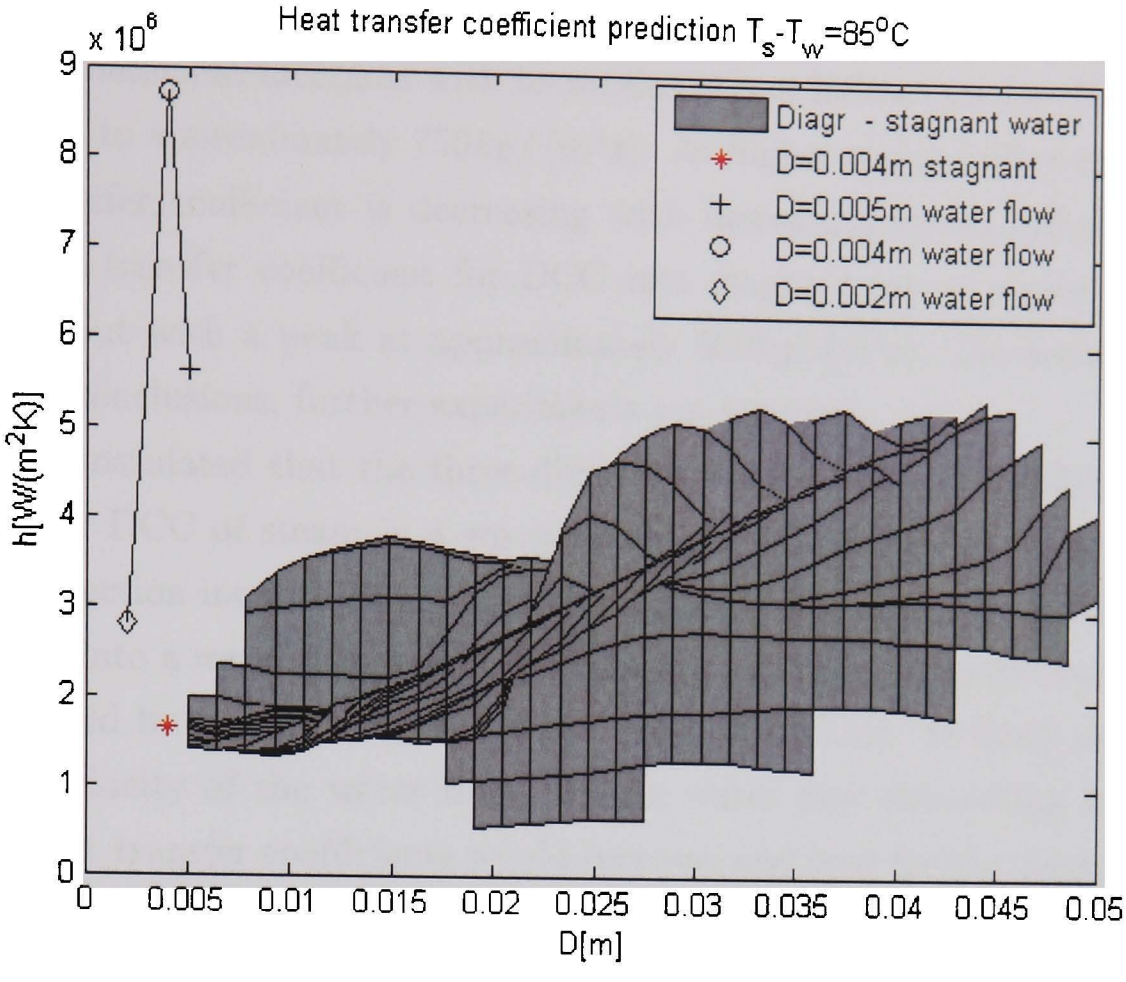

Figure 7.9: Comparison between calculated heat transfer coefficient for stagnant water and calculated heat transfer coefficient for injection into a water flow. Added is also heat transfer coefficient for injection into a stagnant water. Diagram shows the heat transfer coefficient in relation to injector diameter.

flow subcooling temperature in both plots is 85^0C. The surface in grey colour presents heat transfer coefficients from the new 3DHTC diagram. The three heat transfer coefficients for steam injection into water flow are added to the diagram. The heat transfer coefficient of a steam plume injected into stagnant water is added to the diagram and presented as a red star.

From the Figures 7.8 and 7.9 it can be seen, that the heat transfer coefficient in stagnant water is in close agreement with the heat transfer coefficients presented in the developed three-dimensional graph. However, as seen in the Figures 7.8 and 7.9 the water flow results in an increase in heat transfer coefficient. Nevertheless, the trends in heat transfer coefficient found in stagnant water are also seen if a water flow is applied. The heat

transfer coefficient increases with increasing steam inflow rate for the steam inflow up to approximately $750 kg/(m^2 s)$. At higher steam inflow rates the heat transfer coefficient is decreasing with increasing steam inflow rates. The heat transfer coefficient for DCC into stagnant water shows similar feature, but with a peak at approximately $500 kg/(m^2 s)$. To derive more detailed conclusions, further experiments are required.

It is postulated that the three-dimensional heat transfer coefficient diagram for DCC of steam in a water flow shows similar features seen with steam injection into stagnant water. However, the heat transfer coefficient for DCC into a water flow would be higher and the heat transfer coefficient peak would be moved along the steam inflow rate axis. It likely depends on the velocity of the water flow and the water flow subcooling for how much heat transfer coefficients would increase and how far the peak would be moved. From Figure 7.8 it has been calculated, that for the centerline velocity of the water flow of $1.9 m/s$ and water flow subcooling of $85^0 C$, the heat transfer coefficient increases by approximately 84% and the peak is moved along steam inflow rate axis by approximately 74%.

From this it can be concluded, that the heat transfer coefficient of DCC of steam into a water flow is higher than coefficient of DCC of steam into a stagnant water. Furthermore, increased temperature difference, because of the constant supply of a fresh water in a water flow has a bigger effect on a heat transfer coefficient than decreased activity of the interface.

7.5 Discussion

In this chapter, a way of identifying the heat transfer coefficient has been presented. Using information from the new three-dimensional condensation regime diagram and the new two-dimensional steam plume length diagram, the new three-dimensional heat transfer coefficient diagram for predicting the heat transfer coefficient of DCC of steam into water has been developed and presented. As the 3DCR diagram and the 2DSPL diagram are used to construct the 3DHTC diagram all environmental conditions which may affect the heat transfer coefficient are accounted for.

At this time no coherent set of data for the heat transfer coefficient is available in the literature and the new three-dimensional heat transfer

coefficient diagram is therefore believed to be the first attempt to do this. It is likely that the coefficient is dependent on the diameter of steam injector and this dependency is only predicted by the new 3DHTC diagram.

The new 3DHTC diagram shows the decreasing values of the coefficient at high steam inflow rates which has not been predicted by correlations from literature. However, correlations by other researchers have been derived using the data obtained during experiments at low steam inflow rates ($G_0 < 500kg/\left(m^2s\right)$) and therefore it is likely that researchers would not notice the decreasing values of the coefficient at high steam inflow rates. Also, due to the lack data for steam plume length prediction, a large part of the 3DHTC diagram has been left white. It is possible that the coefficient in these areas might decrease with steam inflow rates above $500kg/\left(m^2s\right)$.

Comparison of the heat transfer coefficient for DCC into stagnant water and into water flow showed that the coefficient increases when the water flow is applied. Therefore, increased water subcooling temperature has a bigger effect on the heat transfer coefficient than decreased activity of the interface.

Clearly, it would be of value to obtain more data regarding steam plume length, which would enable improvements to be made in the 3DHTC diagram. Similarly, the collection from experiment of more data concerning the heat transfer coefficient itself would be valuable.

8 General Discussion

In this study a methodology for identifying DCC condensation regimes, lengths of a steam plume and a heat transfer coefficient have been proposed. In addition, the three-dimensional condensation regime, the two-dimensional steam plume length and the three-dimensional heat transfer coefficient diagrams have been developed. These provide important information about DCC for a range of environmental conditions.

The diagrams and models developed in this study are presented in a flow chart in Figure 8.1. In this figure the inter-dependencies of the diagrams and models are presented and calculation procedures are added to the chart.

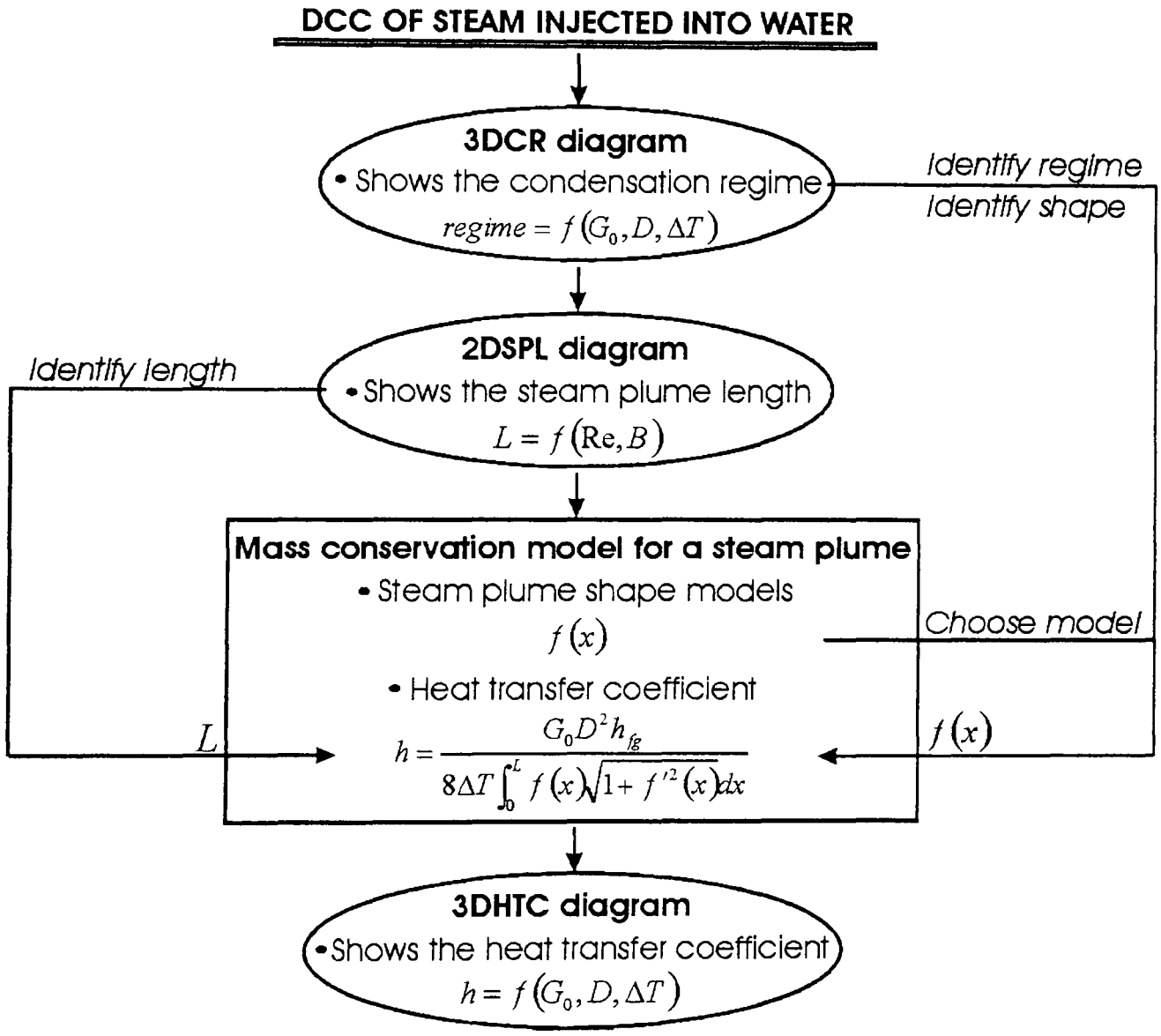

Figure 8.1: Flow chart of the diagrams and models developed in this study. The inter-dependencies of the diagrams and procedures are marked in the chart.

Compared with existing models from the literature, the diagrams developed in this study are based on a comprehensive set of independent experimental studies and data which was brought together to form a combined data bank used for the development of the diagrams. Therefore, developed diagrams include effects of various parameters which affect the flow characteristics of the process. Hence, the diagrams give a more generalised prediction of the DCC characteristics as compared with existing models from literature.

However, due to lack of experimental data the diagrams could not be developed fully for the entire range of environmental conditions and some parts of the 3DCR and the 3DHTC diagrams remain unidentified. Furthermore, due to a lack of knowledge about the steam-water interfacial structures and the effect they might have on a heat transfer coefficient, the latter was calculated using approximated shapes of the plume. There is evidence in the literature to believe that the approximated shapes give better prediction for the heat transfer coefficient compared with irregular shapes. But, structures at the interface have an effect on the heat transfer coefficient and there is a margin of error involved in the use of approximated shapes.

It is postulated that if steam is injected into a water flow two additional mechanisms are introduced which effect the rate of condensation. The supply of cold water in the vicinity of the plume results in an increase in temperature gradient across the interface and accelerates the condensation process. In contrast the water flow speed reduces the relative speed between steam and water and therefore reduces any transient activity at the steam interface. Consequently, the second mechanism decelerates the condensation rate. The results presented in this study indicate that the first mechanism is dominant and that the condensation rate is accelarated when steam is injected into a water flow. It is, however, unclear if this conclusion holds across a wide-range of flow conditions, and more experimental testing is required to establish the effects of water flow.

All diagrams developed in this study can be attached as a table if used in conjunction with CFD computations to model the process of DCC. Compared to existing correlations, used in the modelling to date, the diagrams give more accurate predictions for a wide range of conditions and therefore

the results of numerical modelling would be improved.

Due to the lack of data the validation of the developed diagrams was based on limited sets of data and correlations from literature. The diagrams showed good agreement with data, however the author is aware of the fact that more data is needed in order to provide a sound validation.

All diagrams could still be enhanced providing more experimental data for a wide range of conditions is available. Nevertheless, the study has shown important trends in DCC characteristics and it also identified important physical parameters which affect these characteristics.

9 Conclusions

The aim of this work, as described in the introduction, has been to increase the understanding of the DCC of steam into water process and to propose improved correlations and models of the process.

During the study, information available in the literature has been used together with the experimental data obtained during the development of a ballast water treatment system.

The following conclusions can be drawn from the present study:

Conclusion 1

- The research methodology used has proved to be successful as it provided a framework which resulted in the development of the 3DCR, 2DSPL and 3DHTC diagrams.

Description

In contrast to presently available prediction methods for DCC the diagrams developed in this work enable prediction of the condensation characteristics across a wide range of flow conditions.

Conclusion 2

- Physical parameters with which the DCC process can be described, were identified to be: the steam inflow rate, dimensions of the steam injector, the water subcooling and the velocity of the water flow.

Description

Until now, researchers have identified important parameters to be only the steam inflow rate and the water subcooling. This study has clearly shown, that two additional physical parameters are important for the accurate characterisation of the process. These are the dimension of steam injector and velocity of the water flow.

Conclusion 3

- The three-dimensional condensation regime diagram for DCC of steam injected into water has been developed. Validation of the diagram

against independent experimental data has demonstrated that the diagram can predict the existence of DCC regimes satisfactory across a wide range of flow conditions and injector sizes.

Description
The 3DCR diagram was created from experimental data taken from the literature. This data was independent and published over a period of more than three decades. The diagram has an advantage over maps in the literature, which are able to predict regimes for one injector size only. Furthermore, a validation has shown, that the developed diagram predicts the various jetting regimes accurately.

Conclusion 4

- A two-dimensional steam plume length prediction diagram for DCC of steam injected into a stagnant water has been developed. Validation against experimental data has demonstrated that the diagram predicts lengths of the plume satisfactory for a wide range of flow conditions.

Description
The 2DSPL diagram has been derived from experimental data given in the literature and obtained through a number of independent experiments. Study has shown, that the length of the steam plume, in relation to steam Reynolds number and condensation potential, gives better correlation than the dimensionless steam plume length as a function of steam flow rate and condensation potential, which has been used by earlier researchers. Furthermore, presently available correlations do not provide satisfactory agreements if applied to both high and low Reynolds numbers.

Conclusion 5

- A mass conservation model for the steam plume has been developed.

Description
The mass conservation models for the steam plume have been used also by other researchers. However, the model proposed in this work is designed such that various different shapes can be readily implemented into the model.

Conclusion 6

- A methodology for presenting irregular structures on the interface has been proposed.

Description
A methodology for superimposing periodic and non-periodic structures on the steam-water interface has been presented. As part of this method advanced structures can be imposed at the interface. However, lack of detailed information about the interface has limited the development of a generalised model.

Conclusion 7

- Cross-correlation of the 3DCR and the 2DSPL diagrams has demonstrated that the diagrams are self-consistent.

Description
Evidence for the validity of the prediction made by this combination has been gathered by identifying the flow conditions for the generated steam plume in the shape of a half-sphere from the 2DSPL diagram. These conditions were added to the 3DCR diagram where they matched correctly with the surface, indicating the boundary between the bubbling and jetting regimes. A plume in the shape of a half-sphere is expected to occur at this boundary.

Conclusion 8

- The three-dimensional diagram for the heat transfer coefficient has been developed.

Description
The 3DHTC diagram has been constructed using the 3DCR and 2DSPL diagrams, and mass conservation model. Due to lack of available experimental data the new 3DHTC diagram has been validated against correlations available in literature. Furthermore, in line with information in literature the diagram shows the dependency of the heat transfer coefficient on injector size.

Conclusion 9

- DCC of steam into a water flow showed similar characteristics to DCC of steam into a stagnant water.

Description

The condensation behaviour found in DCC of steam injected into a water flow resembles most of the trends seen with DCC into stagnant water. However, the specific characteristics have been observed at different flow conditions as compared with DCC of steam injected into stagnant water.

10 Recommendations for Further Work

This research has emphasised the complexity of the direct contact condensation process and described the issues related to modelling of DCC of steam injected into water. Effective modelling is critical for the accurate prediction of condensation behaviour, steam plume geometry and heat transfer coefficient.

In this work, a three-dimensional condensation regime diagram, a two-dimensional steam plume length diagram and a three-dimensional heat transfer coefficient diagram have been created. These are capable of providing information about the condensation regime, the size and shape of the steam plume and a heat transfer coefficient for a wide range of conditions.

It is suggested that the following work should be carried out in order to increase the accuracy of the present predictions and to obtain a more universal application of the concept proposed in this thesis:

Recommendation 1

- More experiments of injection of steam into stagnant water at a range of flow conditions should be performed.

Description
More experimental data would increase information about the process. Data should be added to the developed diagrams which would lead to the improvement and the extension of the 3DCR diagram, 2DSPL diagram and the 3DHTC diagram.

Recommendation 2

- Experiments of the injection of steam into a water flow with various velocities should be performed and data collected.

Description
Obtained experimental data should be used to develop regime, steam plume length and heat transfer coefficient diagrams for the DCC into water flow. More data and improved models for DCC into a water flow would increase the understanding of the effect of water flow on the condensation of steam.

Recommendation 3

- Data should be obtained to identify the heat transfer coefficient of DCC of steam into water.

Description
Data can be used to validate the 3DHTC diagram. This validation may show weaknesses of the proposed calculation method and give an indication of the importance of the interface instabilities for heat transfer coefficient calculation.

Recommendation 4

- Experiments should be performed to investigate the structures on the steam-water interface.

Description
Gathered data could be used to configure the proposed method for modelling the interfacial structures. Furthermore, the effect of instabilities on the condensation rate should be thoroughly investigated. These findings could than be compared with information regarding the interface instabilities for the condensation of steam on the water surface from the literature. Following that, the differences between different types of direct contact condensation could be investigated.

Recommendation 5

- Data from the 3DCR, 2DSPL and 3DHTC diagrams should be implemented into the numerical calculation of DCC flow conditions.

Description
Results of these calculations could identify the total flow performance and through that, the performance of many industrial applications like steam driven jet pumps, nuclear reactor coolant system and many others could be improved.

References

[1] Guha, A.: *The Fluid Mechanics of Two-Phase Vapour Droplet Flow With Application to Steam Turbines*, PhD thesis, Trinity College, University of Cambridge, UK (1990)

[2] Whalley, P.B.: *Boiling, Condensation and Gas-Liquid Flow*, Oxford University Press Inc., New York (1987)

[3] I. Hetsroni, G.: *Handbook of Multiphase Systems*, Hemisphere Publishing Corporation, Washington (1982)

[4] Drew, D.A. & Passman, S.L.: *Theory of Multicomponent Fluids*, Springer-Verlag New York, Inc., Printed by Maple-Vail Book Manufacturing Group, York, PA (1999)

[5] Deberne, N., Leone, J.F., Duque, A., Lallemand, A.: *A Model for Calculation of Steam Injector Performance*, International Journal of Multiphase Flow, 25, 841-855 (1999)

[6] Beithou, N & Aybar, H.S.: *A Mathematical Model for Steam-Driven Jet Pump*, International Journal of Multiphase Flow, 26, 1609-1619 (2000)

[7] Sherif, S.A., Lear, W.E., Steadham, J.M., Hunt, P.L., Holladay, J.B.: *Analysis and Modeling of a Two-Phase Jet Pump of a Thermal Management System for Aerospace Applications*, International Journal of Mechanical Sciences, 42, 185-198 (2000)

[8] Kerney, P.J., Faeth, G.M., Olson, D.R.: *Penetration Characteristics of a Submerged Steam Jet*, AIChE Journal, 18(3), 548-553 (1972)

[9] Chan, C.K., & Lee, C.K.B.: *A Regime Map for Direct Contact Condensation*, International Journal of Multiphase Flow, 8(1), 11-20 (1982)

[10] Liang, K.S. & Griffith, P.: *Experimental and Analytical Study of Direct Contact Condensation of Steam in Water*, Nuclear Engineering and Design, 147, 425-435 (1994)

[11] Kim, Y.-S. & Park, J.-W.: *Determination of the Steam-Water Direct Contact Condensation Heat Transfer Coefficient Using Interfacial Transport Models*, Proceedings of American Nuclear Society - Thermal Hydraulics Division, 10, 110-117 (1997)

[12] Youn, D.H., Ko, K.B., Lee, Y.Y., Kim, M.H., Bae, Y.Y., Park, J.K.: *The Direct Contact Condensation of Steam in a Pool at Low Mass Flux*, Journal of Nuclear Science and Technology, 40(10), 881-885 (2003)

[13] Kim, Y.-S., Park, J.-W., Song, C.-H.: *Investigation of the Steam-Water Direct Contact Condensation Heat Transfer Coefficient Using Interfacial Transport Models*, International Comm. Heat Mass Transfer, 31(3), 397-408 (2004)

[14] Kim, H.Y., Bae, Y.Y., Song, C.H., Park, J.K., Choi, S.M.: *Experimental Study on Stable Steam Condensation in Quenching Tank*, International Journal of Energy Research, 25, 239-252 (2001)

[15] Lee, S.I. & No, H.C.: *Gravity-Driven Injector Experiments and Direct-Contact Condensation Regime Map for Passive High-Pressure Injection System*, Nuclear Engineering and Design, 183, 213-234 (1998)

[16] Beithou, N & Aybar, H.S.: *High-Pressure Steam-Driven Jet Pump-Part I: Mathematical Modeling*, Transactions of the ASME: Journal of Engineering for Gas Turbines and Power, 123, 693-700 (2001)

[17] The RELAP5 Code Development Team: *RELAP5/MOD3 Code Manual*, NUREG/CR-5535, Idaho National Engineering Laboratory, Idaho Falls, Idaho, USA (1995)

[18] Petrovic de With, A., Calay, R.K., de With, G.: *Three dimensional regime map for direct contact condensation of steam injected into water*, International Journal of Heat and Mass Transfer, (2006), suggested for publication

[19] Collier, J.G. & Thome J.R.: *Convective Boiling and Condensation 3ed*, Oxford Science Publication, Clarendon Press, Oxford (1996)

[20] Incropera, F.P. & DeWitt, D.P.: *Fundamentals of Heat and Mass Transfer 4th eddition*, John Wiley & Sons, Inc, New York, (1996)

[21] Guha, A.: *Two-Phase Flows with Phase Transition*, Sieverding, C.H.: *von Karman Institute for Fluid Dynamics, Lecture Series 1995-06*, von Karman Institute, Belgium (1995)

[22] Bejan A.: *Heat Transfer Handbook 2th eddition*, John Wiley & Sons, Inc, New York, (1995)

[23] Andrianov, N.: *Analytical and Numerical Investigation of Two-Phase Flows*, PhD thesis, Fakultät für Mathematik der Otto-von-Guericke Universität Magdeburg, DE (2003)

[24] Wallis, G.B.: *One-dimensional Two-Phase Flow*, McGraw-Hill, Inc., New York, USA (1969)

[25] Hewitt, G.F. & Hall-Taylor, N.S.: *Annular Two-Phase Flow*, Pergamon Press, Oxford, New York (1970)

[26] Whalley, P.B.: *Two-Phase Flow and Heat Transfer*, Oxford University Press Inc., New York (1996)

[27] Kleinstreuer, C: *Two-Phase Flow: Theory and Applications*, Teylor & Francis, London, UK (2003)

[28] Andrianov, N., Saurel, R., Warnecke, G.: *A Simple Method for Compressible Multiphase Mixtures and Interfaces*, International Journal for Numerical Methods in Fluids, 41, 109-131 (2003)

[29] Saurel, R. & Abgrall, R.: *A Multiphase Godunov Method for Compressible Multifluid and Multiphase Flows*, Journal of Computational Physics, 150, 425-467 (1999)

[30] Saurel, R. & Lemetayer, O.: *A Multiphase Method for Compressible Flows with Interfaces, Shocks, Detonation Waves and Cavitation*, Journal of Fluid Mechanics, 431, 239-271 (2001)

[31] Lahey, Jr., R.T. & Drew, D.A.: *An Analysis of Two-Phase Flow and Heat Transfer Using a Multidimensional, Multi-Field, Two-Fluid Computational Fluid Dynamics (CFD) Model*, Japan/US Seminar on Two-Phase Flow Dynamics, Santa Barbara, California (2000)

[32] Spalding, D.B.: *Lecture 11: Two Phase Flow* (1982) http://www.simuserve.com/SUPPORT/LECS/IPSA/IPSA.HTM (March 2003)

[33] Baghdadi, A.H.A.: *Numerical Modelling of Two-Phase Flow with Inter-Phase Slip*, PhD thesis, Imperial College of Science and Technology, London (1979)

[34] Saez, M., Tauveron, N., Chataing, T., Geffraye, G., Briottet, L., Alborghetti, N.: *Analysis of the turbine deblading in an HTGR with the CATHARE code*, Nuclear Engineering and Design, 236, 574-586 (2006)

[35] Barten, W., Coddington, P., Ferroukhi, H.: *RETRAN-3D analysis of the base case and the four extreme cases of the OECD/NRC Peach Bottom 2 Turbine Trip benchmark*, Annals of Nuclear Energy 33, 99-118 (2006)

[36] Hainoun, A. & Alissa, S.: *Full-scale modelling of the MNSR reactor to simulate normal operation, transients and reactivity insertion accidents under natural circulation conditions using the thermal hydraulic code ATHLET*, Nuclear Engineering and Design, 235, 33-52 (2005)

[37] Takase, K.: *A Preliminary Study on Direct-Contact Condensation between Water and Vapor in a Suppression Tank for Fusion Reactor Safety*, Fusion Technology, 39, 1056-1060 (2001)

[38] El-Dessouky, H., Ettouney, H., Alatiqi, I., Al-Nuwaibit, G.: *Evaluation of steam jet ejectors*, Chemical Engineering and Processing, 41, 551-561 (2002)

[39] Iwaki, C., Narabayashi, T., Kudo, Y., Nei, H., Mizumachi, W., Shioiri, A.: *Experimental Study on Heat and Momentum Transfer Mechanisms in Steam Injectors for Next-Generation Reactors*, Proceedings of The

2nd International Conference on Multiphase Flow '95-Kyoto, P8-1-7 (1995)

[40] Narabayashi, T., Mizumachi, W., Mori, M.: *Study on Two-Phase Flow Dynamics in Steam Injectors*, Nuclear Engineering and Design, 175, 147-156 (1997)

[41] ESDU: *Ejectors and Jet Pumps - Design for Steam Driven Flow*, IHS Group, ESDU International, London, UK, 86030 (1986)

[42] ESDU: *Ejectors and Jet Pumps - Computer program for Design and Performance for Steam/gas Flow*, IHS Group, ESDU International, London, UK, 94046 (1994)

[43] Beithou, N and Aybar, H.S.: *High-Pressure Steam-Driven Jet Pump-Part I: Parametric Analysis*, Transactions of the ASME: Journal of Engineering for Gas Turbines and Power, 123, 701-706 (2001)

[44] Chen, L.-D. & Faeth, G.M.: *Condensation of Submerged Vapor Jets in Subcooled Liquids*, Transactions of the ASME, Journal of Heat Transfer, 104, 774-780 (1982)

[45] Chun, M.-H., Kim, Y.-S., Park, J.-W.: *An Investigation of Direct Condensation of Steam Jet in Subcooled Water*, International Communications in Heat and Mass Transfer, 23(7), 947-958 (1996)

[46] Simpson, M.E. & Chan, C.K.: *Hydrodynamics of a Subsonic Vapor Jet in Subcooled Liquid*, Journal of Heat Transfer, 104, 271-278 (1982)

[47] Celata, G.P., Cumo, M., Farello, G.E., Focardi, G.: *Direct Contact Condensation of Steam on Slowly Moving Water*, Nuclear Engineering and Design, 96, 21-31 (1986)

[48] Liang, K.S.: *Experimental and Analytical Study of Direct Contact Condensation of Steam in Water*, PhD thesis, Department of Nuclear Engineering, Massachusetts Institute of Technology, USA (1991)

[49] van Wissen, R.J.E., Schreel, K.R.A.M., van der Geld, C.W.M., Wieringa, J.: *Turbulence Production by a Steam-Driven Jet in a Wa-*

ter Vessel, International Journal of Heat and Fluid Flow, 25, 173-179 (2004)

[50] van Wissen, R.J.E., Schreel, K.R.A.M., van der Geld: *Particle Image Velocimetry Measurements of a Steam-Driven Confined Turbulent Water Jet*, Journal of Fluid Mechanics, 530, 353-368 (2005)

[51] Block, J.A.: *Condensation-Driven Fluid Motions*, International Journal of Multiphase Flow, 6, 113-129 (1980)

[52] Aya, I. & Nariai, H.: *Boundaries Between Regimes of Pressure Oscillation Induced by Steam Condensation in Pressure Suppression Containment*, Nuclear Engineering and Design, 99, 31-40 (1987)

[53] Kandlikar, S.G.: *Handbook of Phase Change : Boiling and Condensation*, Taylor & Francis, Philadelphia, London, Printed by Edwards Brothers, MI (1999)

[54] Petrovic, A.: *Analytical Study of Flow Regimes for Direct Contact Condensation Based on Parametrical Investigation*, Journal of Pressure Vessel Technology, 127 (1), 20-25 (2005)

[55] Aya, I. & Nariai, H.: *Evaluation of Heat-Transfer Coefficient at Direct-Contact Condensation of Cold Water and Steam*, Nuclear Engineering and Design, 131, 17-24 (1991)

[56] Weimer, J.C., Faeth, G.M., Olson, D.R.: *Penetration of Vapor Jets Submerged in Subcooled Liquids*, AIChE Journal, 19(3), 552-558 (1973)

[57] Arebi, B. & Dempster, W.M.: *A Theoretical Model for the Growth and Detachment of Condensing Steam Bubbles at a Submerged Orifice*, University of Strathclyde, Glasgow, internal report (2005)

[58] Kim, Y.S. & Song, C.H.: *Overall Review of Steam Jet Condensation in a Next Generation Reactor Water Pool*, Proceedings of IMECE'03, ASME, 1-10 (2003)

[59] Sandwell, D.T.: *Biharmonic Spline Interpolation of GEOS-3 and SEASAT Altimeter Data*, Geophysical Research Letters, 2, 139-142 (1987)

[60] Drazin, P.G. & Reid, W.H.: *Hydrodynamic Stability*, Cambridge University Press, Cambridge, (1981)

[61] Shivamoggi, B.K.: *Theoretical Fluid Dynamics*, John Wiley & Sons, Inc., New York, (1998)

[62] Guyon, E., Hulin, J.-P., Petit, L., Mitescu, C.D.: *Physical Hydrodynamics*, Oxford University Press, Inc., New York, (2001)

[63] Celata, G.P.: *Direct Contact Condensation of Steam on Subcooled Water*, Hewitt, G.F., Mayinger. F., Riznic, J.R.: *Keynote Lecture at the Phase-Interface Phenomena in Multiphase Flow, Dubrovnik, Proceedings of the International Centre for Heat and Mass Transfer*, Hemisphere Publishing Corporation, NY (1991)

[64] Celata, G.P., Cumo, M., Farello, G.E., Focardi, G.: *Direct Contact Condensation of Superheated Steam on Water*, International Journal of Heat and Mass Transfer, 30 (3), 449-458 (1987)

[65] Celata, G.P., Cumo, M., Farello, G.E., Focardi, G.: *A Theoretical Model of Direct Contact Condensation of Steam on a Horizontal Surface*, International Journal of Heat and Mass Transfer, 30 (3), 459-467 (1987)

[66] Celata, G.P., Cumo, M., D'Annibale, F.,Farello, G.E., Focardi, G.: *A Theoretical and Experimental Study of Direct Contact Condensation on Water in Turbulent Flow*, Experimental Heat Transfer, 2, 129-148 (1989)

[67] Mikielewicz, J. & Rageb, A.M.A.: *Simple Theoretical Approach to Direct Contact Condensation on Subcooled Liquid Film*, International Journal of Heat and Mass Transfer, 38 (3), 557-562 (1995)

[68] Mikielewicz, J., Trela, M., Ihnatowicz, E.: *A Theoretical and Experimental Investigation of Direct Contact Condensation on a Liquid Layer*, Experimental Thermal and Fluid Science, 15, 221-227 (1997)

[69] Ruile, H.: *Dependence of Heat Transfer by Direct Contact Condensatio on Liquid Side turbulence in Stratified Two Phase Flow*, Proceedings of the German-Japanese Symposium on Multi-Phase Flow, 313-323 (1994)

[70] Meier, M. & Yadigaroglu, G.: *Numerical and Experimental Study of Large Steam-Air Bubbles Injected in a Water Pool*, Nuclear Science and Engineering, 136, 363-375 (2000)

[71] Yadigaroglu, G.: *Computational Fluid Dynamics for Nucear Applications: from CFD to Multi-scale CMFD*, Nuclear Engineering and Design, 235, 153-164 (2005)

[72] Eden, T.J., Miller, T.F., Jacobs, H.R.: *The Centerline Pressure and Cavity Shape of Horizontal Plane Choked Vapor Jets With Low Condensation Potential*, Journal of Heat Transfer, 120, 999-1007 (1998)

[73] Hun Ju, S., Cheon No, H., Mayinger, F.: *Measurement of Heat Transfer Coefficients for Direct Contact Condensation in Core Makeup Tanks using Holographic Interferometer*, Nuclear Science and Engineering, 199, 75-83 (2000)

[74] Dempster, W.M. & Arebi, B.: *Experimental Characteristics of Steam Bubble Growth at Orifices in Sub-colled Liquid*, University of Strathclyde, Glasgow, internal report (2005)

[75] Peitgen, H.-O., Jürgens, H., Saupe, D.: *Chaos and Fractals, New Frontiers of Science*, Chapter 9 Irregula Shapes: Randomness in Fractal Constructions, Springer-Verlag, New York, (1992)

[76] Kreyszig, E.: *Advanced Mathematical Engineering 7th edition*, John Wiley & Sons, Inc., New York, (1993)

[77] Kuščer, I. & Kodre, A.: *Matematika v Fiziki in Tehniki*, Društvo Matematikov, Fizikov in Astronomov, Ljubljana, (1994)

[78] Bird, R.B., Stewart, W.E., Lightfoot, E.N.: *Transport Phenomena 7th printing*, John Wiley & Sons, Inc, New York (1966)

[79] Young, R.J., Yang, K.T., Novotny, J.L.: *Vapor-Liquid Interaction in a High Velocity Vapor Jet Condensing in a Coaxial Water Flow*, Journal of Heat Transfer, 3, 226-230 (1974)

[80] Tsai, S.S. & Kazimi, M.S.: *The Potential for Penetration of a Hot Vapour Jet into a Subcooled Liquid*, ASME paper, 76-WA/HT-78 (1976)

[81] Kozeki, M. & Kuwabara, S.: *Experimental Studies on Pressure Suppresion Containments for Marine Reactor*, Journal of Marine Engineering Society of Japan, 12, 45-66 (1972)

[82] Fukuda, S.: *Pressure Variations due to Vapor Condensation in Liquid Phenomena at Large Vapor Mass Flow Flux*, Journal of Atomic Energy Society of Japan, 24(6), 466-474 (1982)

[83] Kuščer, I. & Žumer, S.: *Toplota*, Društvo Matematikov, Fizikov in Astronomov, Ljubljana, (1987)

Analytical Study of Flow Regimes for Direct Contact Condensation Based on Parametrical Investigation

Anka Petrovic
e-mail: a.petrovic@herts.ac.uk
Fluid Mechanics Research Group,
AADE Department,
University of Hertfordshire,
Hatfield, AL10 9AB United Kingdom

Various industrial devices exist where direct contact condensation (DCC) of steam in water takes place. Typical examples are the nuclear reactor coolant systems, steam driven jet pumps, and condensers. The modeling of steam condensation is crucial to obtain an appropriate design of such devices. Present models designed for DCC have shown limited agreement with experimental data. Computation of the flow regimes is performed with limited accuracy, due to initial model settings and empirical correlations, which form a main drawback in the computation of DCC related problems. This study, which is a part of a PhD study, presents an investigation of the steam-water interface for various conditions of steam and water, using the computation of balance equations and jump conditions. A simple mathematical model to predict the location of the condensation interface for four different shapes of steam plume at different heat transfer coefficients is presented which will be further developed into an advanced computational model for DCC.
[DOI: 10.1115/1.1845471]

Keywords: Direct Contact Condensation, Condensation Modeling, Flow Regimes, Steam Plume Shapes

Introduction

Multiphase flow is the most common flow in nature. One example of multiphase flows is direct contact condensation (DCC), which occurs when steam is introduced into water. It is a phenomenon of high importance in nuclear, chemical, pumping, and marine industry applications. The behavior of the interface, which is strongly related to the heat transfer during condensation, is the prime interest of the process. This paper presents a model for a DCC. Four different steam plume shapes are proposed and comparison with experimental data and calculations shows good agreement.

DCC was subject of many studies [1–13] and many empirical correlations relevant to the process were proposed [1–3]. Many experiments with the emphasis on different regimes at different parameters were also performed [4–7] proposing some basic steam plume shapes, which occur in the process.

The use of a correct heat transfer coefficient is of big importance in modeling the DCC process. The heat transfer coefficient, which depends on various conditions like position and shape of steam pipe, steam flow rate, temperatures, and velocities of steam and water, has been a subject of study [1–3,8–10] and there exist various empirical relationships for heat transfer coefficients. Correlations describing steam plume length and heat transfer coefficients used in present models are empirical, though based on analytical studies. Some of them show good agreement with experimental data reported and are widely used [3], but are valid only in certain range of parameters. Because of the importance of these correlations and the whole process in which they are involved, more general analytical correlations are needed.

Contributed by the Pressure Vessels and Piping Division for publication in the JOURNAL OF PRESSURE VESSEL TECHNOLOGY. Manuscript received by the PVP Division September 10, 2004; revision received September 17, 2004. Review conducted by: S. Zamrik.

Regions and Processes at DCC of Steam in Pool of Water

When steam is introduced into the pool of water by means of a pipe, DCC of steam in water occurs. DCC consists of four different regions, as shown in Fig. 1. The first region consists of pure steam and is called the steam plume. The second region is called the interface, where DCC starts to take place. The third region is the hot water layer, which contains steam bubbles and is characterized by the increased water temperature. The fourth region is the region of pure pool water.

Steam Plume. The first region in the process of condensation is the steam plume. This region occurs at the steam pipe exit through which the steam with inlet normalized steam flow rate (G_0) is introduced into the pool of water. This region is characterized by pure steam with temperature and velocity gradients in both downstream and perpendicular directions.

The shape of the steam plume is not a physical property of gas and liquid involved in the process but instead it is dependent on the flow conditions. As investigated in different experiments reported in literature [1–4], different regimes for DCC of steam in water can be classified. Figure 2 shows a schematic flow regime map with three main regimes: chugging, bubbling, and jetting. The formation of each regime depends on the steam flow rate and the pool water temperature. Each regime has its own characteristic steam plume shape.

At low steam flow rate water rushes periodically into a steam pipe [1,5,7], causing large amplitude pressure pulses at low frequency. This process is known as chugging. In the case of internal chugging condensation occurs in the steam pipe and the shape of the interface can be approximated by the exit steam pipe cross section. When external chugging occurs, a small bubble of steam surrounded by a layer of hot water forms at the pipe exit. The steam plume shape can be described as a small spherical or ellipsoidal bubble, based on the exit pipe cross section.

Another regime is bubbling, where an irregular spherical or ellipsoidal steam plume is formed at the pipe exit. For lower pool

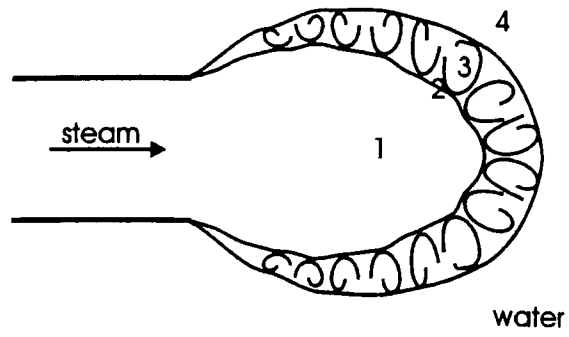

Fig. 1 Different regions in DCC of steam in water: steam plume (1), interface (2), hot water layer (3), and pool water (4)

temperatures bubbles will form and collapse at the pipe exit, causing high frequency pressure oscillations. For higher pool temperatures bubbles will detach from the pipe and collapse at a certain distance from the injector. Consequently, the associated oscillation frequencies will be lower [2].

The last main condensation flow regime is jetting which has conical or ellipsoidal steam plume shapes. Irregularity of the jetting shape depends on the nozzle diameter, steam velocity, and pool water temperature. At low steam velocities irregularity is high for low pool water temperatures, but becomes smaller with increasing pool water temperature. In contrast, the steam plume shape for sonic steam velocities is clear and stable at low pool water temperatures. Oscillations in the steam plume occur as the temperature increases. The pressure fluctuations associated with this jetting oscillation are low and occur at high frequency.

Interface Between Steam and Water. The outer surface of the steam plume is the interface. It is the region where steam and water meet and along which DCC occurs as a convective heat and mass transfer through the interface. The exact shape and position of interface depend on interfacial eddies in the hot water layer [1]. The size of the interface is related to the amount of condensed steam.

Hot Water Layer. The hot water layer is also named bulk water. It is a two-phase layer of conductively heated water towards the saturation temperature at the interface, mixed with small steam bubbles. Both phases in the hot water layer are in turbulent motion with eddies created mainly by the momentum or kinetic energy carried by the condensing steam [1] and the velocity of the water [8].

Eddies have a strong effect on the interface shape and control the interfacial transport. Eddies are for interfacial transport modeling proposed to be of two different size ranges [2]. Large eddies have enough inertia to travel away from the interface and dominate the transport process if the turbulent Reynolds number is not too large ($Re_t<500$). On the other hand there are small eddies, which are strongly influenced by the liquid viscosity and are confined around the interface. These eddies typically exist at large turbulent Reynolds numbers ($Re_t>500$).

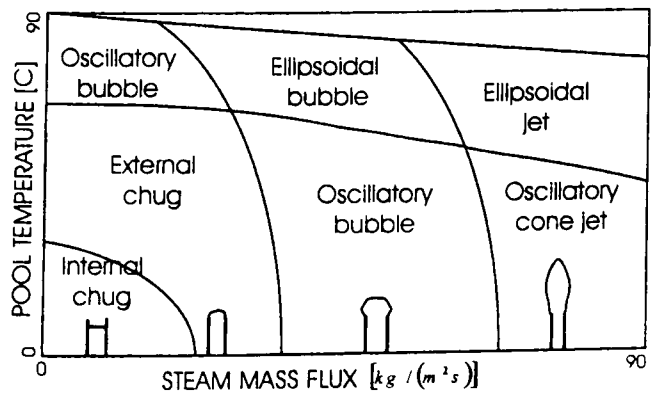

Fig. 2 Schematic flow regime map of steam in water from the literature

Pool Water. The pool water is a one-phase area of water at certain temperature. This water can be stagnant or moving. As shown by Celata [8] the water velocity has an effect on turbulence in the hot water layer and consequently on the steam plume shape and the heat transfer coefficient.

Analytical Model for DCC

An appropriate model describing condensation of steam in water must incorporate fundamental aspects of two-phase flow and flow dynamics.

The approach taken by Drew and Passman [11] derives the equations of motion from balance equations valid inside each material for Newtonian fluids using the ensemble-averaging technique. Through averaging, information is lost and a derived system of balance equations, governing three-dimensional unsteady two-phase flow, is underdetermined. Therefore, lost information must be replaced by the constitutive equations based on behavior of the various phases.

The one-dimensional governing equations used in this study are based on the general equations governing three-dimensional unsteady two-phase model derived by Drew and Passman [11]. The equations are described as follows:

Continuity equation:

$$\frac{\partial}{\partial t}(\alpha_k\rho_k)+\frac{\partial}{\partial x}(\alpha_k\rho_k v_k)=\Gamma_k \tag{1}$$

Momentum equation:

$$\begin{aligned}\frac{\partial}{\partial t}(\alpha_k\rho_k v_k)+\frac{\partial}{\partial x}(\alpha_k\rho_k v_k^2)&=-\frac{\partial}{\partial x}(\alpha_k p_k)+\Gamma_k(v_{in}-v_k)-\alpha_k\rho_k FI_k(v_k-v_{k'})\\&-C\alpha_k\alpha_{k'}\rho_m\left[\frac{\partial}{\partial t}(v_k-v_{k'})+v_{k'}\frac{\partial v_k}{\partial x}-v_k\frac{\partial v_{k'}}{\partial x}\right]\end{aligned} \tag{2}$$

where the last two elements of the equations describe the interfacial momentum transfer and Energy equation:

$$\begin{aligned}\frac{\partial}{\partial t}\left[\alpha_k\rho_k\left(e_k+\frac{v_k^2}{2}\right)\right]+\frac{\partial}{\partial x}\left[\alpha_k\rho_k v_k\left(e_k+\frac{v_k^2}{2}\right)\right]\\=-\frac{\partial}{\partial x}(\alpha_k p_k v_k)+Q_k+W_k+\Gamma_k\left(e_{ki}+\frac{v_{ki}^2}{2}\right)\end{aligned} \tag{3}$$

Although mass, momentum, and energy are conserved, discontinuities in the fluid flow exist at the interface, and hence, there is a need for jump conditions. Jump conditions are boundary conditions at the interface of phases which describe exchanges of mass, momentum and energy between different phases.

Jump conditions for the one-dimensional model of DCC of steam in water are as follows:

Continuity jump condition:

$$\Gamma_g+\Gamma_f=0 \tag{4}$$

Momentum jump condition:

$$\begin{aligned}\Gamma_g(v_{in}-v_g)+\Gamma_f(v_{in}-v_f)-\alpha_g\rho_g FI_g(v_g-v_f)\\-\alpha_f\rho_f FI_f(v_f-v_g)=m\end{aligned} \tag{5}$$

Energy jump condition:

$$Q_g+Q_f+W_g+W_f+\Gamma_g\left(e_{gi}+\frac{v_{gi}^2}{2}\right)+\Gamma_f\left(e_{fi}+\frac{v_{fi}^2}{2}\right)=\varepsilon \tag{6}$$

From the balance Eqs. (1)–(3) with a use of jump conditions (4)–(6) where interfacial energy and surface tension sources are set to zero, a system of six equations describing transient, one-dimensional condensation can be derived [Eqs. (7)–(12)].

Continuity equations for gas and liquid phase:

$$\frac{\partial}{\partial t}(\alpha_g\rho_g)+\frac{\partial}{\partial x}(\alpha_g\rho_g v_g)=\Gamma_g \tag{7}$$

$$\frac{\partial}{\partial t}(\alpha_f\rho_f)+\frac{\partial}{\partial x}(\alpha_f\rho_f v_f)=-\Gamma_g \tag{8}$$

Momentum equations for gas and liquid phase:

$$\frac{\partial}{\partial t}(\alpha_g\rho_g v_g)+\frac{\partial}{\partial x}(\alpha_g\rho_g v_g^2)$$

$$=-\frac{\partial}{\partial x}(\alpha_g p)+\Gamma_g(v_{in}-v_g)-\alpha_g\rho_g FI_g(v_g-v_f)$$

$$-C\alpha_g\alpha_f\rho_m\left[\frac{\partial}{\partial t}(v_g-v_f)+v_f\frac{\partial v_g}{\partial x}-v_g\frac{\partial v_f}{\partial x}\right] \tag{9}$$

$$\frac{\partial}{\partial t}(\alpha_f\rho_f v_f)+\frac{\partial}{\partial x}(\alpha_f\rho_f v_f^2)$$

$$=-\frac{\partial}{\partial x}(\alpha_f p)-\Gamma_g(v_{\text{in}}-v_g)+\alpha_g\rho_g FI_g(v_g-v_f)$$

$$+C\alpha_g\alpha_f\rho_m\left[\frac{\partial}{\partial t}(v_g-v_f)+v_f\frac{\partial v_g}{\partial x}-v_g\frac{\partial v_f}{\partial x}\right] \tag{10}$$

Energy equations for gas and liquid phase:

$$\frac{\partial}{\partial t}\left[\alpha_g\rho_g\left(e_g+\frac{v_g^2}{2}\right)\right]+\frac{\partial}{\partial x}\left[\alpha_g\rho_g v_g\left(e_g+\frac{v_g^2}{2}\right)\right]$$

$$=-\frac{\partial}{\partial x}(\alpha_g p v_g)+Q_g+W_g+\Gamma_g\left(e_{\text{gi}}+\frac{v_{\text{gi}}^2}{2}\right) \tag{11}$$

$$\frac{\partial}{\partial t}\left[\alpha_f\rho_f\left(e_f+\frac{v_f^2}{2}\right)\right]+\frac{\partial}{\partial x}\left[\alpha_f\rho_f v_f\left(e_f+\frac{v_f^2}{2}\right)\right]$$

$$=-\frac{\partial}{\partial x}(\alpha_f p v_f)-Q_g-W_g-\Gamma_g\left(e_{\text{gi}}+\frac{v_{\text{gi}}^2}{2}\right) \tag{12}$$

To compute pressure, gas and fluid density, gas and fluid velocity, and gas and fluid internal energy, the system of equations can be solved numerically with the use of a finite difference method. Crucial to the modeling of the steam condensation is the approximation of the variables Q, W, and Γ as well as the shape of the steam plume and a hot water layer. These quantities are computed simultaneously with the general equations. It is the computation of Γ which is the most critical as it depends on the heat transfer processes that take place in the flow. To obtain an accurate approximation of Γ a heat transfer coefficient must be calculated, which depends on the steam plume shape and the processes in the hot water layer.

In this study we investigated the effect of the steam plume shape on the flow field prediction. A model is developed to simulate DCC of steam to predict interface characteristics for a range of steam-water temperature differences.

Parametrical Study of Different Steam Plume Shapes

The characteristics of the steam plume depend on the temperature difference between pool water and steam, steam flow rate, shape of the pool, position, and direction of the steam pipe. Considering the case of the horizontal steam pipe releasing steam in an open area of water, a simple calculation showing the relation between different plume shapes, plume lengths, and heat transfer coefficients can be performed.

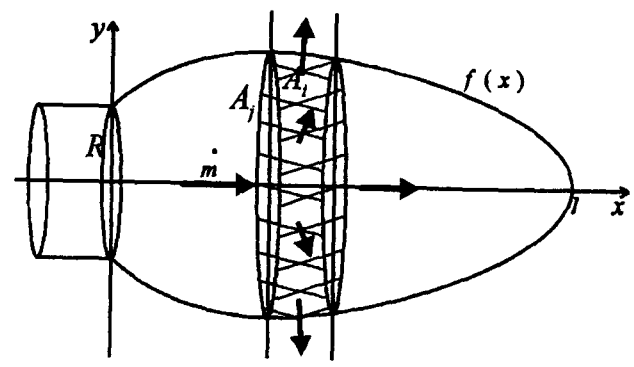

Fig. 3 Change in volume of steam mass is equal to the mass of steam, which condensed through the surface of the volume

Following the laws of conservation, the change of mass of the steam in a plume volume must be equal to the mass of steam, which condenses through a surface of the same volume [Eq. (13)]:

$$\rho v(x)A_j(x)-\rho v(x+dx)A_j(x+dx)=\frac{h_i}{h_{fg}}\Delta TA_i(x) \tag{13}$$

Assuming an axially symmetric steam plume (Fig. 3) Eq. (13) can be transformed into an integral equation [Eq. (14)]. In here the surface through which condensation occurs is calculated correctly using the declination of the function. This is in contrast with many models to date that use only an approximation of the area.

$$\int_{\dot{m}_0}^{0}d\dot{m}=-\frac{h_i}{h_{fg}}\Delta T2\pi\int_0^l f(x)\sqrt{1+f'^2(x)}dx \tag{14}$$

The form of Eq. (14) is such that it can be easily used for different plume shapes, described by function $f(x)$. In this study we tested four different steam plume shapes

- Conical $f(x)=-(R/l)x+R$
- Parabolic $f(x)=R\sqrt{1-x/l}$
- Ellipsoidal $f(x)=R\sqrt{1-x^2/l^2}$
- Spherical $f(x)=\sqrt{(l-a)^2-(x-a)^2}$

where the sphere's center can be moved along the x axis in and out of the pipe's exit for $a=\pm(l^2-R^2)/(2l)$.

In order to evaluate the computational predictions, experimental data by Chun et al. [3] is used. They performed an experiment with steam entering horizontally in open water. The experiment was performed with a normalized steam flow rate G_0 ranging from 200 to 1600 kg/(m^2 s).

A full set of experimental data for a normalized steam flow rate of 1488 kg/(m^2 s) was used in this study for validation. According to the paper the dimensionless steam plume length l/d is in the range of 1–15 and the average heat transfer coefficient of DCC is in the range of 1–3.5 MW/(m^2 K). The heat transfer coefficient was not measured for the upper part of the normalized steam flow rate range and is reported to increase with increasing flow rate. Therefore, we cannot rely completely on the proposed range for the heat transfer coefficient. Furthermore, the heat transfer coefficient, measured for high steam flow rates, is reported to be in the order of 10 MW/(m^2 K) as reported by Kerney et al. [12] and Young et al. [13].

Figures 4–7 show a comparison for the dimensionless plume length between experimental data and the results calculated from Eq. (14) for different plume shapes. Calculations were performed for the normalized steam flow rate $G_0=1488$ kg/(m^2 s) to be comparable with data from Chun's experiment, which was performed for the same normalized steam flow rate.

All four figures show dimensionless plume length in relation to the temperature difference between pool water and steam. The heat transfer coefficient used for the calculation was set in order to obtain the best comparison between experimental data and calcu-

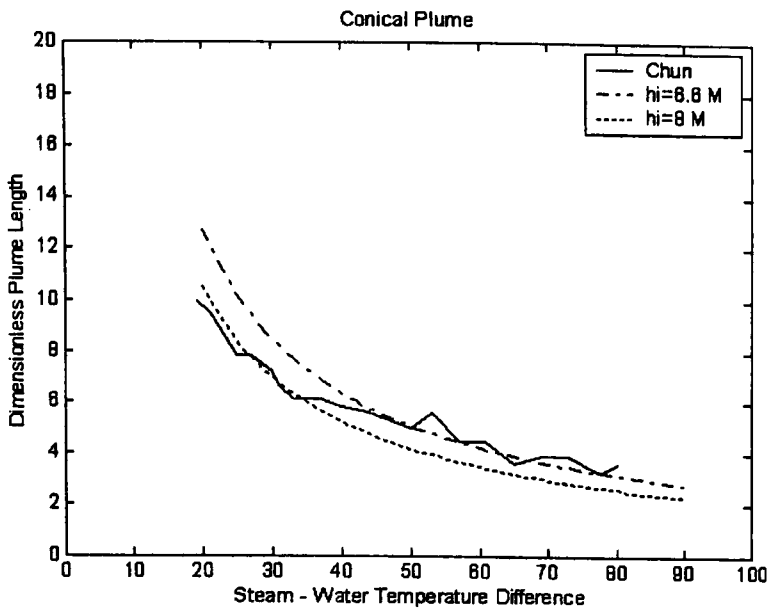

Fig. 4 Dimensionless plume length dependent on temperature difference in (°C) for conical plume shape compared with experimental data from Chun et al. [3]

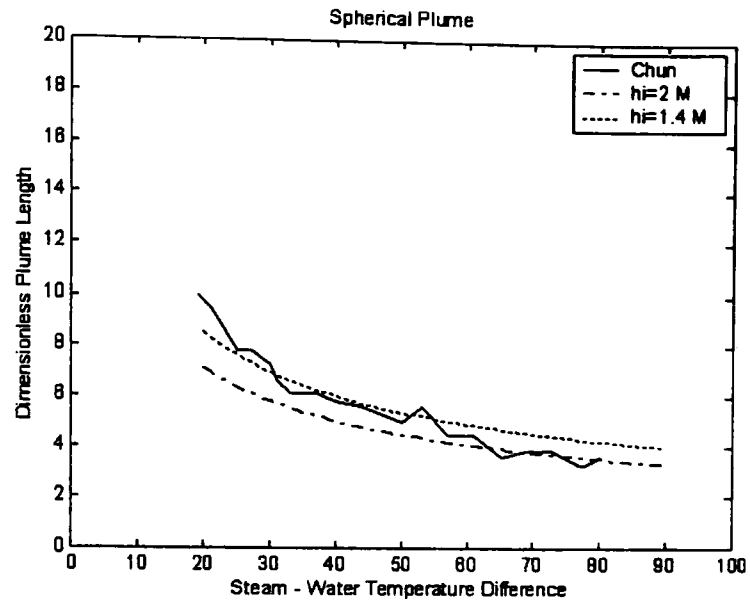

Fig. 6 Dimensionless plume length dependent on temperature difference in (°C) for spherical plume shape compared with experimental data from Chun et al. [3]

lations. Comparing heat transfer coefficients used for calculations for different steam plume shapes show the efficiency of DCC heat transfer for different shapes.

Figure 4 shows good agreement with experimental data for high temperature differences when the heat transfer coefficient was set to 6.6 MW/(m^2 K).

For low temperature differences the error between data and calculations is approximately 25%. For low temperature differences better agreement is obtained with a higher heat transfer coefficient. Both heat transfer coefficients are above the range reported by Chun, but fall in the range reported by Kerney and Young.

Figure 5 shows the comparison between the predicted nondimensional plume lengths for two different heat transfer coefficients for a parabolic plume shape. The plume length for both heat transfer coefficients increases with increasing steam-water difference which is opposite to the trend seen in the conical plume (see Fig. 4).

Also the predicted plume lengths are much smaller when compared to the plume length for a conical shape for a similar temperature difference. These results suggest that the use of parabolic plume shape can be considered inaccurate.

Use of a spherical plume (Fig. 6) also shows good agreement with experimental data. The plume length prediction for a spherically shaped plume is in better agreement with experimental data for a lower heat transfer coefficient at low temperature differences than for high temperature differences. The maximum disagreement between data and predictions for the higher temperature difference is approximately 15%; that is lower than the error for the conical shape.

Both heat transfer coefficients used are in the range reported by Chun and are lower than those used in the calculations with conical shape.

Calculations performed with an ellipsoidal plume shape show the best agreement with experimental data (Fig. 7) and confirm the observation reported by Chun et al. In here the heat transfer coefficient was set to 5.4 MW/(m^2 K). The disagreement between data and calculations, which occurs for lower temperature difference, is approximately 10%.

Measurements of heat transfer coefficients are unclear because of the difficulty involved in obtaining mean steam flow rate, correct length of plume, and complicated heat transfer in the hot water layer. However, the DCC heat transfer coefficient for horizontal steam inflow in stagnant water is reported to be in the range

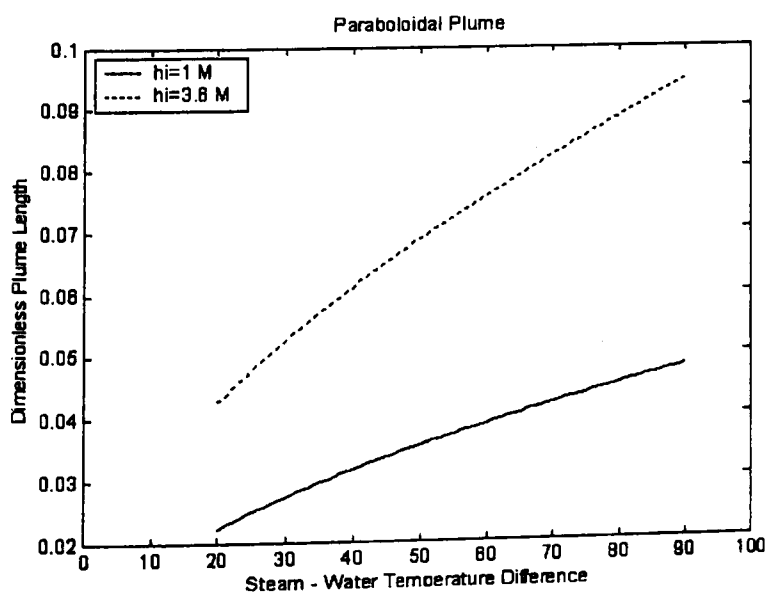

Fig. 5 Dimensionless plume length dependent on temperature difference in (°C) for parabolic plume shape

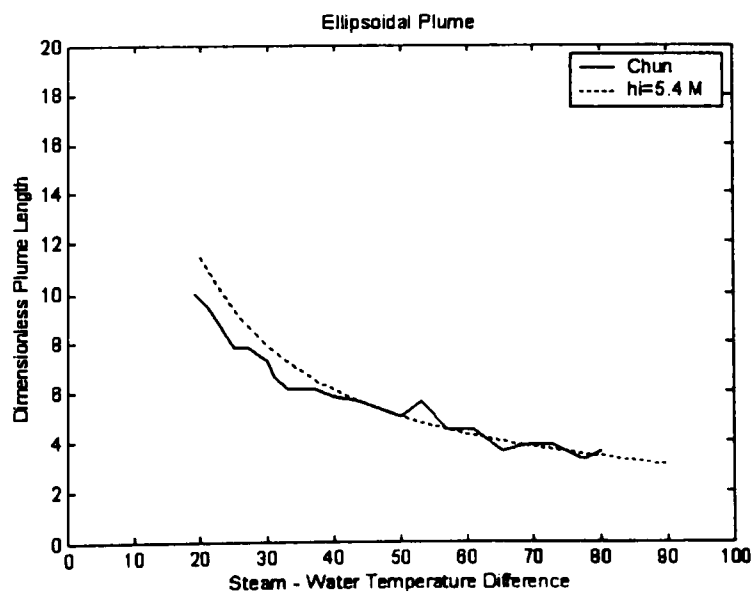

Fig. 7 Dimensionless plume length dependent on temperature difference in (°C) for ellipsoidal plume shape compared with experimental data from Chun et al. [3]

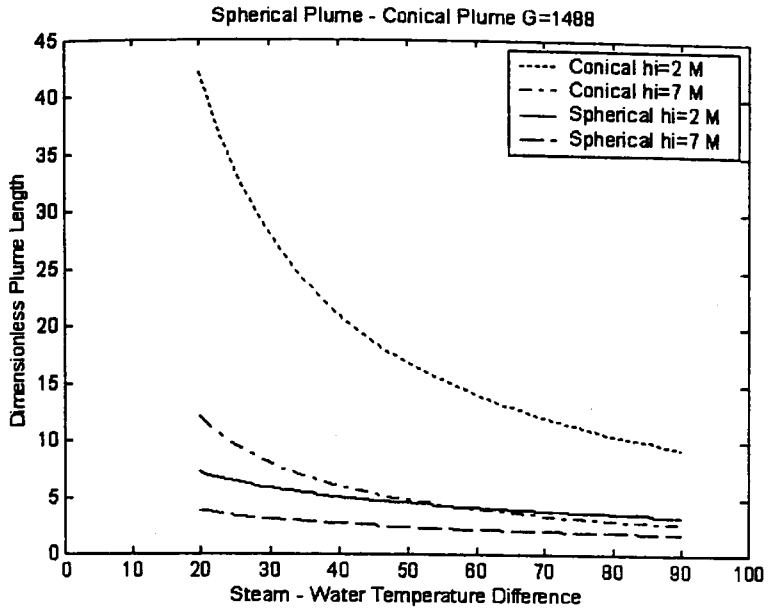

Fig. 8 Dimensionless plume length for spherical plume shape compared with results for conical plume for two different heat transfer coefficients for high normalized steam flow rate

from 1 to 12 MW/(m^2 K). All heat transfer coefficients used during the calculations in this study are in the same range and so are considered to be close to reality.

Calculations performed with an ellipsoidal plume shape show the best agreement with experimental data for a normalized steam flow rate of 1488 kg/(m^2 s). Unfortunately experimental data for dimensionless plume length for different steam flow rates are not available; therefore, we cannot perform similar investigations which might show better agreement for different shapes used for different steam flow rates.

Figures 8 and 9 show calculated dimensionless plume lengths for spherical and conical shape for two different heat transfer coefficients and normalized steam flow rates in order to compare these two models.

Results, shown in Fig. 8 were calculated at a high normalized steam flow rate of 1488 kg/(m^2 s) in order to be comparable with previous figures. Predictions of the nondimensional plume length for a low heat transfer coefficient are too high with the conically shaped plume. With increasing heat transfer coefficient the length reduces and falls into the range proposed by Chun. On the other hand the spherical model is less affected by the change of heat transfer coefficient.

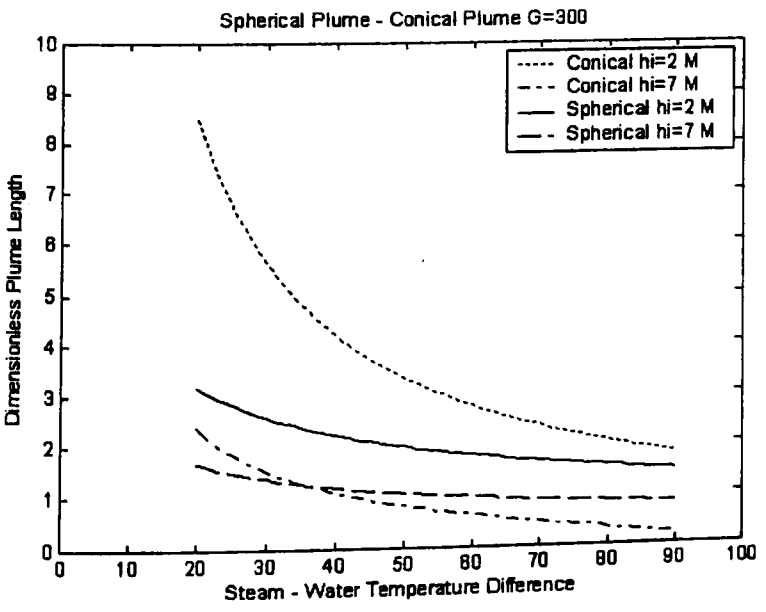

Fig. 9 Dimensionless plume length for spherical plume shape compared with results for conical plume for two different heat transfer coefficients for low normalized steam flow rate

Dimensionless plume lengths calculated at a low normalized steam flow rate $G_0 = 300\ \mathrm{kg/m^2\ s}$ show the same trend for two different models, but the ranges are smaller (Fig. 9). Calculations obtained with the conical model are much more dependent on input parameters; hence, the range where the conical model may be used is small. On the other hand, the spherical model showed a more stable prediction and should be considered to cover a wider range of steam flow rates.

Conclusions

In the paper a model for DCC of steam in water is presented. Difficulties arise in the predictions of heat transfer coefficient and steam plume shape. In existing models partly empirically obtained equations for calculating heat transfer coefficient and steam plume length are used.

The proposed model was employed to predict steam plume length for four different axially symmetrical steam plume shapes. The results showed, that the use of an appropriate shape for inlet conditions give predictions for dimensionless steam plume close to experimentally obtained lengths.

The ellipsoidal model showed the best agreement with experimental data and is believed to be the most appropriate shape for a wide range of data. This confirms observations on DCC reported in literature. Spherical and conical shapes should only be considered as appropriate in specific ranges and should be further investigated.

The study also showed that the spherical model gives better agreement with experimental data for the lowest heat transfer coefficient and the conical model for the highest one. This result was expected because the condensation area for spherical shape is the biggest and for conical the smallest for the same plume length. In order to obtain exact correlations between heat transfer coefficient and different shapes, further work should be performed.

Further work will involve a modified model taking other variables into account and incorporating the modified model into a computational model of condensation.

Acknowledgments

The author would like to thank Dr. R. K. Calay for her interesting discussions. The author would also like to thank Dr. G. de With for his support during this study.

Nomenclature

A = area
a = x coordinate of a center of a sphere
C = coefficient of virtual mass
d = injector exit diameter
e = internal energy
f = steam plume shape function
FI = interface drag coefficient
G = normalized steam flow rate
h_{ef} = heat of vaporization
h_i = heat transfer coefficient
l = length of steam plume
m = surface tension source
$\dot{m}$ = change of mass
p = pressure
Q = interfacial heat exchange
R = injector exit radius
Re = reynolds number
T = temperature
t = time
v = velocity
W = interfacial work exchange
x = space coordinate
α = void fraction
Γ = interfacial mass exchange

ε = interfacial energy source
ρ = density

Subscripts

f = fluid
fi = relative fluid-interface index
g = gas
gi = relative gas-interface index
i = interface for area of interface
in = interface
j = position of steam flux cross section
k = phase index
k' = opposite index to phase index $_k$
ki = relative phase-interface index
0 = injector exit condition
t = turbulent

References

[1] Liang, K.-S., and Griffith, P., 1994, "Experimental and Analytical Study of Direct Contact Condensation of Steam in Water," Nucl. Eng. Des., **147**, pp. 425–435.

[2] Liang, K.-S., 1991, "Experimental and Analytical Study of Direct Contact Condensation of Steam in Water," PhD thesis, Massachusetts Institute of Technology, Cambridge, MA.

[3] Chun, M.-H., Kim, Y.-S., and Park, J.-W., 1996, "An Investigation of Direct Condensation of Steam Jet in Subcooled Water," Int. Commun. Heat Mass Transfer, **23**(7), pp. 947–958.

[4] Chan, C. K., and Lee, C. K. B., 1982, "A Regime Map for Direct Contact Condensation," Int. J. Multiphase Flow, **8**(1), pp. 11–20.

[5] Aya, I., and Nariai, H., 1987, "Boundaries Between Regimes of Pressure Oscillation Induced by Steam Condensation in Pressure Suppression Containment," Nucl. Eng. Des., **99**, pp. 31–40.

[6] Weimer, J. C., Faeth, G. M., and Olson, D. R., 1973, "Penetration of Vapor Jets Submerged in Subcooled Liquids," AIChE J., **19**(3), pp. 552–558.

[7] Youn, D. H., Ko, K. B., Lee, Y. Y., Kim, M. H., Bae, Y. Y., and Park, J. K., 2003, "The Direct Contact Condensation of Steam in a Pool at Low Mass Flux," Technical Report, J. Nucl. Sci. Technol., **40**(10), pp. 881–885.

[8] Celata, G. P., Cumo, M., Farello, G. E., and Focardi, G., 1986, "Direct Contact Condensation of Steam on Slowly Moving Water," Nucl. Eng. Des., **96**, pp. 21–31.

[9] Celata, G. P., Cumo, M., Farello, G. E., and Focardi, G., 1987, "Direct Contact Condensation of Steam of Superheated Steam on Water," Int. J. Heat Mass Transfer, **30**(3), pp. 449–458.

[10] Celata, G. P., 1991, "Direct Contact Condensation of Steam on Subcooled Water," *Proc., International Center for Heat and Mass Transfer*, G. F. Hewitt et al., eds., Hemisphere, New York, No. 33, pp. 345–372.

[11] Drew, D. A., and Passman, S. L., 1999, *Theory of Multicomponent Fluids*, Applied Mathematical Sciences Series Vol. 135, Springer-Verlag, New York, pp. 121–128.

[12] Kerney, P. J., Faeth, G. M., and Olson, D. R., 1972, "Penetration Characteristics of a Submerged Steam Jet," AIChE J., **18**(3), pp. 548–553.

[13] Young, R. J., Yang, K. T., and Novotny, J. L., 1974, "Vapor-Liquid Interaction in a High Velocity Vapor Jet Condensing in a Coaxial Water Flow," ASME J. Heat Transfer, **3**, pp. 226–230.